Supplementary Information (SI) for Organic & Biomolecular Chemistry.
This journal is © The Royal Society of Chemistry 2024

Supporting Information

Conservation of Structure and Dynamic Behavior in Triazine Macrocycles: Opportunities for Subtle Control of Hinge Motion

Casey J. Patterson-Gardner,[a] Hongjun Pan,[b] Benjamin G. Janesko,[a] Eric E. Simanek[a,*]

[a]*Department of Chemistry & Biochemistry, Texas Christian University, Fort Worth, TX, 76129 USA*

[b]*Department of Chemistry, University of North Texas, Denton, TX, 76203, USA*

Table of Contents

General Experimental Details

NMR Spectroscopy. **S-5**
Modeling NMR Spectra. **S-5**
Determination of the Temperature of Coalescence, T_c, and Error. **S-5**
Determination of Chemical Shift Difference, Δν, at T_c. **S-5**
Determination of the barrier to hinging, $\Delta G^{\ddagger}$, from Δν and T_c. **S-5**
Determination of the Thermodynamics of the barrier to hinging from ln(k) vs 1/T. **S-6**
Determination of the Thermodynamics of the barrier to hinging from the plot of ln(k/T) vs 1/T. **S-6**
General Computational Details. **S-6**

Computational Structures and Energies

Table S1. Computed M06-2x Free Energies of Potential Hinging Intermediates. **S-7**
Table S2. Macrocycle SMILES Strings and AlogP Values.
Table S3. Gaussian M06-2x Optimized from CREST Potential Hinging Intermediate Structures. **S-8**

Variable-Temperature NMR and Analysis

Figure S1. Stacked ^{1}H VT-NMR Spectra of $\mathbf{G^{NNMe}}$. **S-9**
Figure S2. Annotated Stacked ^{1}H VT-NMR Spectra of $\mathbf{G^{NNMe}}$. **S-10**
Figure S3. Chemical Shift Dependence on Temperature for $\mathbf{G^{NNMe}}$. **S-11**
Figure S4. Log_{10} of the Difference in Chemical Shift with Temperature for $\mathbf{G^{NNMe}}$. **S-11**
Table S4. Chemical Shift and Δν dependence on temperature for $\mathbf{G^{NNMe}}$. **S-12**
Table S5. Relevant Variables for the Determination of $\Delta G^{\ddagger}$ for $\mathbf{G^{NNMe}}$. **S-12**
Figure S5. DNMR Traces for α and the respective fit for $\mathbf{G^{NNMe}}$. **S-13**
Figure S6. Thermodynamics derived from DNMR for $\mathbf{G^{NNMe}}$. **S-14**
Figure S7. Stacked ^{1}H VT-NMR Spectra of $\mathbf{G^{NNEt}}$. **S-15**

Figure S8. Annotated Stacked ^{1}H VT-NMR Spectra of **G^{NNEt}**. **S-16**
Figure S9. Chemical Shift Dependence on Temperature for **G^{NNEt}**. **S-17**
Figure S10. Log_{10} of the Difference in Chemical Shift with Temperature for **G^{NNEt}**. **S-17**
Table S6. Chemical Shift and Δν dependence on temperature for **G^{NNEt}**. **S-18**
Table S7. Relevant Variables for the Determination of $\Delta G^{\ddagger}$ for **G^{NNEt}**. **S-18**
Figure S11. DNMR Traces for α and the respective fit for **G^{NNEt}**. **S-19**
Figure S12. Thermodynamics derived from DNMR for the α resonance of **G^{NNEt}**. **S-20**
Figure S13. DNMR Traces for a and the respective fit for **G^{NNEt}**. **S-21**
Figure S14. Thermodynamics derived from DNMR for the a resonance of **G^{NNEt}**. **S-22**
Figure S15. Stacked ^{1}H VT-NMR Spectra of **G^{NNiPr}**. **S-23**
Figure S16. Annotated Stacked ^{1}H VT-NMR Spectra of **G^{NNiPr}**. **S-24**
Figure S17. Chemical Shift Dependence on Temperature for **G^{NNiPr}**. **S-25**
Figure S18. Log_{10} of the Difference in Chemical Shift with Temperature for **G^{NNiPr}**. **S-25**
Table S8. Chemical Shift and Δν dependence on temperature for **G^{NNiPr}**. **S-26**
Table S9. Relevant Variables for the Determination of $\Delta G^{\ddagger}$ for **G^{NNiPr}**. **S-26**
Figure S19. DNMR Traces for α and the respective fit for **G^{NNiPr}**. **S-27**
Figure S20. Thermodynamics derived from DNMR for **G^{NNiPr}**. **S-28**
Figure S21. Stacked ^{1}H VT-NMR Spectra of **G^{NNBn}**. **S-29**
Figure S22. Annotated Stacked ^{1}H VT-NMR Spectra of **G^{NNBn}**. **S-30**
Figure S23. Chemical Shift Dependence on Temperature for **G^{NNBn}**. **S-31**
Figure S24. Log_{10} of the Difference in Chemical Shift with Temperature for **G^{NNBn}**. **S-31**
Table S10. Chemical Shift and Δν dependence on temperature for **G^{NNBn}**. **S-32**
Table S11. Relevant Variables for the Determination of $\Delta G^{\ddagger}$ for **G^{NNBn}**. **S-32**
Figure S25. DNMR Traces for α and the respective fit for **G^{NNBn}**. **S-33**
Figure S26. Thermodynamics derived from DNMR for the α resonance of **G^{NNBn}**. **S-34**
Figure S27. DNMR Traces for a and the respective fit for **G^{NNBn}**. **S-35**
Figure S28. Thermodynamics derived from DNMR for the a resonance of **G^{NNBn}**. **S-36**
Figure S29. Stacked ^{1}H VT-NMR Spectra of **G^{NNHx}**. **S-37**
Figure S30. Annotated Stacked ^{1}H VT-NMR Spectra of **G^{NNHx}**. **S-38**
Figure S31. Chemical Shift Dependence on Temperature for **G^{NNHx}**. **S-39**
Figure S32. Log_{10} of the Difference in Chemical Shift with Temperature for **G^{NNHx}**. **S-39**
Table S12. Chemical Shift and Δν dependence on temperature for **G^{NNHx}**. **S-40**
Table S13. Relevant Variables for the Determination of $\Delta G^{\ddagger}$ for **G^{NNHx}**. **S-40**
Figure S33. DNMR Traces for α and the respective fit for **G^{NNHx}**. **S-41**
Figure S34. Thermodynamics derived from DNMR for the α resonance of **G^{NNHx}**. **S-42**
Figure S35. DNMR Traces for a and the respective fit for **G^{NNHx}**. **S-43**
Figure S36. Thermodynamics derived from DNMR for the a resonance of **G^{NNHx}**. **S-44**

^{1}H NMR Spectra of Macrocycles

Figure S37. The 400 MHz ^{1}H NMR Spectrum of **G^{NNMe}** in DMSO. **S-45**
Figure S38. The 400 MHz ^{1}H NMR Spectrum of **G^{NNEt}** in DMSO. **S-46**
Figure S39. The 400 MHz ^{1}H NMR Spectrum of **G^{NNiPr}** in DMSO. **S-47**

Figure S40. The 400 MHz ^{1}H NMR Spectrum of **G^{NNBn}** in DMSO. **S-48**
Figure S41. The 400 MHz ^{1}H NMR Spectrum of **G^{NNHx}** in DMSO. **S-49**

^{13}C NMR Spectra of Macrocycles

Figure S42. The 100 MHz ^{13}C NMR Spectrum of **G^{NNMe}** in DMSO. **S-50**
Figure S43. The 100 MHz ^{13}C NMR Spectrum of **G^{NNEt}** in DMSO. **S-51**
Figure S44. The 100 MHz ^{13}C NMR Spectrum of **G^{NNiPr}** in DMSO. **S-52**
Figure S45. The 100 MHz ^{13}C NMR Spectrum of **G^{NNBn}** in DMSO. **S-53**
Figure S46. The 100 MHz ^{13}C NMR Spectrum of **G^{NNHx}** in DMSO. **S-54**

2D rOesy and COSY NMR Spectra of Macrocycles

Figure S47. The 400 MHz rOesy and COSY NMR Spectrum of **G^{NNMe}** in DMSO. **S-55**
Figure S48. The 400 MHz rOesy and COSY NMR Spectrum of **G^{NNEt}** in DMSO. **S-56**
Figure S49. The 400 MHz rOesy and COSY NMR Spectrum of **G^{NNiPr}** in DMSO. **S-57**
Figure S50. The 400 MHz rOesy and COSY NMR Spectrum of **G^{NNBn}** in DMSO. **S-58**
Figure S51. The 400 MHz rOesy and COSY NMR Spectrum of **G^{NNHx}** in DMSO. **S-59**

Mass Spectra of Macrocycles

Figure S52. HRMS (ESI) of **G^{NNMe}**. **S-60**
Figure S53. HRMS (ESI) of **G^{NNEt}**. **S-61**
Figure S54. HRMS (ESI) of **G^{NNiPr}**. **S-62**
Figure S55. HRMS (ESI) of **G^{NNBn}**. **S-63**
Figure S56. HRMS (ESI) of **G^{NNHx}**. **S-64**

General Chemistry

General Chemistry Details **S-65**

Synthetic Details

Synthesis of Hydrazones **S-66**
Synthesis of Esters **S-75**
Synthesis of Monomers **S-89**

Characterization of Hydrazone Intermediates

Figure S57. The 400 MHz ^{1}H and 100 MHz ^{13}C NMR spectra of **tert-butyl 2-benzylhydrazonecarboxylate** in $CDCl_3$. **S-69**
Figure S58. The 400 MHz ^{1}H and 100 MHz ^{13}C NMR spectra of **tert-butyl 2-hexylhydrazonecarboxylate** in $CDCl_3$. **S-70**
Figure S59. The 400 MHz ^{1}H and 100 MHz ^{13}C NMR spectra of **tert-butyl 2-benzylhydrazinecarboxylate** in $CDCl_3$. **S-71**
Figure S60. The 400 MHz ^{1}H and 100 MHz ^{13}C NMR spectra of **tert-butyl 2-benzylhydrazinecarboxylate** in $CDCl_3$. **S-72**
Figure S61. HRMS (ESI) of **tert-butyl 2-hexylhydrazonecarboxylate**. **S-73**

Figure S62. HRMS (ESI) of **tert-butyl 2-hexylhydrazinecarboxylate**. **S-73**
Figure S63. HRMS (ESI) of **tert-butyl 2-benzylhydrazinecarboxylate**. **S-73**
Figure S64. HRMS (ESI) of **tert-butyl 2-benzylhydrazonecarboxylate**. **S-74**

Characterization of Ester Intermediates

Figure S65. The 400 MHz ^{1}H and 100 MHz ^{13}C NMR spectra of **G^{NNMe}-Ester** in DMSO. **S-79**
Figure S66. The 400 MHz ^{1}H and 100 MHz ^{13}C NMR spectra of **G^{NNEt}-Ester** in DMSO. **S-80**
Figure S67. The 400 MHz ^{1}H and 100 MHz ^{13}C NMR spectra of **G^{NNiPr}-Ester** in DMSO. **S-81**
Figure S68. The 400 MHz ^{1}H and 100 MHz ^{13}C NMR spectra of **G^{NNBn}-Ester** in DMSO. **S-82**
Figure S69. The 400 MHz ^{1}H and 100 MHz ^{13}C NMR spectra of **G^{NNHx}-Ester** in DMSO. **S-83**
Figure S70. HRMS (ESI) of **G^{NNMe}-Ester**. **S-84**
Figure S71. HRMS (ESI) of **G^{NNEt}-Ester**. **S-85**
Figure S72. HRMS (ESI) of **G^{NNiPr}-Ester**. **S-86**
Figure S73. HRMS (ESI) of **G^{NNBn}-Ester**. **S-87**
Figure S74. HRMS (ESI) of **G^{NNHx}-Ester**. **S-88**

Characterization of Monomer Intermediates

Figure S75. The 400 MHz ^{1}H and 100 MHz ^{13}C NMR spectra of **G^{NNMe}-Monomer** in DMSO. **S-94**
Figure S76. The 400 MHz ^{1}H and 100 MHz ^{13}C NMR spectra of **G^{NNEt}-Monomer** in DMSO. **S-95**
Figure S77. The 400 MHz ^{1}H and 100 MHz ^{13}C NMR spectra of **G^{NNiPr}-Monomer** in DMSO. **S-96**
Figure S78. The 400 MHz ^{1}H and 100 MHz ^{13}C NMR spectra of **G^{NNBn}-Monomer** in DMSO. **S-97**
Figure S79. The 400 MHz ^{1}H and 100 MHz ^{13}C NMR spectra of **G^{NNHx}-Monomer** in DMSO. **S-98**
Figure S80. HRMS (ESI) of **G^{NNMe}-Mononer**. **S-99**
Figure S81. HRMS (ESI) of **G^{NNEt}-Monomer**. **S-100**
Figure S82. HRMS (ESI) of **G^{NNiPr}-Monomer**. **S-101**
Figure S83. HRMS (ESI) of **G^{NNBn}-Monomer**. **S-102**
Figure S84. HRMS (ESI) of **G^{NNHx}-Monomer**. **S-103**

References **S-104**

GENERAL EXPERIMENTAL DETAILS

NMR Spectroscopy. Variable-temperature NMR was taken 500 MHz Varian NMR spectrometer at the University of North Texas. All other spectra were taken on a 400 MHz Bruker Avance spectrometer at Texas Christian University. Chemical shifts for ^{1}H and $^{13}C\{^{1}H\}$ spectra were calibrated to their corresponding solvent resonance (i.e., DMSO-*d_6* with δ = 2.50 ppm for ^{1}H spectra and δ = 39.52 for $^{13}C\{^{1}H\}$ spectra, $CDCl_3$ with δ = 7.26 for ^{1}H spectra and δ = 77.16 for $^{13}C\{^{1}H\}$ spectra, and CD_3OD with δ = 3.31 for ^{1}H and δ = 49.00 for $^{13}C\{^{1}H\}$ spectra). Identification of splitting of NMR signals was assigned by the following: s = singlet, d = doublet, t = triplet, q = quartet, bs = broad singlet, m = multiplet (if the center of the multiplet could not be determined, a range for the peak was reported).

The contours of 2D Spectra (COSY and rOesy) were calibrated to the center of their corresponding NNR-A ^{1}H resonances (i.e., the methylene/methyl/methine vinyl to the Ar-hydrazone nitrogen). 2D rOesy spectra underwent a freeze/thaw cycle by freezing the macrocycle in DMSO solution in a dry ice/acetone bath and thawing under vacuum. After evolution of bubbles stopped, the NMR tube was removed from vacuum and backfilled with N_2. This cycle was repeated until evolution of gas was no longer noticed. Variable temperature ^{1}H NMR was taken with temperatures between -50°C and 50°C.

Modeling NMR Spectra. Dynamic NMR (DNMR) was performed using TopSpin 3.7.0 using the "Fit Dynamic NMR Models" command. The rate constant, k, for each spectrum was determined by optimizing the k, line broadening (LB), the J-value when necessary, intensity, and chemical shift of the simulated peaks until the highest fit was achieved. The original spectra is shown in black and simulated spectra are shown in green or magenta.

Determination of the Temperature of Coalescence, T_c, and Error. The temperature of coalescence was determined from the halfway point between the first observed coalesced point and the last observed decoalesced point. e.g., with the α proton of **G^{NNMe}**, the last decoalesced temperature was 263K, and the first coalesced temperature was 268K, so T_c was taken to be 265.5K (see **Figure S2** for an example of a coalescence plot). Consequently, the upper and lower temperature bounds were taken and used to find the uncertainty of $\Delta G^{\ddagger}$ for these bounds. For example, the reported $\Delta G^{\ddagger}$ for the α proton of **G^{NNMe}** uses T_c at 265.5K, and the uncertainty is derived from the deviation from $\Delta G^{\ddagger}$@265.5K with $\Delta G^{\ddagger}$@268K as an upper bound and $\Delta G^{\ddagger}$@263K as a lower bound.

Determination of chemical shift difference, Δν, at T_c. The difference in chemical shift at T_c was determined by a plot between log(Δν) and its respective temperature. The linear portion of the plot was used to generate a linear regression (see **Figure S4** for an example). The T_c was used with the linear equation to give log(Δν) at T_c, which then allows for determination the Δν at T_c.

Determination of the barrier to hinging, $\Delta G^{\ddagger}$, from Δν and T_c. The barriers to hinging were obtained from the Eyring-Polanyi equation where κ is the transmission coefficient (assumed to be 1), h is Planck's constant, k_{exch} is the exchange rate, k_B is the Boltzmann constant, and R is the ideal gas constant. The exchange rate is acquired from equation 2 where Δν is in Hz.

$$\Delta G = -RT_c \ln\left(\frac{\kappa h k_{exch}}{k_B T_c}\right) \quad \text{(equation 1)}$$

$$k_{exch} = \frac{\pi(\Delta\nu)}{\sqrt{2}} \approx 2.22\Delta\nu \quad \text{(equation 2)}$$

Determination of the thermodynamics of the barrier to hinging, $\Delta H^{‡}$, $\Delta S^{‡}$, and $\Delta G^{‡}$ from the plot of ln(k) vs 1/T. The $\Delta G^{‡}$ was determined from the equation 3 where a is constant 0.004575 kcal/mol, T is desired temperature in K (in this case, T = T_c), T_c is the temperature of coalescence (previously determined), and Δν is the chemical shift difference at the desired temperature in 1/s (here, Δν = Δν at T_c).

$$\Delta G = aT\left(9.972 + \log\left(\frac{T_c}{\Delta\nu}\right)\right) \quad \text{(equation 3)}$$

Enthalpy, $\Delta H^{‡}$, is obtained from the slope of the plot of ln(k) vs 1/T, with k being the rate constant determined with DNMR line shape analysis, with equation 4. E_a is determined by equation 5. where R is the gas constant 1.987e-3 kcal/mol, and T_c is the previously determined temperature of coalescence. Entropy, $\Delta S^{‡}$, is yielded from the Gibbs free energy equation, giving equation 6, where ΔG and ΔH are the previously determined free energy and enthalpy, and T_c is the previously determined temperature of coalescence.

$$\Delta H = E_a - RT_c, \quad \text{(equation 4)}$$

$$E_a = -slope * R \quad \text{(equation 5)}$$

$$\Delta S = -\frac{\Delta G - \Delta H}{T_c} \text{(equation 6)}$$

Determination of the thermodynamics of the barrier to hinging, $\Delta H^{‡}$, $\Delta S^{‡}$, and $\Delta G^{‡}$ from the plot of ln(k/T) vs 1/T. A plot of ln(k/T) vs 1/T was generated and a linear regression was performed to yield the slope and intercept values. Enthalpy, ΔH, was determined from equation 7. Entropy was determined from equation 8 where k_b is the Boltzmann constant 8.314 J/Kmol, *h* is 6.6e-34 Js, and R is 1.987e-3 kcal/mol. ΔG is thereby determined from the Gibbs free energy equation (Equation 5.).

$$\Delta H = -slope/R. \text{ (equation 7)}$$

$$\Delta S = \left(y - intercept - \ln\left(\frac{k_b}{h}\right)\right) * R \text{ (equation 8)}$$

General Computational Details. The $\mathbf{G^{NNMe}}$ conformer ensemble was generated using CREST with the keywords --gnf2, --alpb dmso, --chrg 2 on a previously optimized structure in Gaussian. The folded conformer, acute conformer, and canted conformer were identified as possible intermediates from $\mathbf{G^{NNMe'}}$s CREST conformer output. The selected conformers were modified in GaussView 6 to match their respective macrocycle (e.g., adding a methyl to $\mathbf{G^{NNMe}}$ methyl hydrazone to generate $\mathbf{G^{NNEt}}$, appending a hexyl chain to $\mathbf{G^{NNMe}}$ to generate $\mathbf{G^{NNHx}}$) for the folded conformer, acute conformer, and canted conformer for each macrocycle. These structures were then optimized in Gaussian16 and thermochemical values were obtained with the input:

```
opt freq empiricaldispersion=gd3 scrf=(solvent=dmso) scf=xqc def2svp m062x
```

M06-2x was chosen due to success in other triazine computation.[A] Tight exchange (scf=xqc) was needed for convergence of $\mathbf{G^{NNBn}}$ folded conformation, and so was appended to the other macrocycles and conformers as well. Grimme's dispersion 3 (Ref. B) was invoked due to an otherwise ovular shape that was obtained from optimization in the absence of dispersion correction. Free energies are reported in **Table S1**. The optimized structures are reported in **Table S3**.

Table S1. Computed M06-2x Free Energies of Potential Hinging Intermediates.

	G_{folded} (kcal/mol)	$G_{stairstep}$ (kcal/mol)	$\Delta G_{stairstep-folded}$ (kcal/mol)	G_{acute} (kcal/mol)	$\Delta G_{acute-folded}$ (kcal/mol)
$\mathbf{G^{NNH}}$	-1133466	-1133461	4.617795	-1133460	6.120664
$\mathbf{G^{NNMe}}$	-1182707.452	-1182700.018	7.433400538	-1182699	8.865362
$\mathbf{G^{NNEt}}$	-1231953.806	-1231944.561	9.245001699	-1231945	8.520863
$\mathbf{G^{NNiPr}}$	-1281189	-1281185	4.294631	-1281185	3.715445
$\mathbf{G^{NNBn}}$	-1472260.188	-1472253.096	7.092038906	-1472254	6.099957
$\mathbf{G^{NNHx}}$	-1428925	-1428916	9.071811	-1428916	8.688407

Space filling structures and $\mathbf{G^{NNiPr}}$ ajar figures were generated in UCSF Chimera 1.16. RMSD values were obtained from the Gaussian16 optimized structures using the "match" command on the respective macrocycles. The hydrazone sidechain atoms were removed to minimize error stemming from disorder of the hydrazone chain.

AlogP values for the alkyl hydrazone macrocycles were obtained using RDKit's MolLogP command. The SMILES strings and respective logP values are reported in **Table S2.**

Table S2. Macrocycle SMILES Strings and AlogP Values.

	Macrocycle SMILES String	AlogP
$\mathbf{G^{NNMe}}$	n1c(N(C)C)nc(N(C)N=CCCNC(=O)CN3)nc(NCC(=O)NCCC=NN(C)(c2nc(N(C)C)nc3n2))1	-1.4172
$\mathbf{G^{NNEt}}$	n1c(N(C)C)nc(N(CC)N=CCCNC(=O)CN3)nc(NCC(=O)NCCC=NN(CC)(c2nc(N(C)C)nc3n2))1	-0.6370
$\mathbf{G^{NNiPr}}$	n1c(N(C)C)nc(N(C(C)C)N=CCCNC(=O)CN3)nc(NCC(=O)NCCC=NN(C(C)C)(c2nc(N(C)C)nc3n2))1	0.1400
$\mathbf{G^{NNBn}}$	n1c(N(C)C)nc(N(C(c1ccccc1))N=CCCNC(=O)CN3)nc(NCC(=O)NCCC=NN(C(c1ccccc1))(c2nc(N(C)C)nc3n2))1	0.7933
$\mathbf{G^{NNHx}}$	n1c(N(C)C)nc(N(CCCCCC)N=CCCNC(=O)CN3)nc(NCC(=O)NCCC=NN(CCCCCC)(c2nc(N(C)C)nc3n2))1	2.4838

Table S3. Gaussian M06-2x Optimized Potential Hinging Intermediate Structures.

Macrocycle	Folded	Stairstep	Acute
G^{NNH}	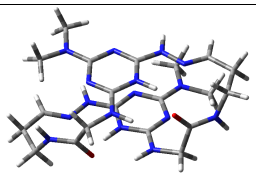	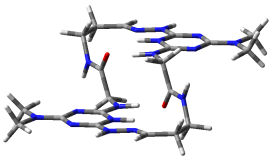	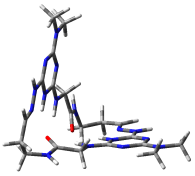
G^{NNMe}	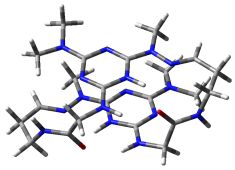	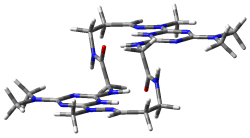	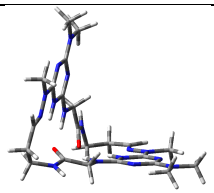
G^{NNEt}	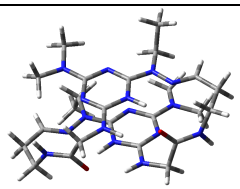	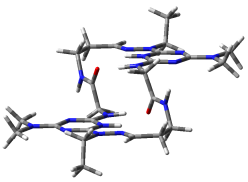	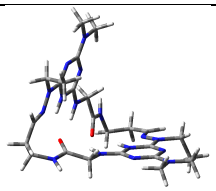
G^{NNiPr}	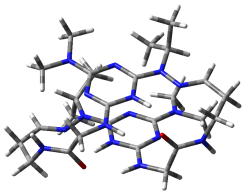	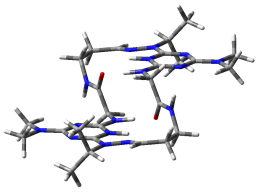	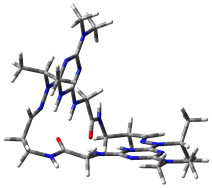
G^{NNBn}	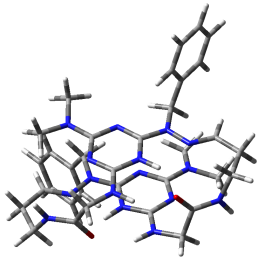	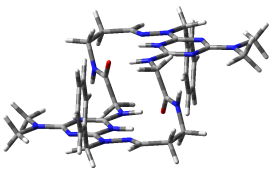	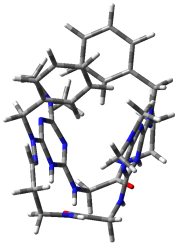
G^{NNHx}	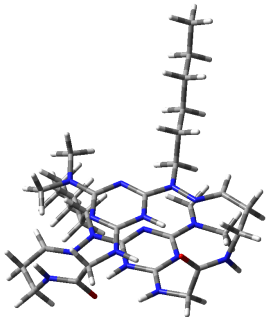	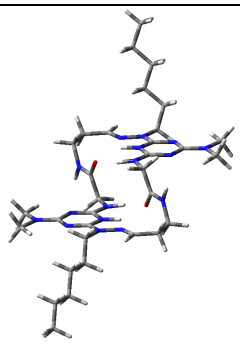	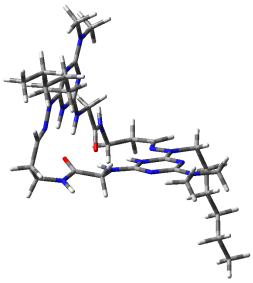

Figure S1. Stacked ^{1}H VT-NMR Spectra of $\mathbf{G^{NNMe}}$. To assess the impact of additional acid, difluoroacetic acid was added to the sample and additional spectra were collected. These spectra are incorporated into this figure at the appropriate temperature and are evident from the DFA resonance at 6.5 ppm.

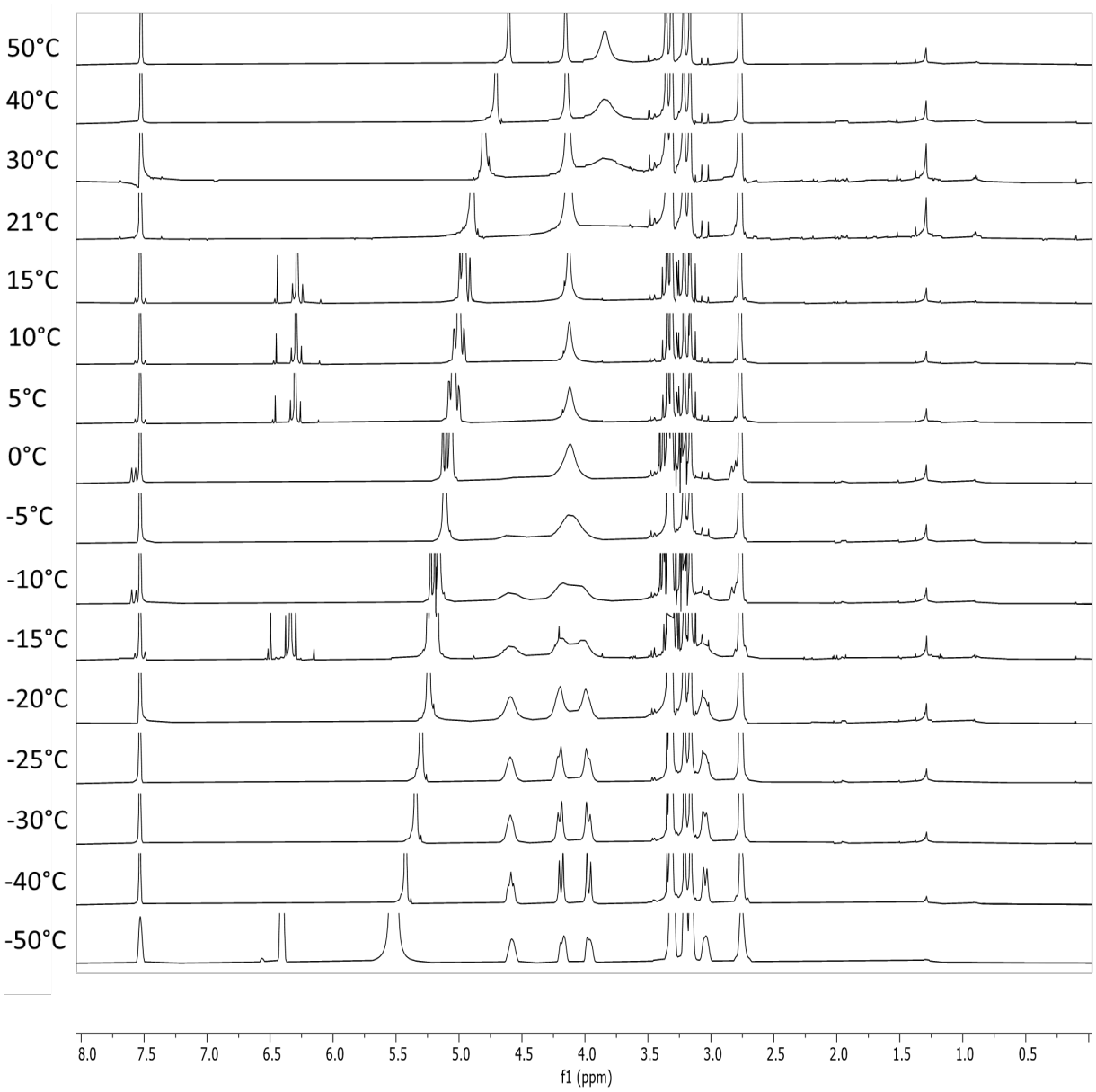

Figure S2. Annotated Stacked ^{1}H VT-NMR Spectra of $\mathbf{G^{NNMe}}$. The resonances corresponding to α are highlighted with red with a black border. The resonances corresponding to C are highlighted with blue without a border. The inlet highlights the temperatures around coalescence for C, with the resonances denoted by blue squares with a black border. The first spectrum post coalescence is denoted with the T_c in the respective resonance's color.

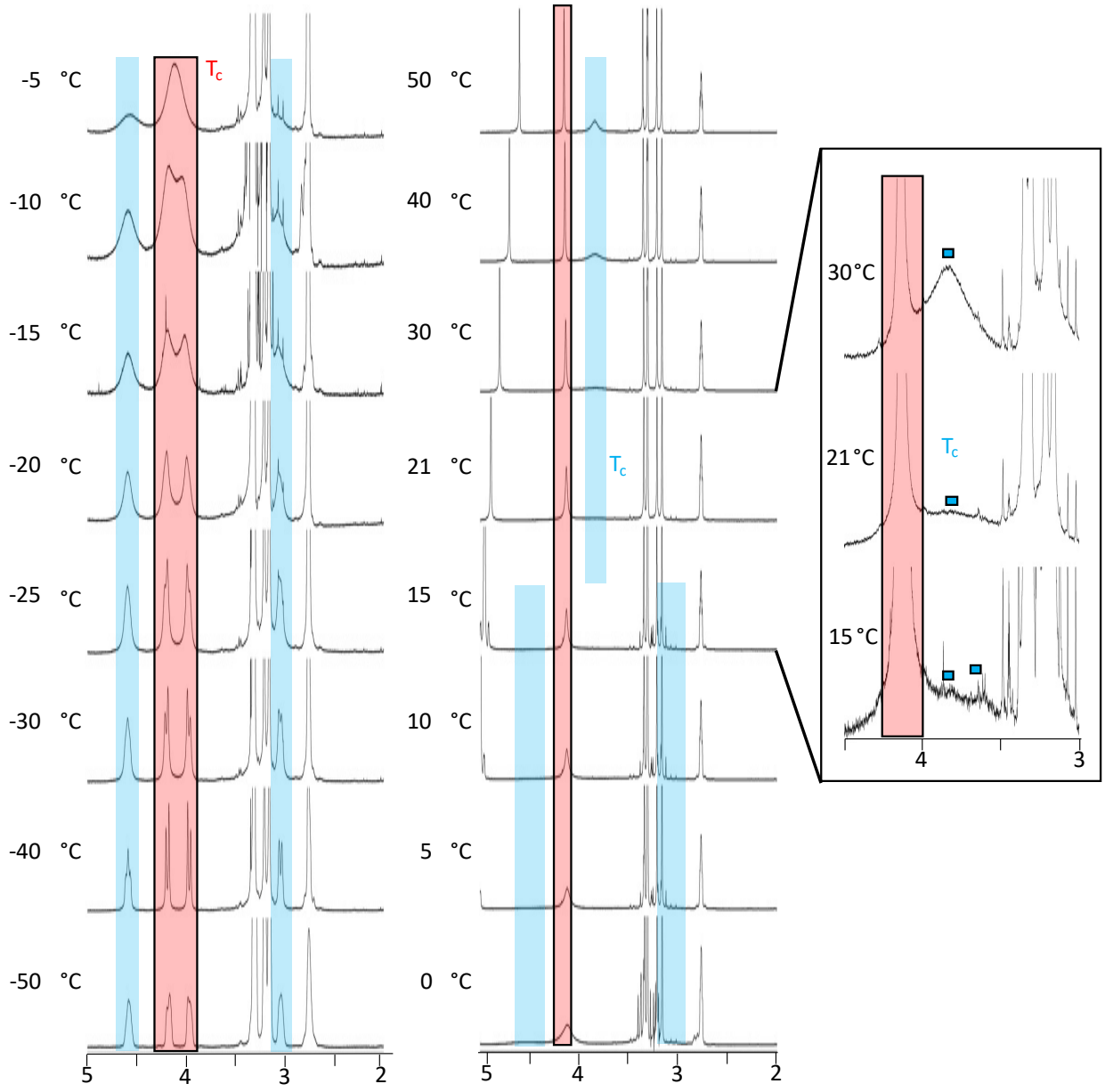

Figure S3. Chemical Shift Dependence on Temperature for $\mathbf{G}^{\mathbf{NNMe}}$.

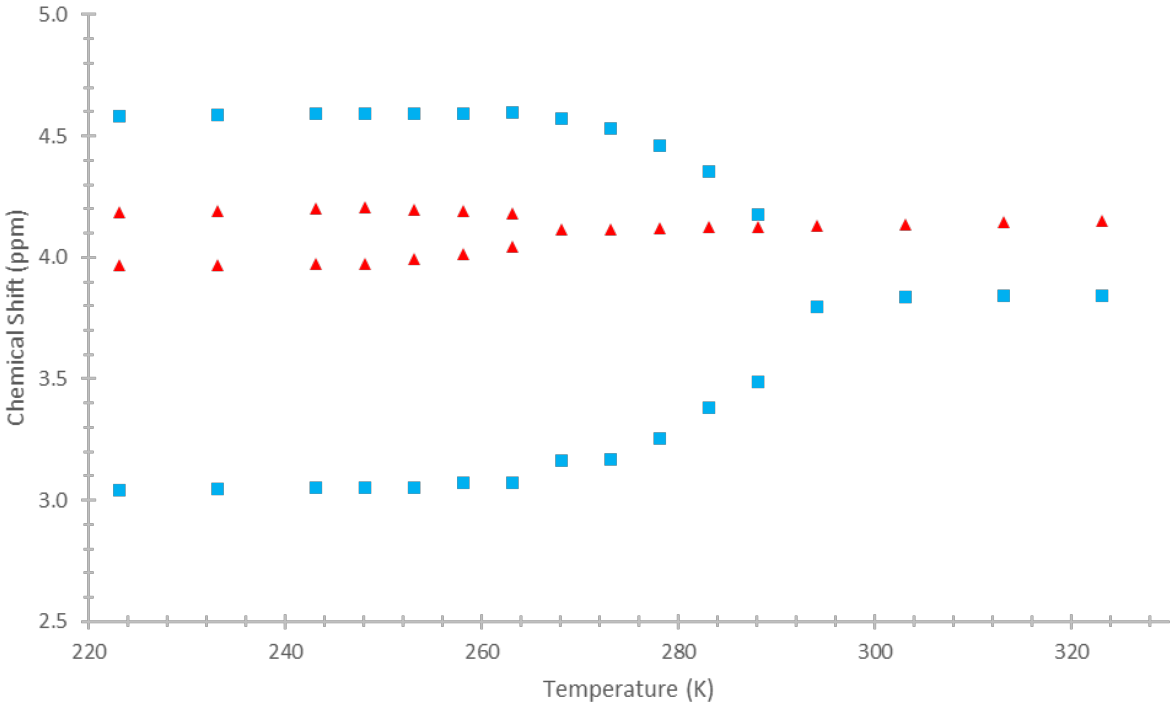

Figure S4. Log_{10} of the Difference in Chemical Shift with Temperature for $\mathbf{G}^{\mathbf{NNMe}}$. Lines are derived from the linear sections of the graph.

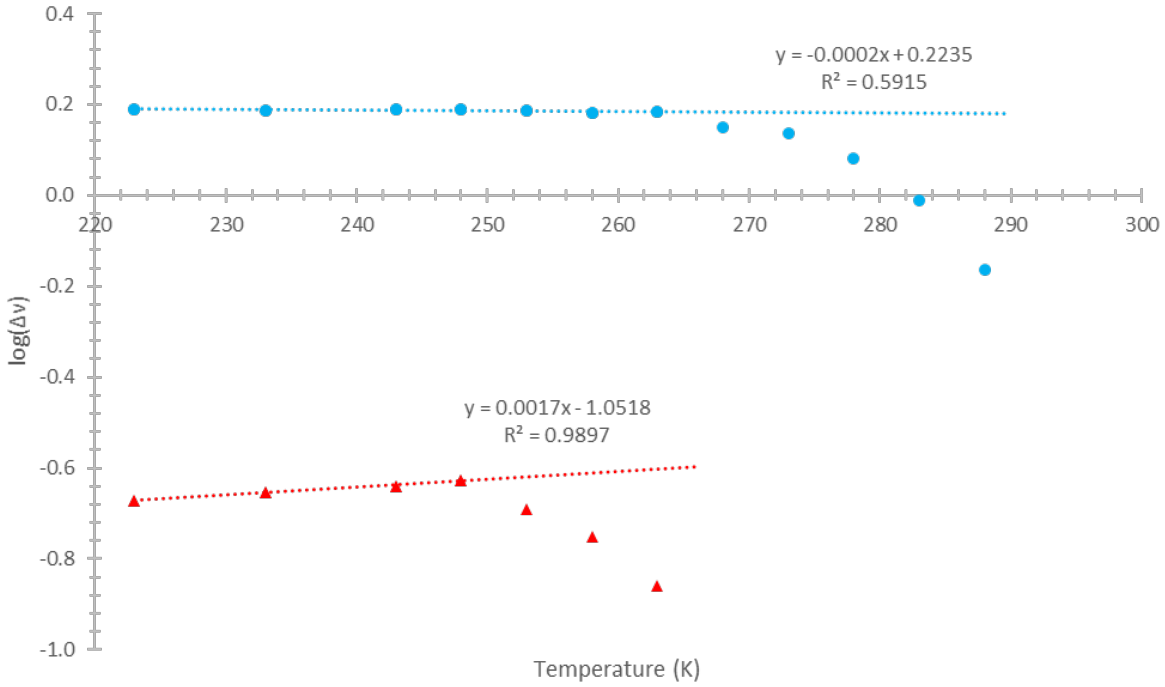

Table S4. Chemical shift and Δν dependence on temperature for $\mathbf{G^{NNMe}}$.

T (K)	α				C			
	Chemical Shift (ppm)		Δν (ppm)	log(Δν)	Chemical Shift (ppm)		Δν (ppm)	log(Δν)
323	4.1523	-	-	-	3.8412	-	-	-
313	4.1440	-	-	-	3.8397	-	-	-
303	4.1355	-	-	-	3.8351	-	-	-
294	4.1286	-	-	-	3.7979	-	-	-
288	4.1273	-	-	-	4.1740	3.4870	0.6870	-0.1630
283	4.1236	-	-	-	4.3560	3.3833	0.9727	-0.0120
278	4.1204	-	-	-	4.4580	3.2542	1.2038	0.0806
273	4.1181	-	-	-	4.5334	3.1678	1.3656	0.1353
268	4.1151	-	-	-	4.5730	3.1646	1.4084	0.1487
263	4.1809	4.0425	0.1384	-0.8589	4.5961	3.0708	1.5253	0.1834
258	4.1920	4.0150	0.1770	-0.7520	4.5900	3.0714	1.5186	0.1814
253	4.1965	3.9931	0.2034	-0.6916	4.5906	3.0537	1.5369	0.1866
248	4.2080	3.9721	0.2359	-0.6273	4.5926	3.0509	1.5417	0.1880
243	4.2015	3.9726	0.2289	-0.6404	4.5922	3.0500	1.5422	0.1881
233	4.1911	3.9693	0.2218	-0.6540	4.5873	3.0460	1.5413	0.1879
223	4.1840	3.9710	0.2130	-0.6716	4.5831	3.0394	1.5437	0.1886

Table S5. Relevant variables for the determination of $\Delta G^{\ddagger}$ for $\mathbf{G^{NNMe}}$.

	T_c (K)	log(Δν)	Δν@Tc (ppm)	k (MHz)	$\Delta G^{\ddagger}$ (kcal/mol)
α	265.5	-0.5993	0.2516	279.4	12.51
C	291	0.1795	1.5120	1679.0	12.73
				Average	12.62

Figure S5. DNMR traces for α and the respective fit for C for $\mathbf{G^{NNMe}}$. The original spectra are shown in black, while the simulated spectra are shown in green or mauve.

Temperature	k_α	k_C @ k_α
-40°C	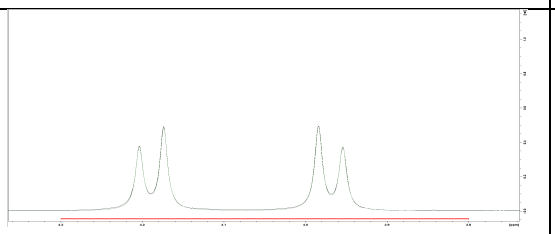	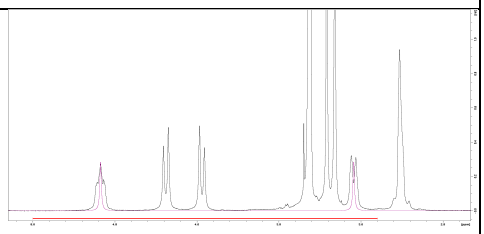
-30°C	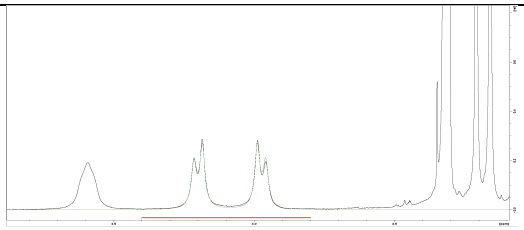	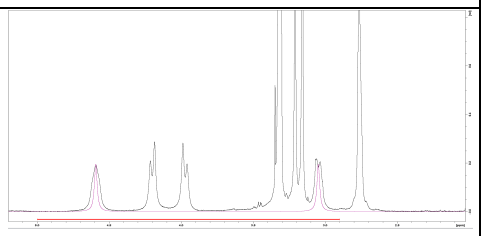
-25°C	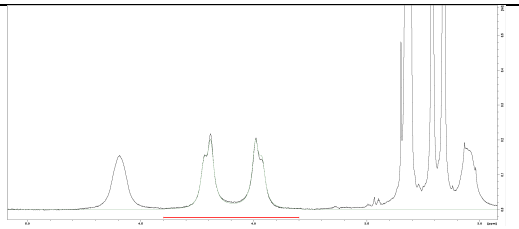	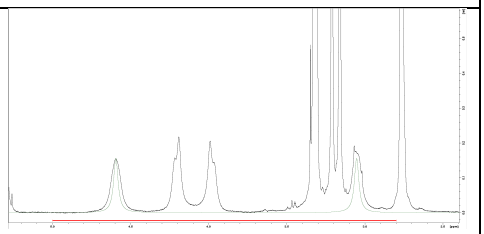
-20°C	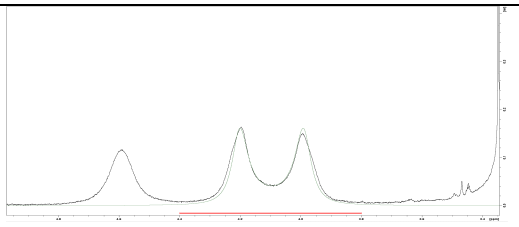	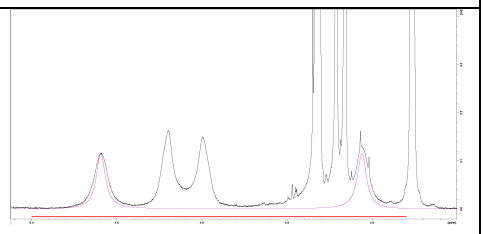
-15°C	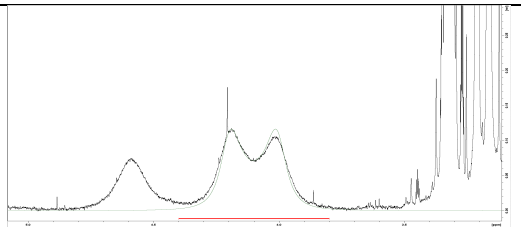	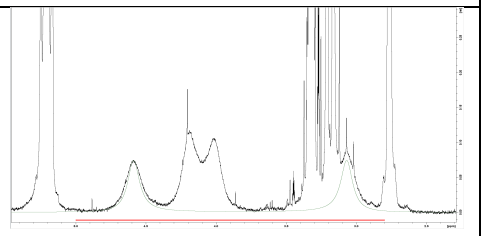
-10°C	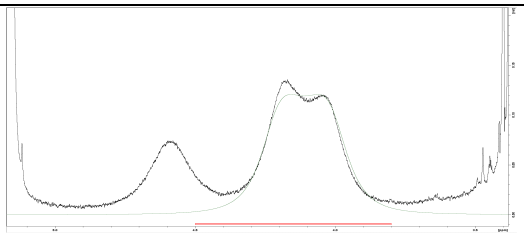	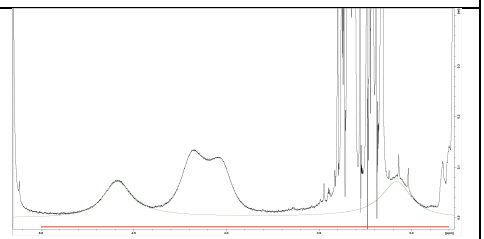

Figure S6. Thermodynamics Derived from DNMR for $\mathbf{G}^{\mathbf{NNMe}}$. a) Temperature dependent rate constant for the selected temperatures. b) Enthalpy, entropy, and free energy calculated from the Arrhenius and Eyring plots. c) The Arrhenius plot for $\mathbf{G}^{\mathbf{NNMe}}$. d) The Eyring plot for $\mathbf{G}^{\mathbf{NNMe}}$.

a)

T (°C)	T (K)	1/T	k	ln(k)	ln(k/T)
-40	233.15	0.00429	1.0565	0.05493	-5.397
-30	243.15	0.00411	3.9579	1.376	-4.118
-25	248.15	0.00403	22.5488	3.116	-2.398
-20	253.15	0.00395	68.3431	4.225	-1.309
-15	258.15	0.00387	127.2810	4.846	-1.001
-10	263.15	0.00380	275.7020	5.619	0.04660

b)

Method	$\Delta H^{\ddagger}$	$\Delta S^{\ddagger}$	$\Delta G^{\ddagger}$
ln(k) vs 1/T	23.32	0.041	12.51
ln(k/T) vs 1/T	22.84	0.040	12.31

c)

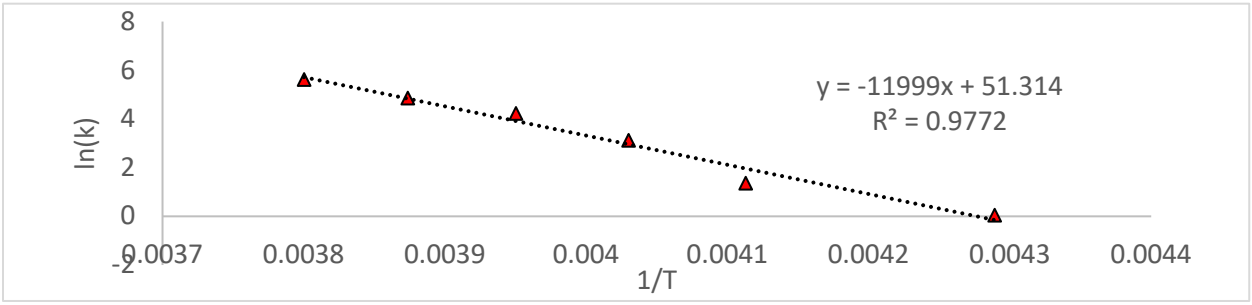

d)

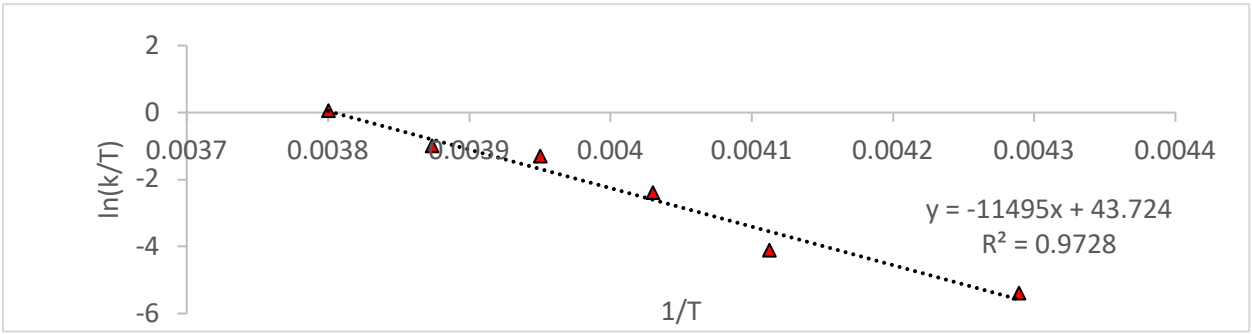

Figure S7. Stacked ^{1}H VT-NMR Spectra of $\mathbf{G}^{\mathbf{NNEt}}$.

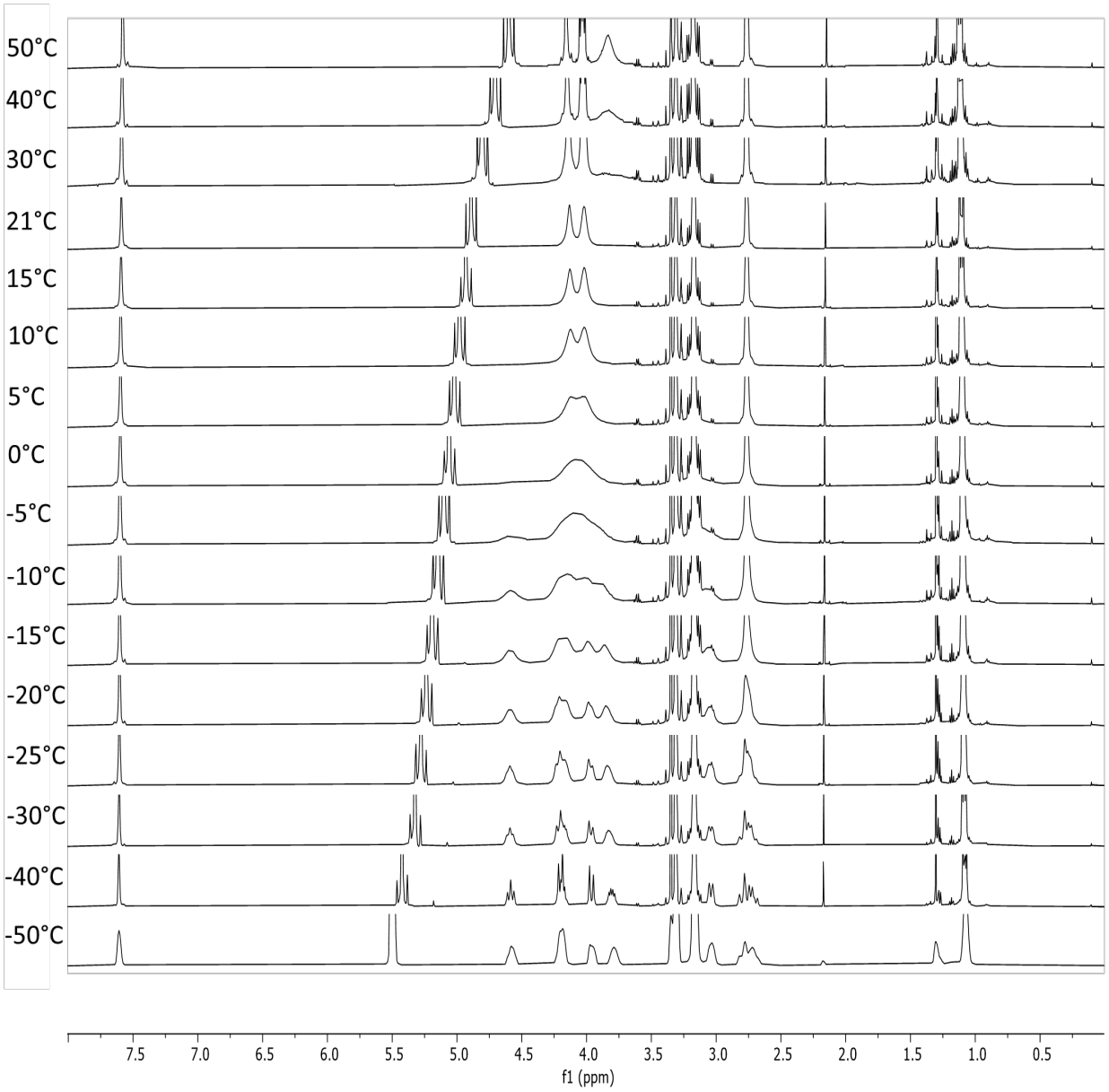

Figure S8. Annotated Stacked ^{1}H VT-NMR Spectra of $\mathbf{G}^{\mathbf{NNEt}}$. The resonances corresponding to α are highlighted with red with a black border. The resonances corresponding to C are highlighted with blue without a border. The resonances corresponding to a are highlighted with green with a dashed border. The inlet highlights the temperatures around coalescence for C, with the resonances denoted by blue squares with a black border. The first spectrum post coalescence is denoted with the T_c in the respective resonance's color.

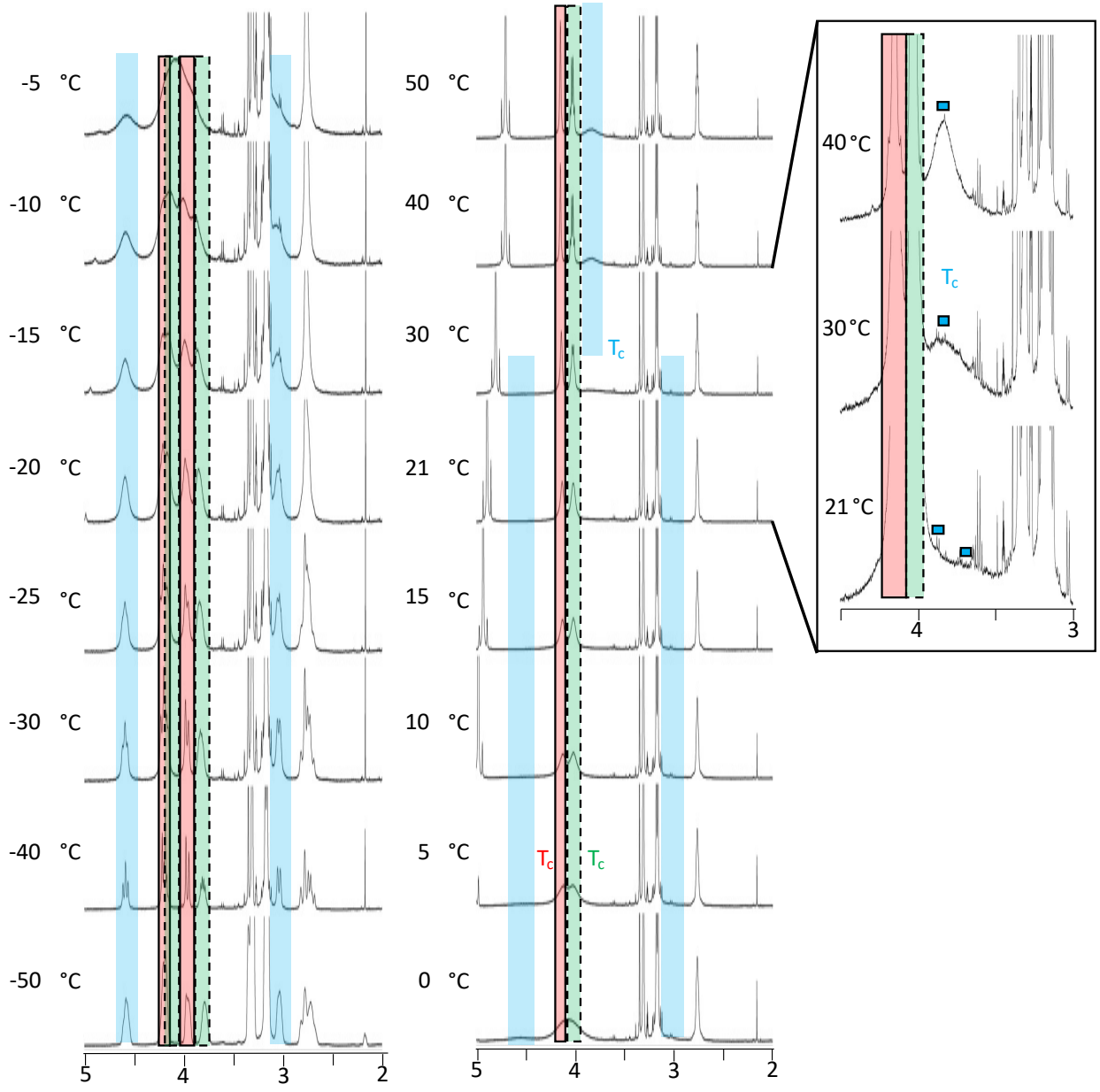

Figure S9. Chemical Shift Dependence on Temperature for $\mathbf{G}^{\mathbf{NNEt}}$.

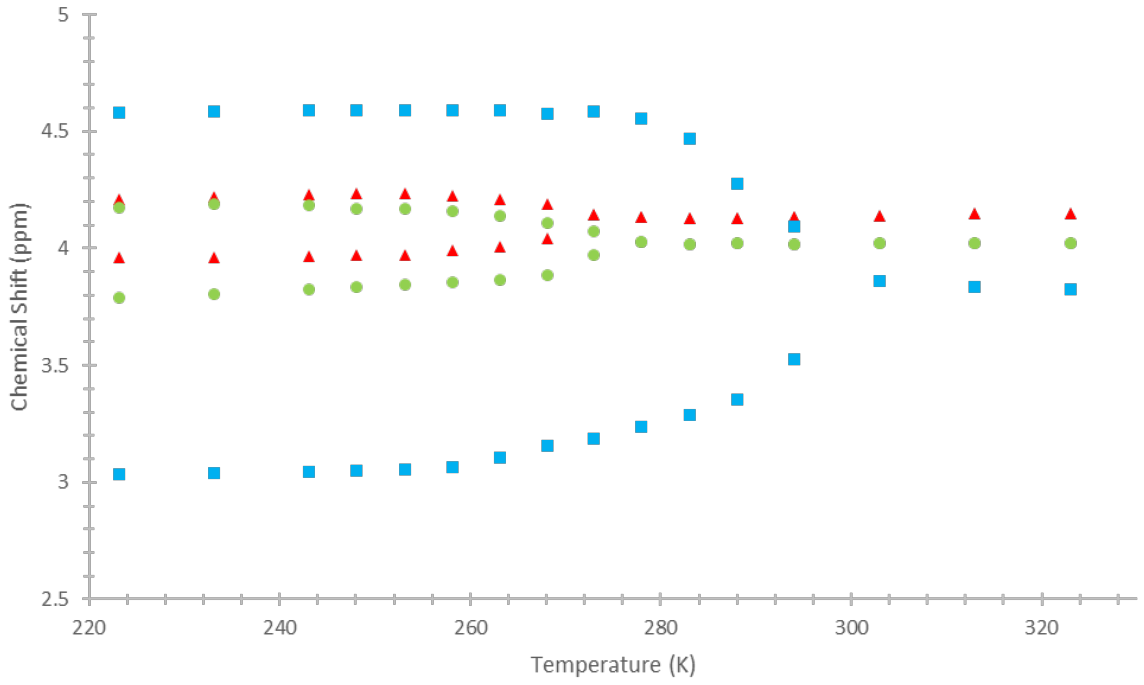

Figure S10. Log10 of the Difference in Chemical Shift with Temperature for $\mathbf{G}^{\mathbf{NNEt}}$. Lines are derived from the linear sections of the graph.

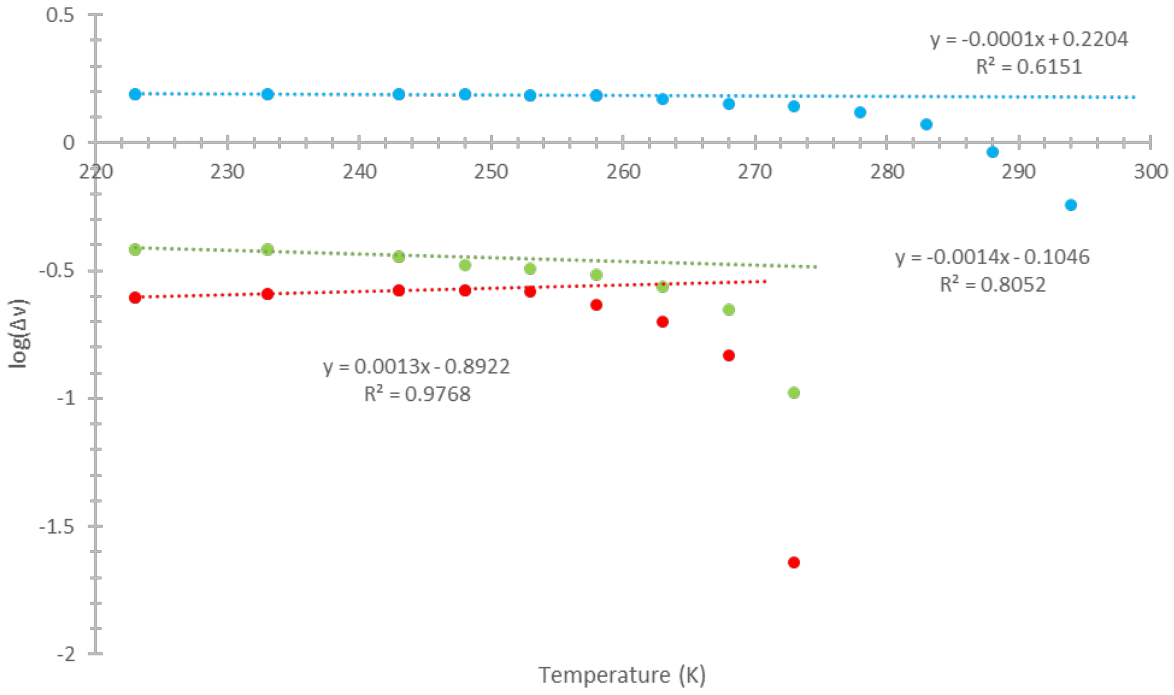

Table S6. Chemical Shift and Δv Dependence on Temperature for $\mathbf{G^{NNEt}}$.

	α				C				a			
T (K)	Chemical Shift (ppm)		Δv (ppm)	log(Δv)	Chemical Shift (ppm)		Δv (ppm)	log(Δv)	Chemical Shift (ppm)		Δv (ppm)	log(Δv)
323	4.1490	4.1490	-	-	3.8268	3.82680	-	-	4.0214	4.0214	-	-
313	4.1491	4.1491	-	-	3.8340	3.8340	-	-	4.0215	4.0215	-	-
303	4.1403	4.1403	-	-	3.8610	3.8610	-	-	4.0235	4.0235	-	-
294	4.1330	4.1330	-	-	4.0930	3.5240	0.5690	-0.2449	4.0197	4.0197	-	-
288	4.1300	4.1300	-	-	4.2750	3.3519	0.9231	-0.0348	4.0210	4.0210	-	-
283	4.1300	4.1300	-	-	4.4680	3.2887	1.1793	0.0716	4.0184	4.0184	-	-
278	4.1350	4.1350	-	-	4.5530	3.2390	1.3140	0.1186	4.0250	4.0250	-	-
273	4.1420	4.1190	-	-	4.5830	3.1868	1.3962	0.1449	4.0750	3.9700	0.1050	-0.9788
268	4.1900	4.0420	0.0230	-1.6383	4.5723	3.1554	1.4169	0.1513	4.1090	3.8860	0.2230	-0.6517
263	4.2080	4.0080	0.2000	-0.6990	4.5880	3.1051	1.4829	0.1711	4.1380	3.8640	0.2740	-0.5622
258	4.2240	3.9920	0.2320	-0.6345	4.5888	3.0624	1.5264	0.1837	4.1600	3.8560	0.3040	-0.5171
253	4.2340	3.9720	0.2620	-0.5817	4.5910	3.0528	1.5382	0.1870	4.1690	3.8460	0.3230	-0.4908
248	4.2370	3.9710	0.2660	-0.5751	4.5922	3.0494	1.5428	0.1883	4.1680	3.8340	0.3340	-0.4763
243	4.2314	3.9661	0.2653	-0.5763	4.5911	3.0446	1.5465	0.1894	4.1864	3.8260	0.3604	-0.4432
233	4.2177	3.9619	0.2558	-0.5921	4.5853	3.0397	1.5456	0.1891	4.1879	3.8057	0.3822	-0.4177
223	4.2120	3.9640	0.2480	-0.6056	4.5810	3.0340	1.5470	0.1895	4.1730	3.7890	0.3840	-0.4157

Table S7. Relevant Variables for the Determination of $\Delta G^{\ddagger}$ for $\mathbf{G^{NNEt}}$.

	T_c (K)	log(Δv)	Δv@T_c (ppm)	k (MHz)	$\Delta G^{\ddagger}$ (kcal/mol)
α	275.5	-0.5373	0.2902	322.3	12.92
C	298.5	0.1804	1.5150	1682.6	13.07
a	275.5	-0.4841	0.3280	364.4	12.85
				Average	12.95

Figure S11. DNMR Traces for α and the Respective Fit for C for $\mathbf{G^{NNEt}}$. The original spectra are shown in black, while the simulated spectra are shown in green or mauve.

Temperature	k_α	k_C @ k_α
-40°C	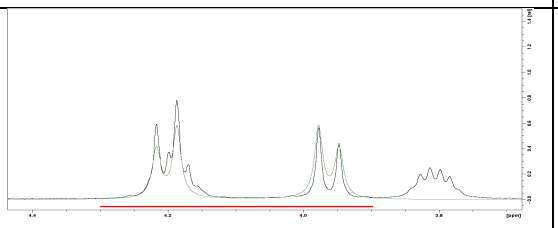	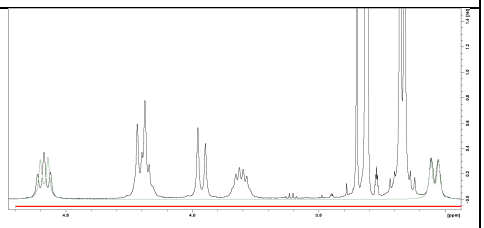
-30°C	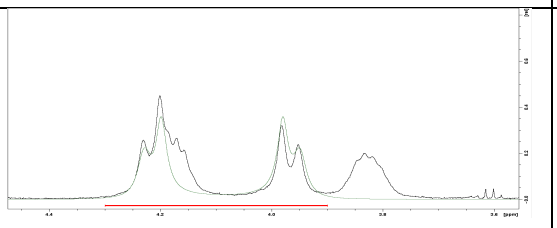	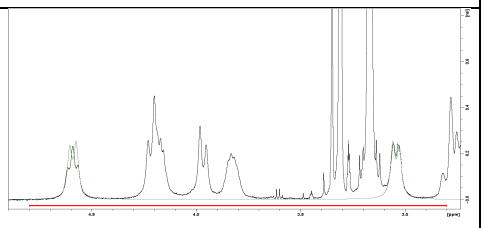
-25°C	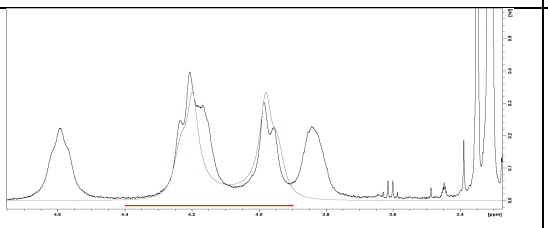	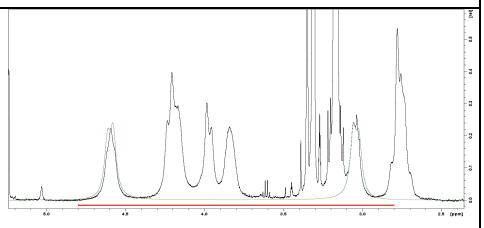
-20°C	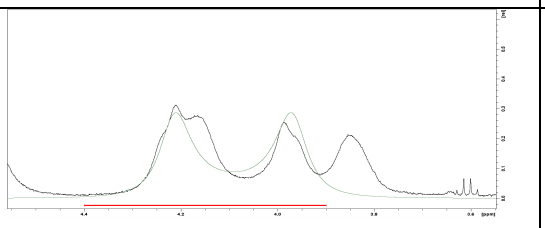	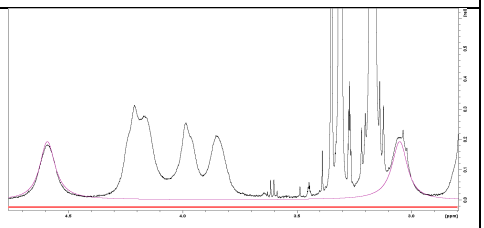
-15°C	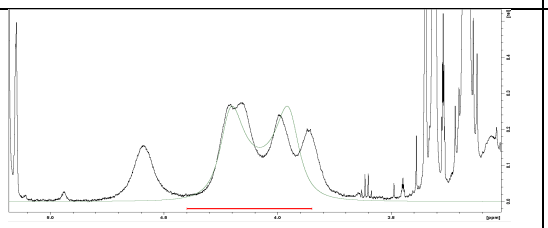	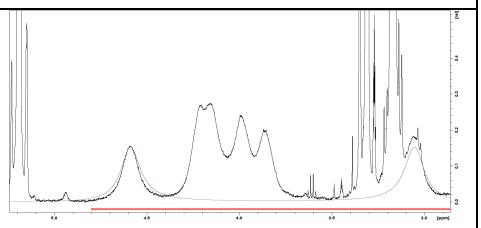
-10°C	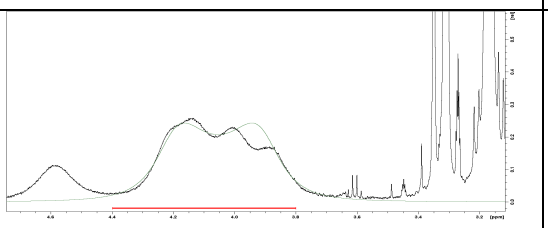	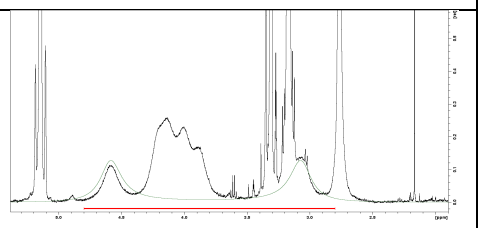

Figure S12. Thermodynamics Derived from DNMR for the α Resonance of $\mathbf{G^{NNEt}}$. a) Temperature dependent rate constant for the selected temperatures. b) Enthalpy, entropy, and free energy calculated from the Arrhenius and Eyring plots. c) The Arrhenius plot for α. d) The Eyring plot for α.

a)

T (°C)	T (K)	1/T	K	ln(k)	ln(k/T)
-40	233.15	0.00429	8.7957	2.174	-3.277
-30	243.15	0.00411	40.4429	3.700	-1.794
-25	248.15	0.00403	70.7230	4.259	-1.255
-20	253.15	0.00395	105.000	4.654	-0.880
-15	258.15	0.00387	168.5710	5.127	-0.426
-10	263.15	0.00380	274.1160	5.614	0.0408

b)

Method	$\Delta H^{\ddagger}$	$\Delta S^{\ddagger}$	$\Delta G^{\ddagger}$
ln(k) vs 1/T	13.11	0.00070	12.92
ln(k/T) vs 1/T	13.17	0.0031	12.32

c)

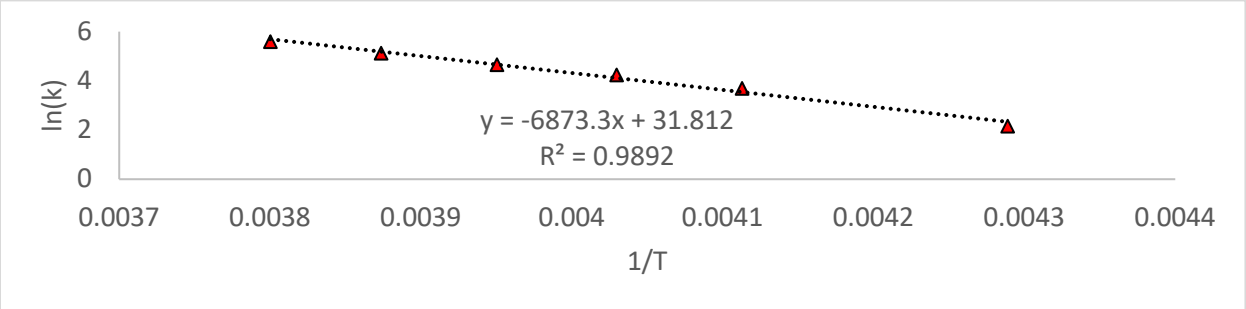

d)

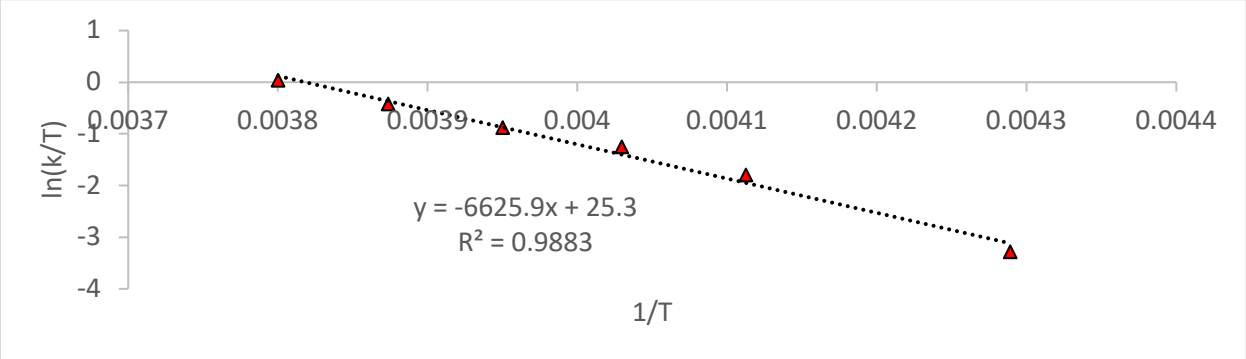

Figure S13. DNMR Traces for a and the Respective Fit for C for $\mathbf{G}^{\mathbf{NNEt}}$. The original spectra are shown in black, while the simulated spectra are shown in green or mauve.

Temperature	k_a	k_C @ k_a
-40°C	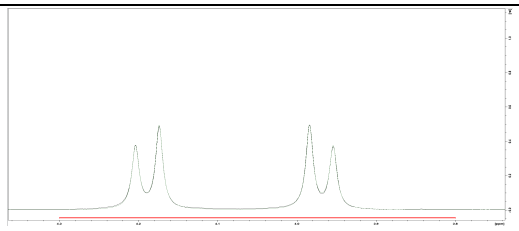	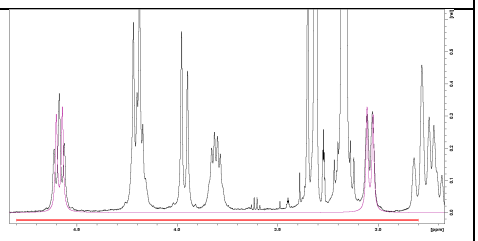
-30°C	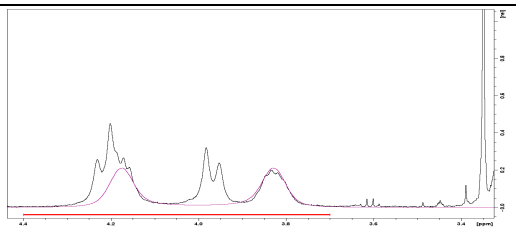	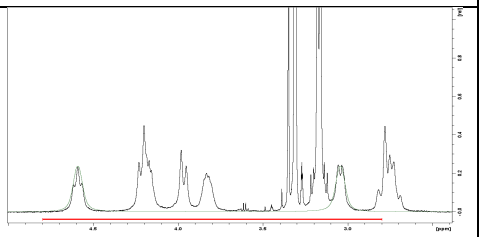
-25°C	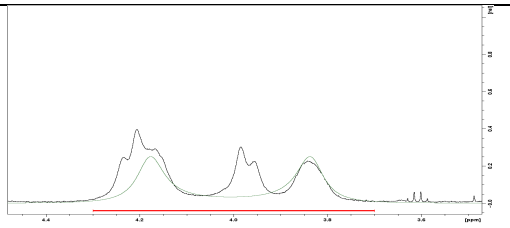	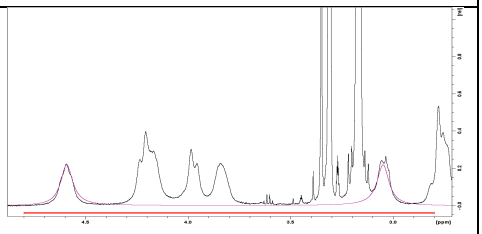
-20°C	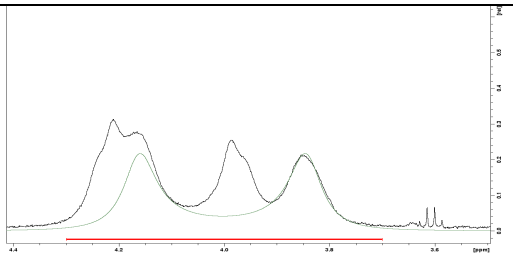	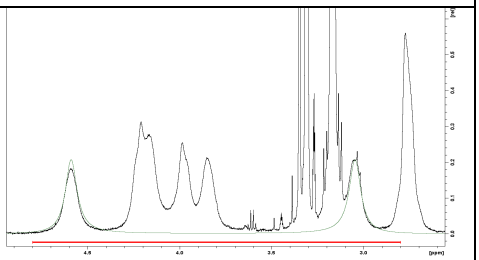
-15°C	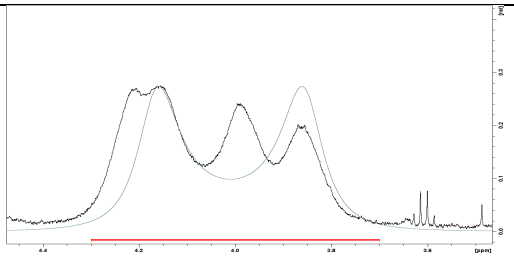	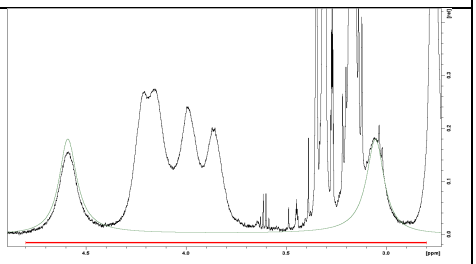
-10°C	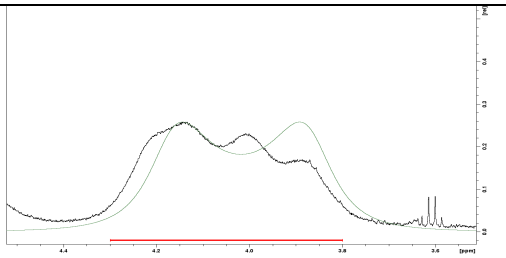	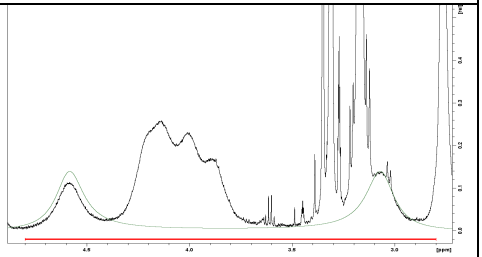

Figure S14. Thermodynamics Derived from DNMR for the a Resonance of $\mathbf{G^{NNEt}}$. a) Temperature dependent rate constant for the selected temperatures. b) Enthalpy, entropy, and free energy calculated from the Arrhenius and Eyring plots. c) The Arrhenius plot for a. d) The Eyring plot for a.

a)

T (°C)	T (K)	1/T	K	ln(k)	ln(k/T)
-40	233.15	0.004289	15.0000	2.708	-2.744
-30	243.15	0.004113	50.1210	3.914	-1.579
-25	248.15	0.00403	83.6348	4.426	-1.088
-20	253.15	0.00395	104.3380	4.648	-0.886
-15	258.15	0.003874	160.5000	5.078	-0.475
-10	263.15	0.0038	250.5000	5.523	-0.0493

b)

Method	$\Delta H^{\ddagger}$	$\Delta S^{\ddagger}$	$\Delta G^{\ddagger}$
ln(k) vs 1/T	10.54	-0.0084	12.85
ln(k/T) vs 1/T	10.59	-0.0070	12.52

c)

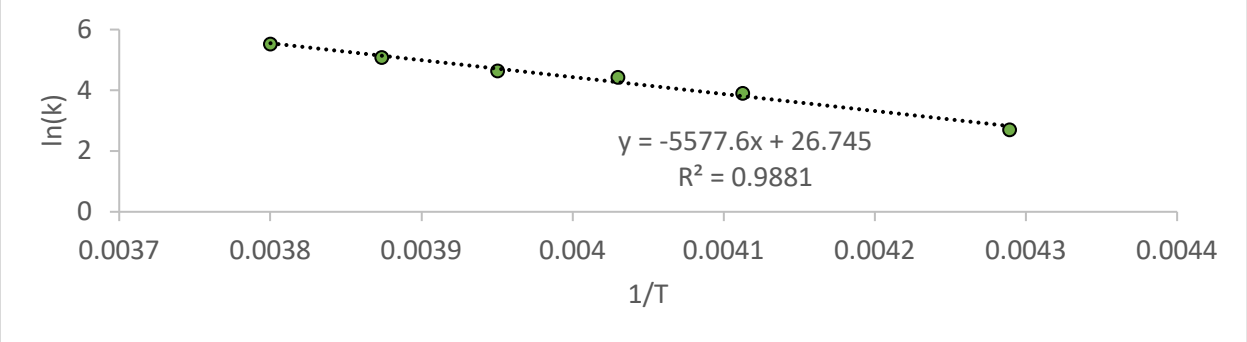

d)

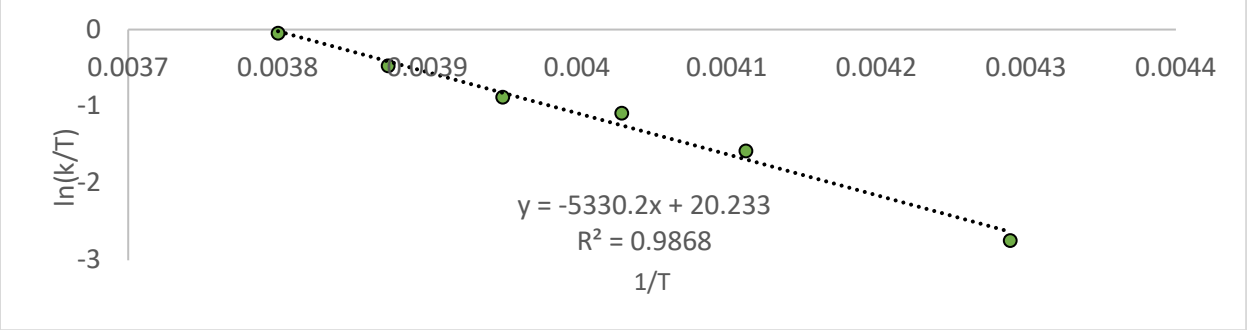

Figure S15. Stacked ^{1}H VT-NMR Spectra of $\mathbf{G^{NNiPr}}$.

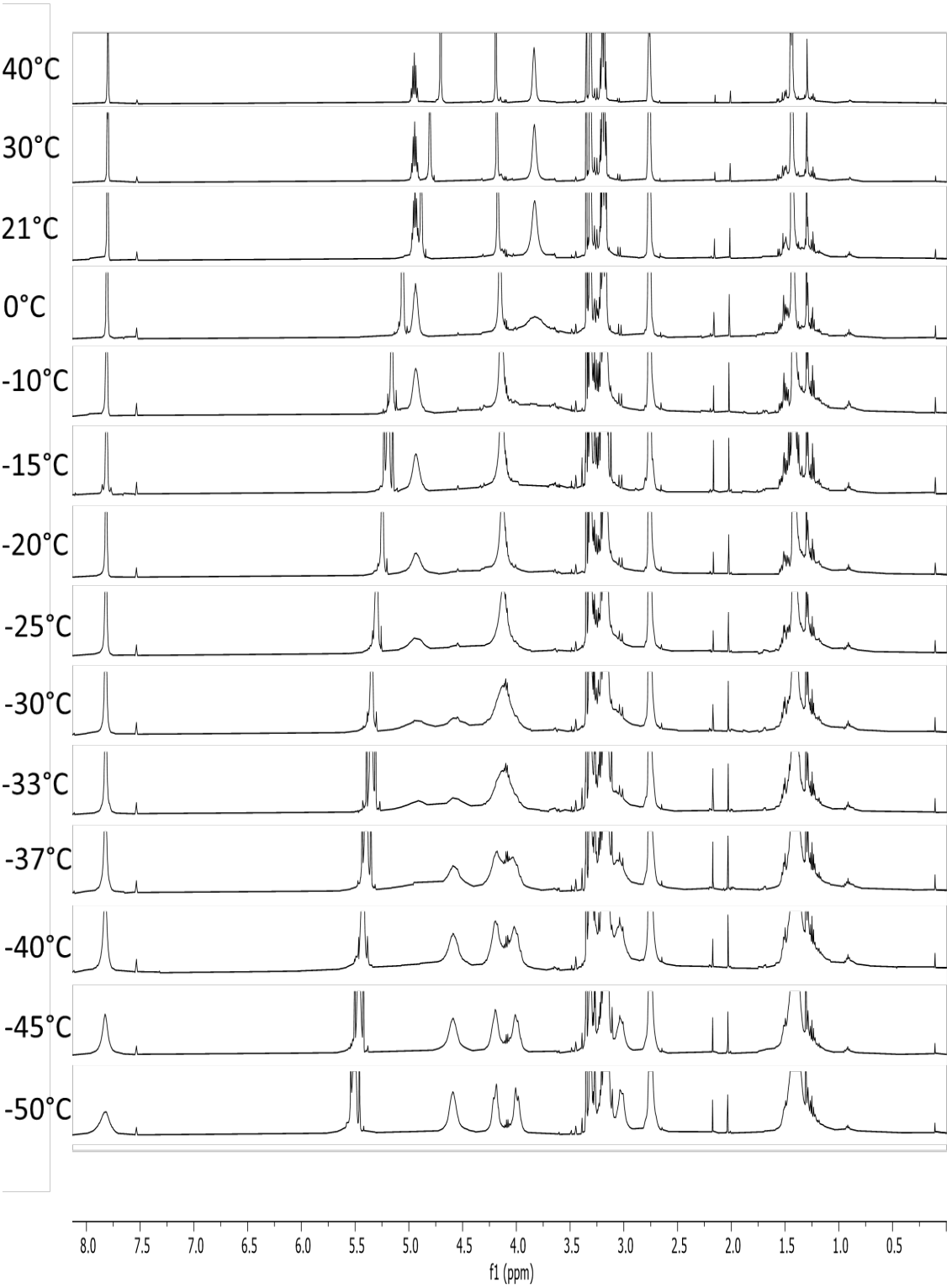

Figure S16. Annotated Stacked ^{1}H VT-NMR Spectra of **G^{NNiPr}**. The resonances corresponding to α are highlighted with red with a black border. The resonances corresponding to C are highlighted with blue without a border. The resonances corresponding to a are highlighted with green with a dashed border. The inlet highlights the temperatures around coalescence for C, with the resonances denoted by blue squares with a black border. The first spectrum post coalescence is denoted with the T_c in the respective resonance's color.

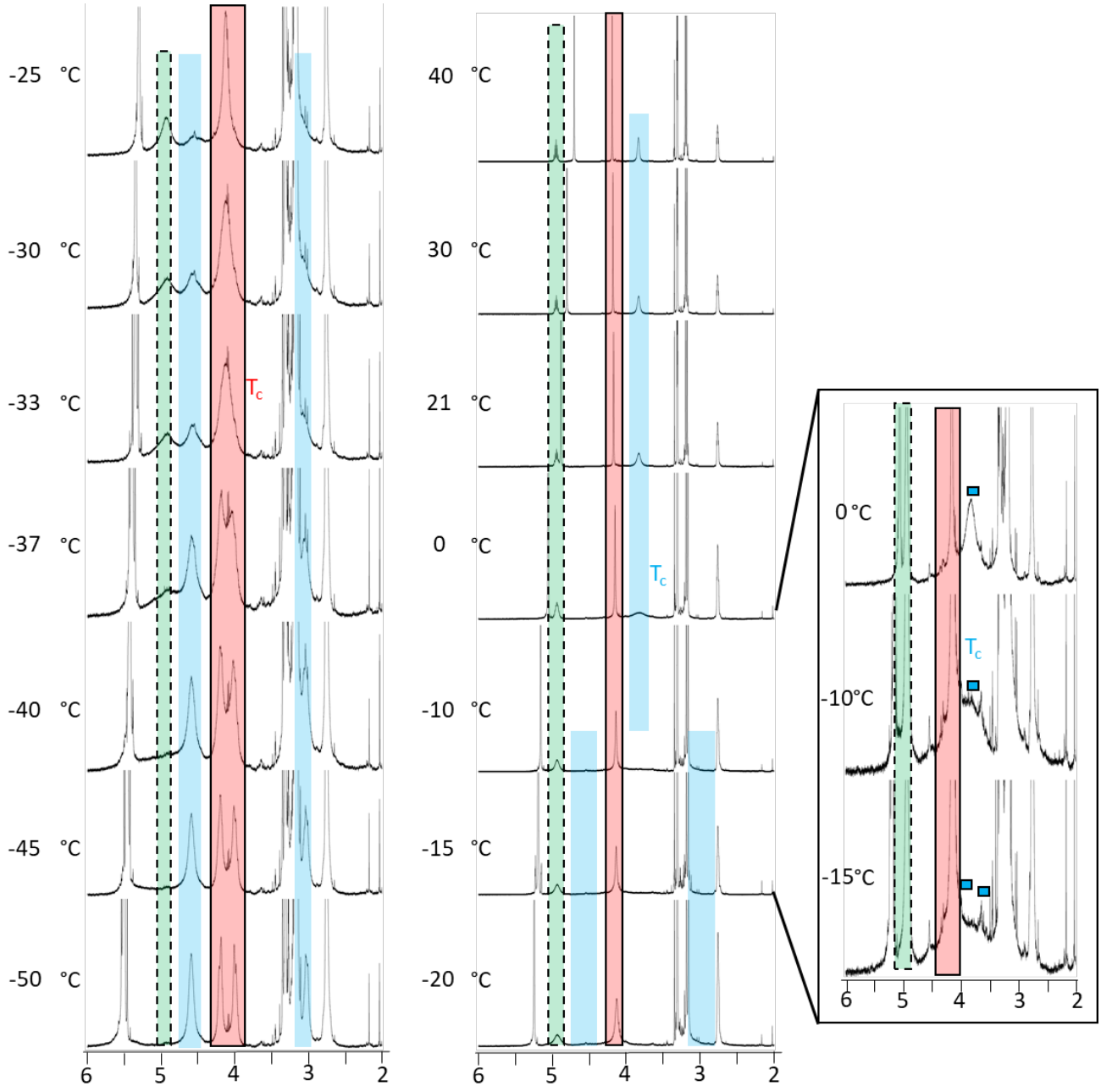

Figure S17. Chemical Shift Dependence on Temperature for $\mathbf{G}^{\mathbf{NNiPr}}$.

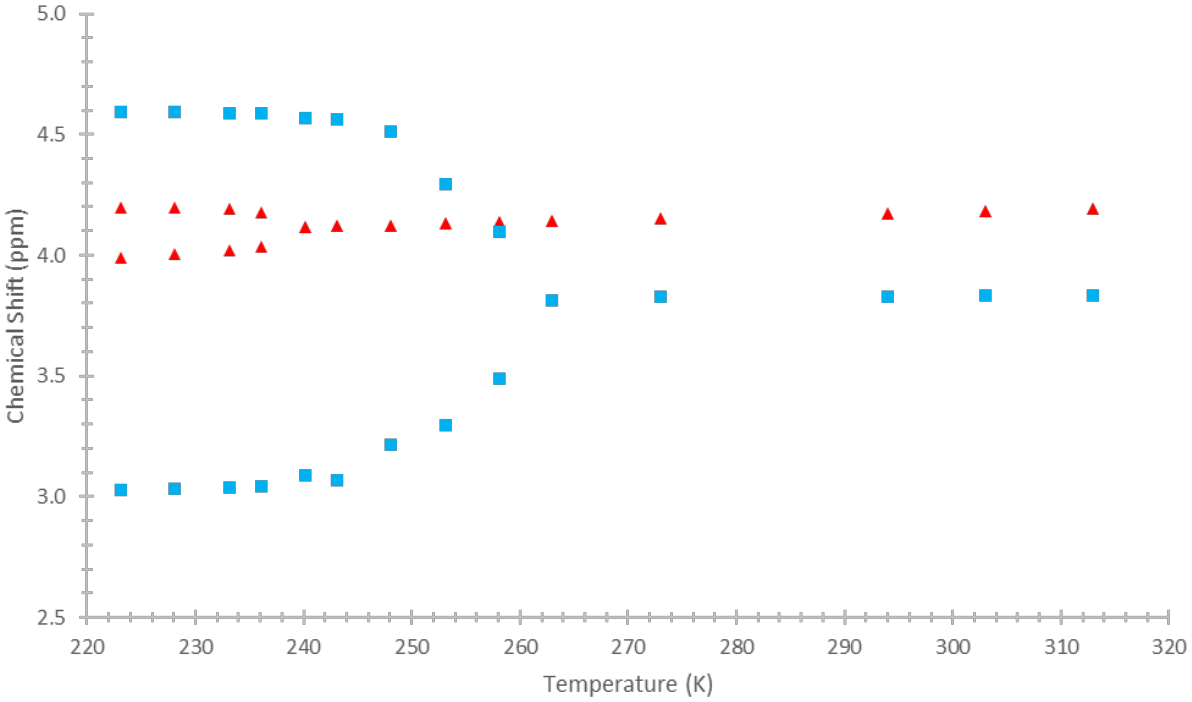

Figure S18. Log10 of the Difference in Chemical Shift with Temperature for $\mathbf{G}^{\mathbf{NNiPr}}$. Lines are derived from the linear sections of the graph.

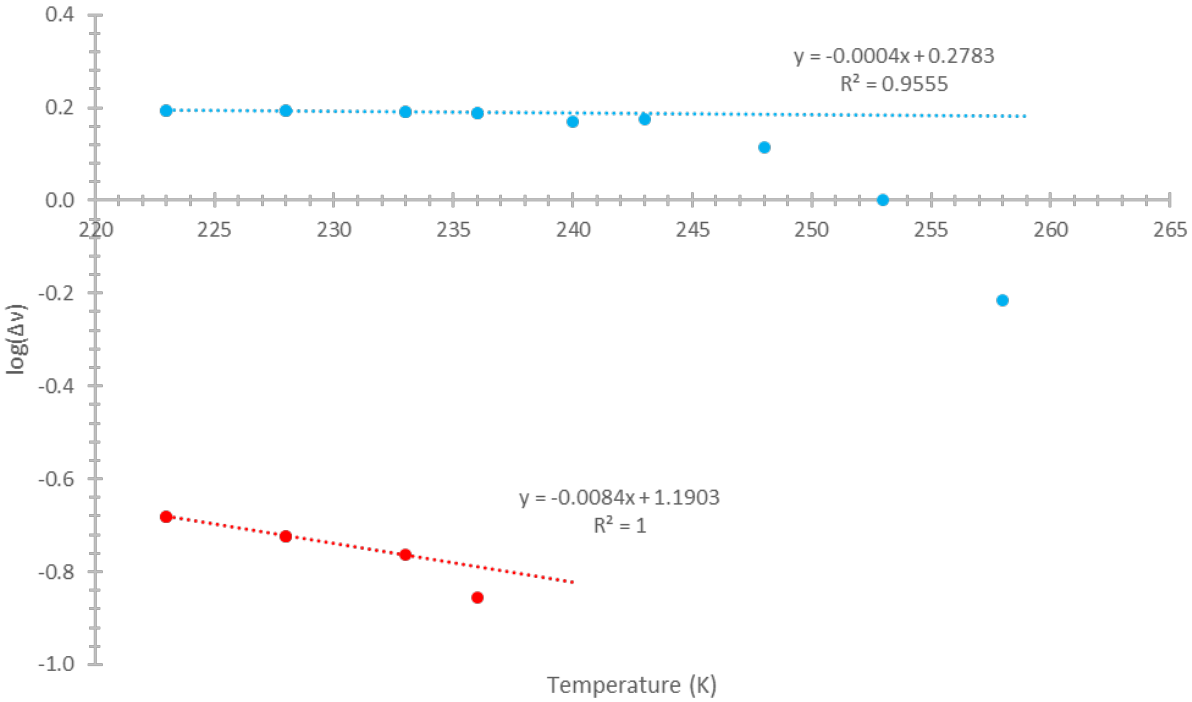

Table S8. Chemical Shift and Δv Dependence on Temperature for $\mathbf{G^{NNiPr}}$.

	α				C			
T (K)	Chemical Shift (ppm)		Δv (ppm)	log(Δv)	Chemical Shift (ppm)		Δv (ppm)	log(Δv)
313	4.1903	4.1903	-	-	3.8350	3.8350	-	-
303	4.1804	4.1804	-	-	3.8318	3.8318	-	-
294	4.1716	4.1716	-	-	3.8294	3.8294	-	-
273	4.1518	4.1518	-	-	3.8260	3.8260	-	-
263	4.1397	4.1397	-	-	3.8142	3.8142	-	-
258	4.1359	4.1359	-	-	4.0953	3.4869	0.6084	-0.2158
253	4.1297	4.1297	-	-	4.2960	3.2948	1.0012	0.0005
248	4.1223	4.1223	-	-	4.5120	3.2129	1.2991	0.1136
243	4.1200	4.1200	-	-	4.5640	3.0650	1.4990	0.1758
240	4.1160	4.1160	-	-	4.5690	3.0900	1.4790	0.1700
236	4.1760	4.0362	0.1398	-0.8545	4.5880	3.0420	1.5460	0.1892
233	4.1903	4.0179	0.1724	-0.7635	4.5899	3.0389	1.5510	0.1906
228	4.1962	4.0069	0.1893	-0.7228	4.5930	3.0330	1.5600	0.1931
223	4.1973	3.9888	0.2085	-0.6809	4.5923	3.0293	1.5630	0.1940

Table S9. Relevant Variables for the Determination of $\Delta G^{\ddagger}$ for $\mathbf{G^{NNiPr}}$.

	T_c (K)	log(Δv)	Δv@T_c (ppm)	k (MHz)	$\Delta G^{\ddagger}$ (kcal/mol)
α	238	-0.8068	0.1560	173.3	11.39
C	260.5	0.1803	1.5140	1682.1	11.33
				Average	11.36

Figure S19. DNMR Traces for α and the Respective Fit for C for $\mathbf{G^{NNiPr}}$. The original spectra are shown in black, while the simulated spectra is shown in green or mauve.

Temperature	k_α	k_C @ k_α
-50°C	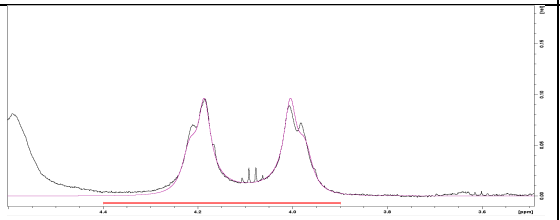	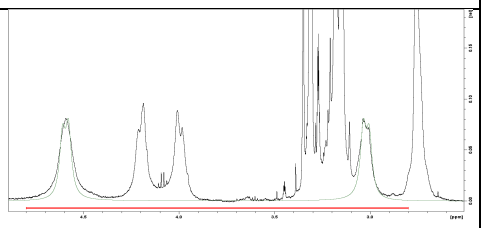
-45°C	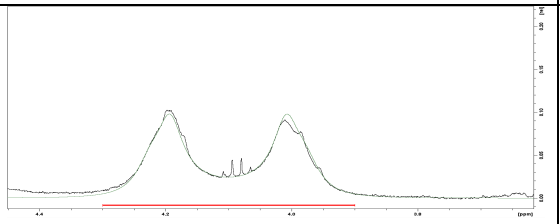	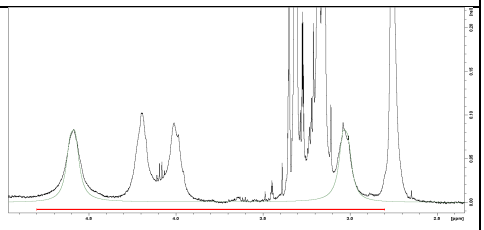
-40°C	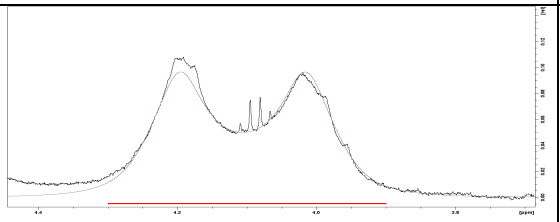	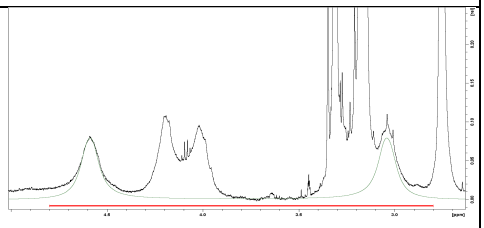
-37°C	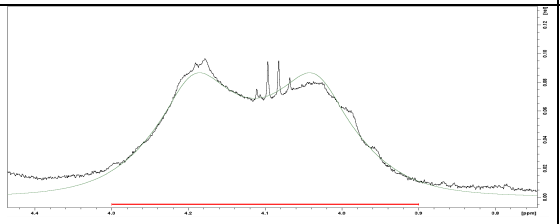	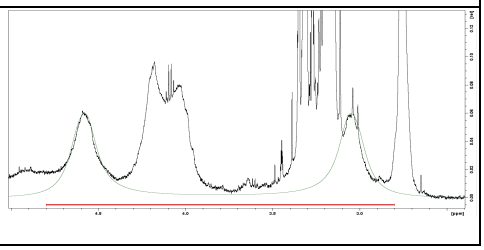

Figure S20. Thermodynamics Derived from DNMR for $\mathbf{G}^{\mathbf{NNiPr}}$. a) Temperature dependent rate constant for the selected temperatures. b) Enthalpy, entropy, and free energy calculated from the Arrhenius and Eyring plots. c) The Arrhenius plot for $\mathbf{G}^{\mathbf{NNiPr}}$. d) The Eyring plot for $\mathbf{G}^{\mathbf{NNiPr}}$.

a)

T (°C)	T (K)	1/T	K	ln(k)	ln(k/T)
-50	223.15	0.00448	56.5757	4.036	-1.372
-45	228.15	0.00438	82.8880	4.417	-1.013
-40	233.15	0.00429	141.6530	4.953	-0.498
-37	236.15	0.00424	222.2060	5.404	-0.0609

b)

Method	$\Delta H^{\ddagger}$	$\Delta S^{\ddagger}$	$\Delta G^{\ddagger}$
ln(k) vs 1/T	10.39	-0.0042	11.39
ln(k/T) vs 1/T	10.41	-0.0034	11.23

c)

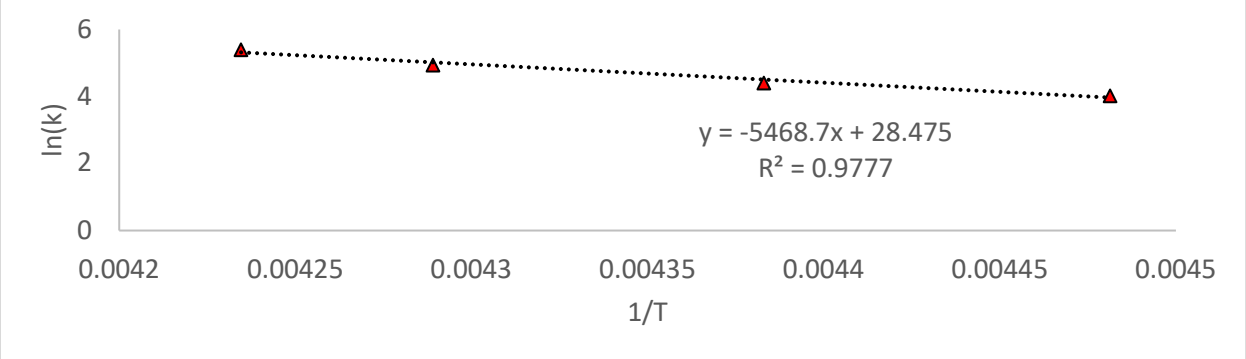

d)

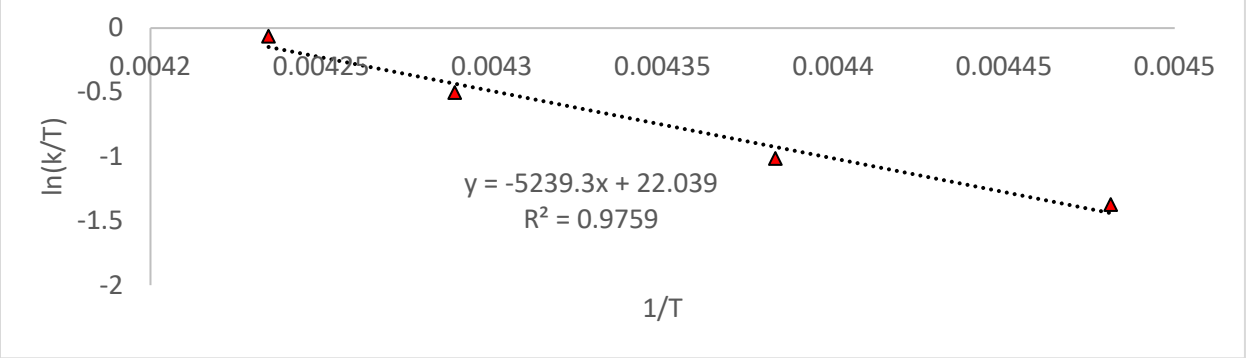

Figure S21. Stacked ^{1}H VT-NMR Spectra of $\mathbf{G^{NNBn}}$.

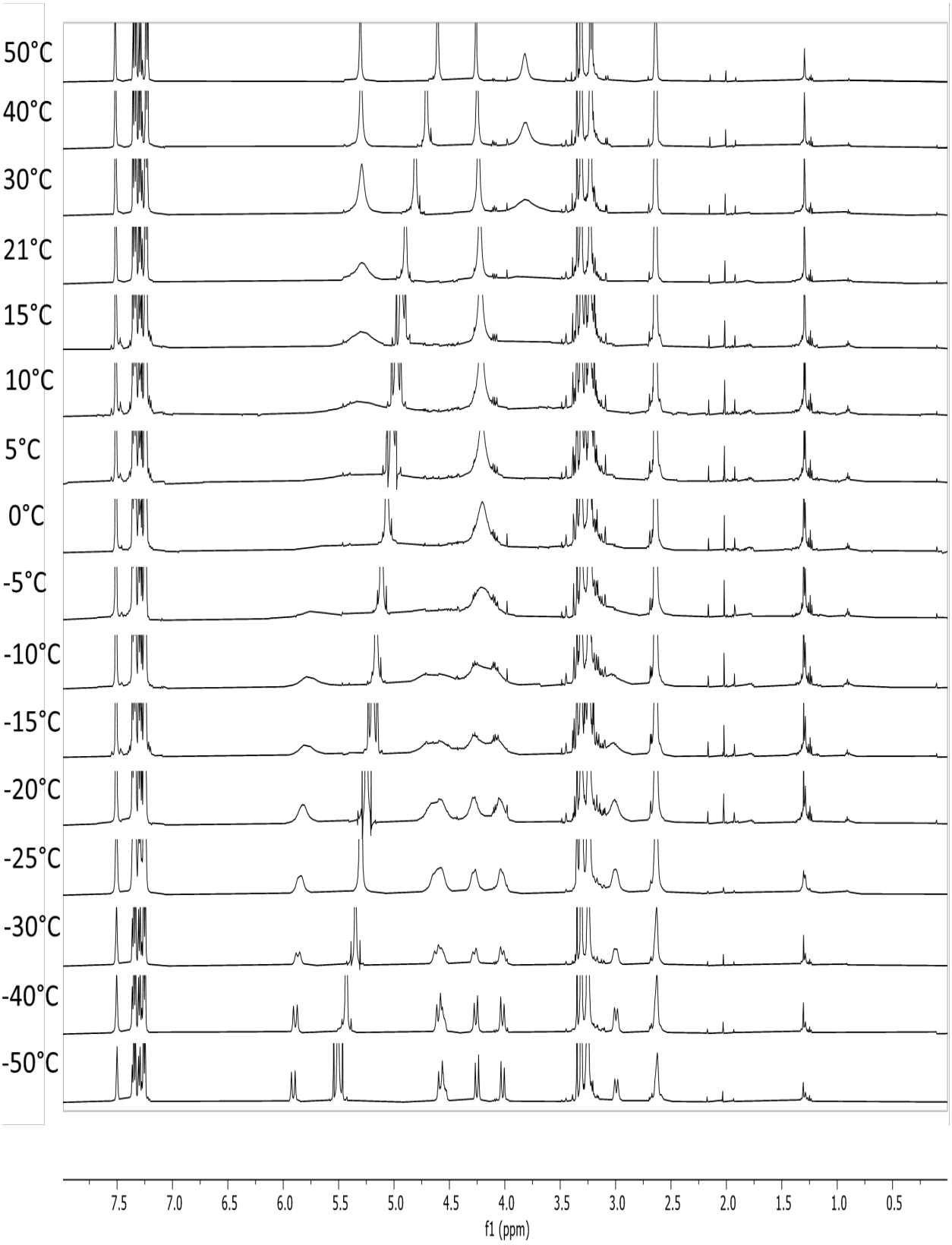

Figure S22. Annotated Stacked ^{1}H VT-NMR Spectra of **G^{NNBn}**. The resonances corresponding to α are highlighted with red with a black border. The resonances corresponding to C are highlighted with blue without a border. The resonances corresponding to a are highlighted with green with a dashed border. The inlet highlights the temperatures around coalescence for C, with the resonances denoted by blue squares with a black border. The first spectrum post coalescence is denoted with the T_c in the respective resonance's color.

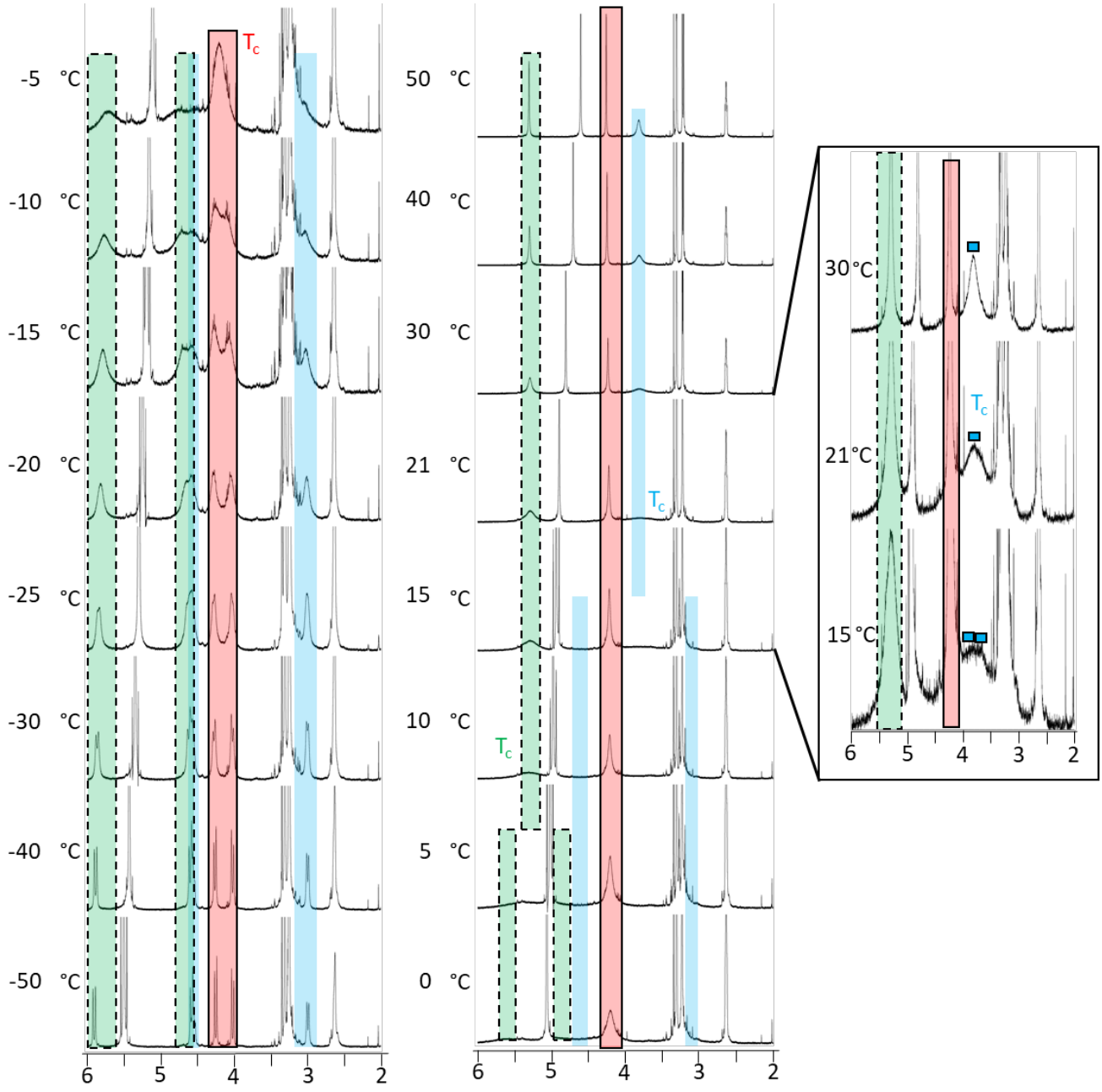

Figure S23. Chemical Shift Dependence on Temperature for $\mathbf{G^{NNBn}}$.

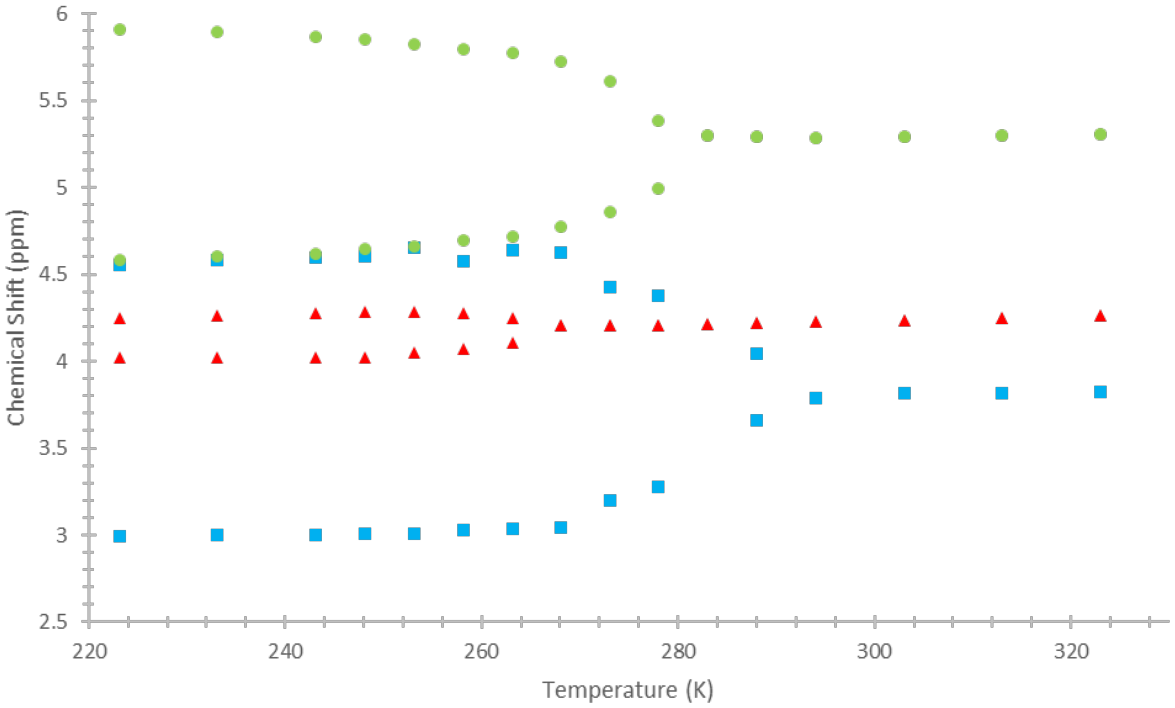

Figure S24. Log10 of the Difference in Chemical Shift with Temperature for $\mathbf{G^{NNBn}}$. Lines are derived from the linear sections of the graph.

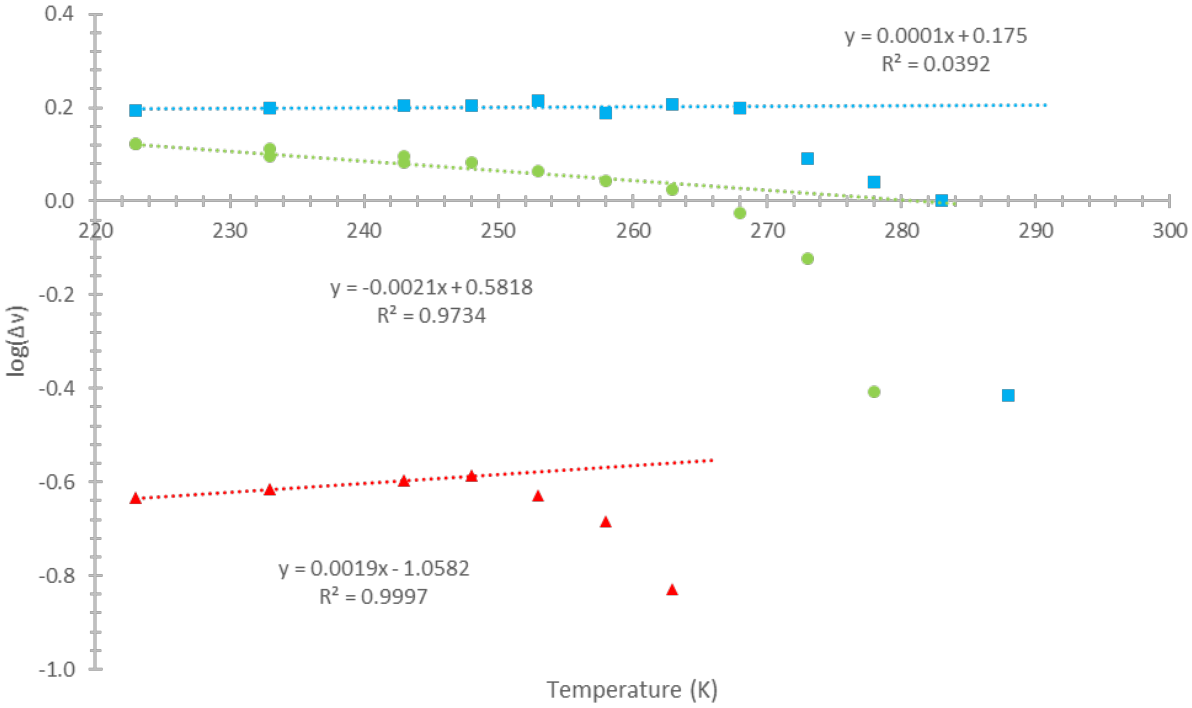

Table S10. Chemical Shift and Δv Dependence on Temperature for $\mathbf{G^{NNBn}}$.

	α				C				*N*CH2			
T (K)	Chemical Shift (ppm)		Δv (ppm)	log(Δv)	Chemical Shift (ppm)		Δv (ppm)	log(Δv)	Chemical Shift (ppm)		Δv (ppm)	log(Δv)
323	4.2601	4.2601	-	-	3.8202	3.8202	-	-	5.3041	5.3041	-	-
313	4.2491	4.2491	-	-	3.8144	3.8144	-	-	5.2981	5.2981	-	-
303	4.2372	4.2372	-	-	3.8152	3.8152	-	-	5.2921	5.2921	-	-
294	4.2253	4.2253	-	-	3.7903	3.7903	-	-	5.2876	5.2876	-	-
288	4.2196	4.2196	-	-	4.0430	3.6580	0.3850	-0.4145	5.2890	5.2890	-	-
283	4.2164	4.2164	-	-	-	-	-	-	5.3010	5.3010	-	-
278	4.2073	4.2073	-	-	4.3760	3.2751	1.1009	0.0417	5.3870	4.9962	0.3908	-0.4080
273	4.2049	4.2049	-	-	4.4291	3.1956	1.2335	0.0911	5.6110	4.8560	0.7550	-0.1221
268	4.2074	4.2074	-	-	4.6263	3.0424	1.5839	0.1997	5.7236	4.7770	0.9466	-0.0238
263	4.2517	4.1038	0.1479	-0.8300	4.6415	3.0356	1.6059	0.2057	5.7735	4.7142	1.0593	0.0250
258	4.2770	4.0700	0.2070	-0.6840	4.5730	3.0310	1.5420	0.1881	5.7960	4.6940	1.1020	0.0422
253	4.2817	4.0466	0.2351	-0.6287	4.6499	3.0085	1.6414	0.2152	5.8211	4.6590	1.1621	0.0652
248	4.2820	4.0230	0.2590	-0.5867	4.6022	3.0041	1.5981	0.2036	5.8516	4.6440	1.2076	0.0819
243	4.2749	4.0220	0.2529	-0.5971	4.5996	3.0010	1.5986	0.2037	5.8687	4.6194	1.2493	0.0967
233	4.2640	4.0216	0.2424	-0.6155	4.5814	2.9980	1.5834	0.1996	5.8909	4.5998	1.2911	0.1110
223	4.2515	4.0195	0.2320	-0.6345	4.5567	2.99385	1.5629	0.1939	5.9092	4.5811	1.3281	0.1232

Table S11. Relevant Variables for the Determination of $\Delta G^{\ddagger}$ for $\mathbf{G^{NNBn}}$.

	T_c (K)	log(Δv)	Δv@T_c (ppm)	k (MHz)	$\Delta G^{\ddagger}$ (kcal/mol)
α	265.5	-0.5538	0.2794	310.3	12.45
C	291	0.2057	1.6057	1783.5	12.69
a	280.5	0.0025	1.0058	1117.1	12.47
				Average	12.54

Figure S25. DNMR Traces for α and the Respective Fit for C for $\mathbf{G^{NNBn}}$. The original spectra are shown in black, while the simulated spectra are shown in green or mauve.

Temperature	k_α	k_C @ k_α
-40°C	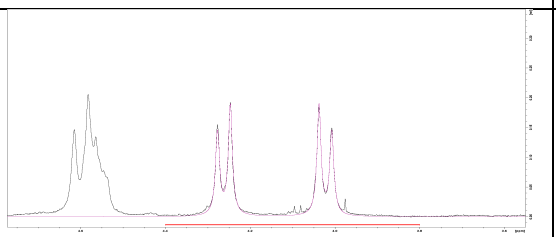	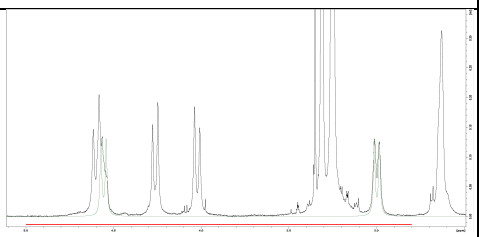
-30°C	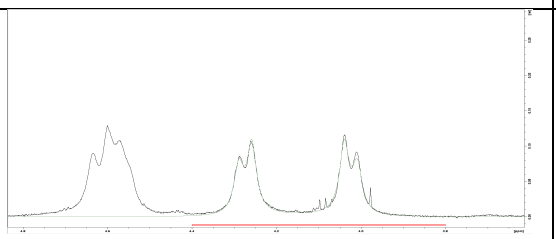	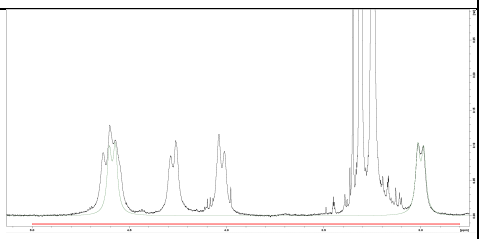
-25°C	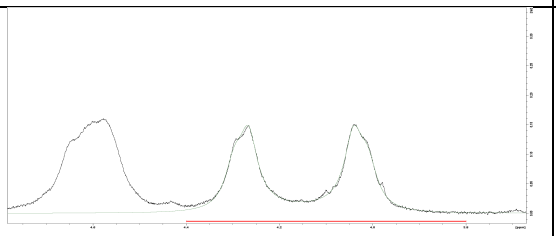	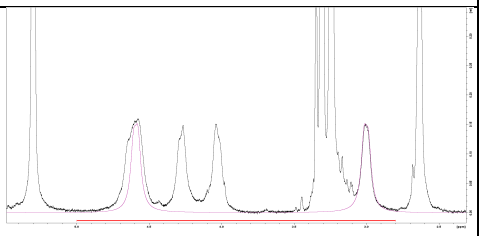
-20°C	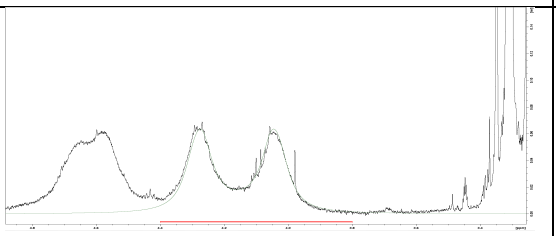	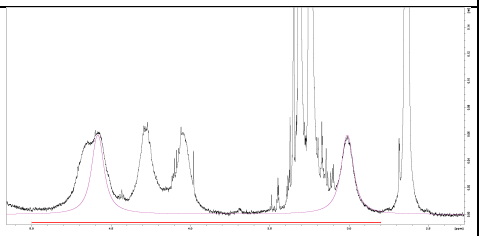
-15°C	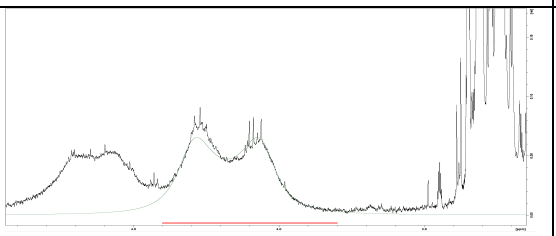	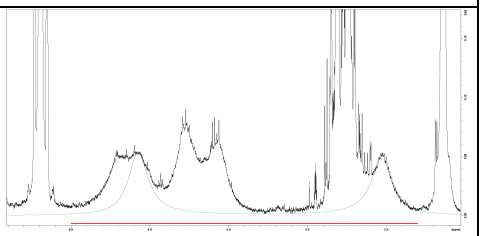
-10°C	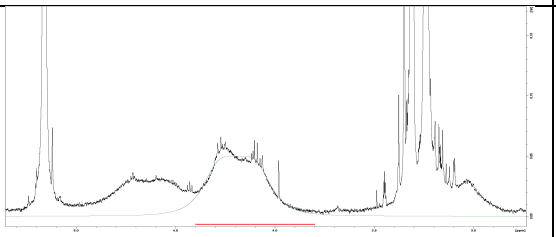	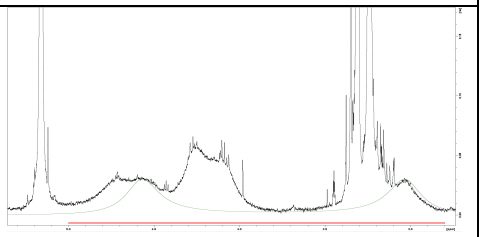

Figure S26. Thermodynamics Derived from DNMR for the α Resonance of $\mathbf{G^{NNBn}}$. a) Temperature dependent rate constant for the selected temperatures. b) Enthalpy, entropy, and free energy calculated from the Arrhenius and Eyring plots. c) The Arrhenius plot for α. d) The Eyring plot for α.

a)

T (°C)	T (K)	1/T	K	ln(k)	ln(k/T)
-40	233.15	0.00429	1.9983	0.692	-4.759
-30	243.15	0.00411	17.0574	2.837	-2.657
-25	248.15	0.00403	39.3406	3.672	-1.842
-20	253.15	0.00395	45.2247	3.812	-1.722
-15	258.15	0.00387	143.2420	4.965	-0.589
-10	263.15	0.00380	337.5820	5.822	0.249

b)

Method	$\Delta H^{\ddagger}$	$\Delta S^{\ddagger}$	$\Delta G^{\ddagger}$
ln(k) vs 1/T	19.38	0.026	12.45
ln(k/T) vs 1/T	19.42	0.027	12.28

c)

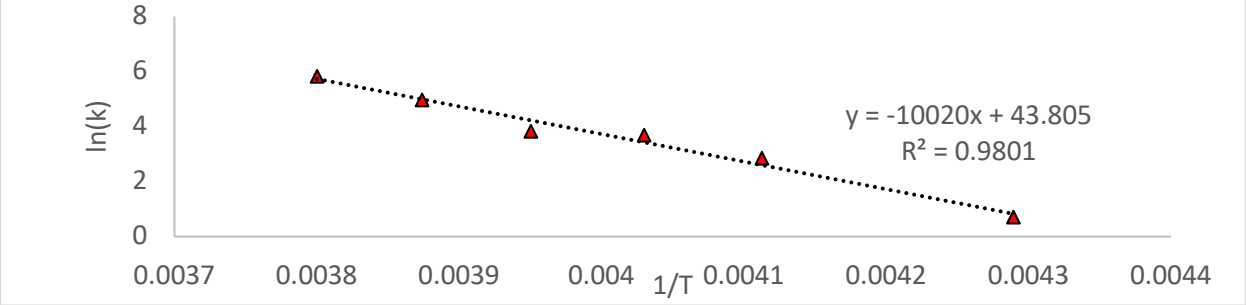

d)

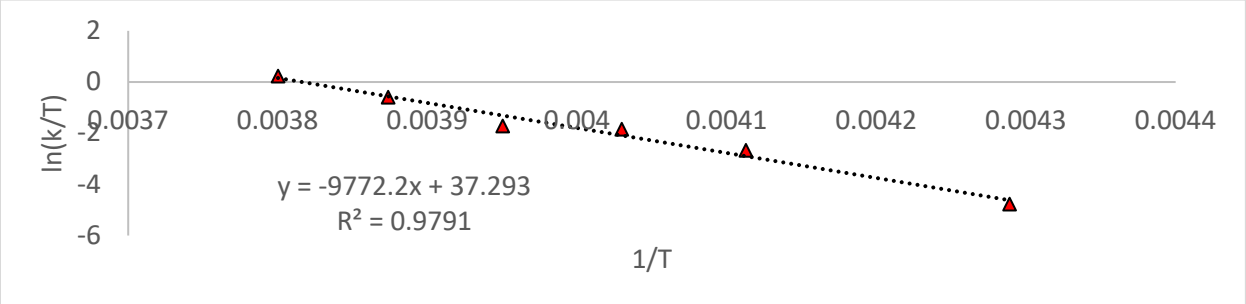

Figure S27. DNMR Traces for a and the Respective Fit for C for $\mathbf{G^{NNBn}}$. The original spectra are shown in black, while the simulated spectra are shown in green or mauve.

Temperature	k_a	k_C @ k_a
-40°C	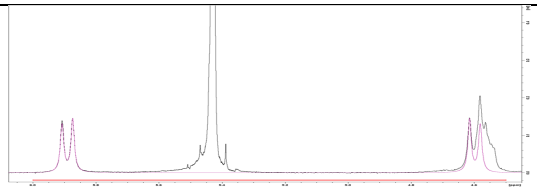	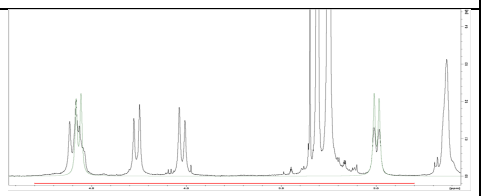
-30°C	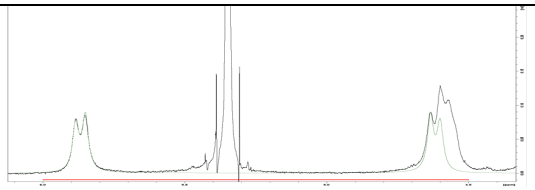	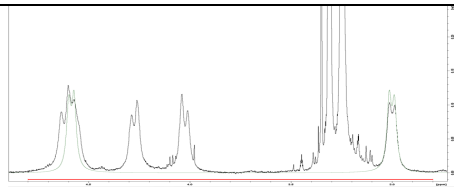
-25°C	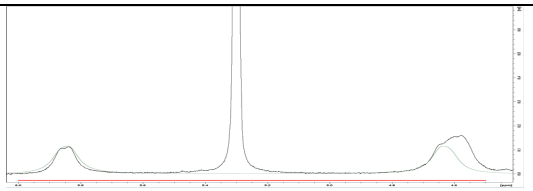	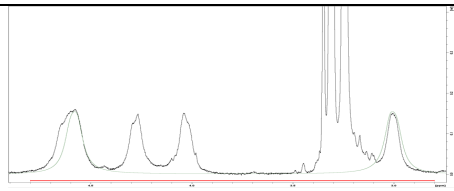
-20°C	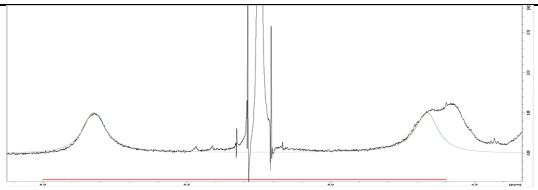	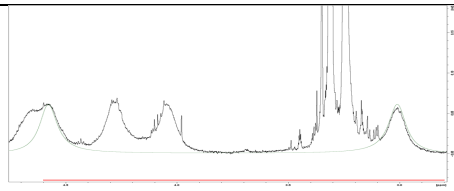
-15°C	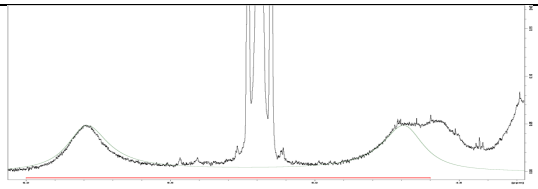	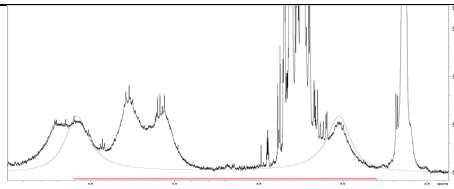
-10°C	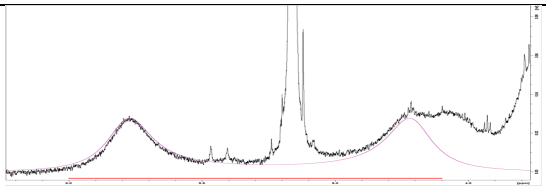	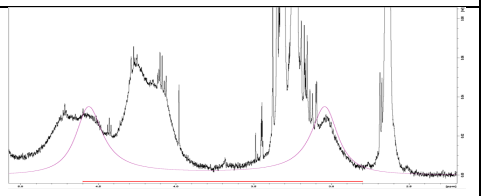
-5°C	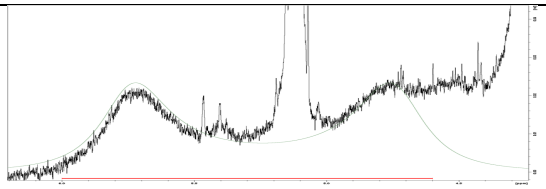	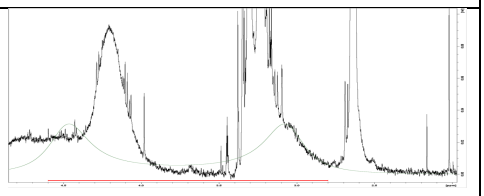

Figure S28. Thermodynamics Derived from DNMR for the a Resonance of $\mathbf{G^{NNBn}}$. a) Temperature dependent rate constant for the selected temperatures. b) Enthalpy, entropy, and free energy calculated from the Arrhenius and Eyring plots. c) The Arrhenius plot for a. d) The Eyring plot for a.

a)

T (°C)	T (K)	1/T	K	ln(k)	ln(k/T)
-40	233.15	0.00429	19.5276	6.206	-2.480
-30	243.15	0.00411	40.5199	2.972	-1.792
-25	248.15	0.00403	78.1166	3.702	-1.156
-20	253.15	0.00395	146.0670	4.358	-0.550
-15	258.15	0.00387	269.2690	4.984	0.0422
-10	263.15	0.00380	295.5500	5.596	0.116
-5	268.15	0.00373	495.6800	5.689	0.614

b)

Method	$\Delta H^{\ddagger}$	$\Delta S^{\ddagger}$	$\Delta G^{\ddagger}$
ln(k) vs 1/T	11.39	-0.00385	12.47
ln(k/T) vs 1/T	11.45	-0.00324	12.31

c)

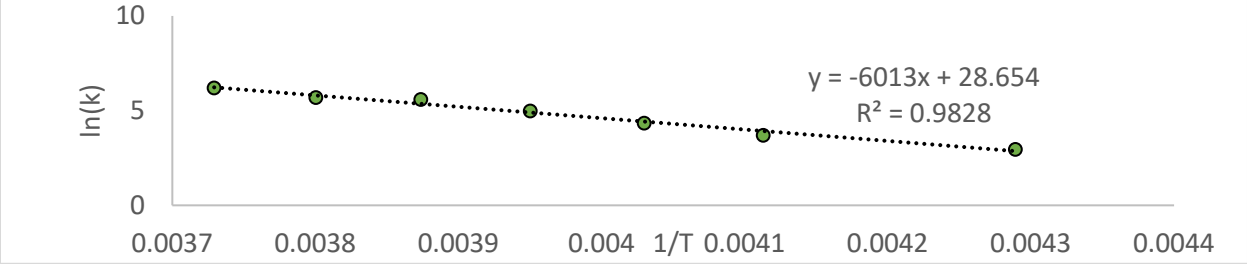

d)

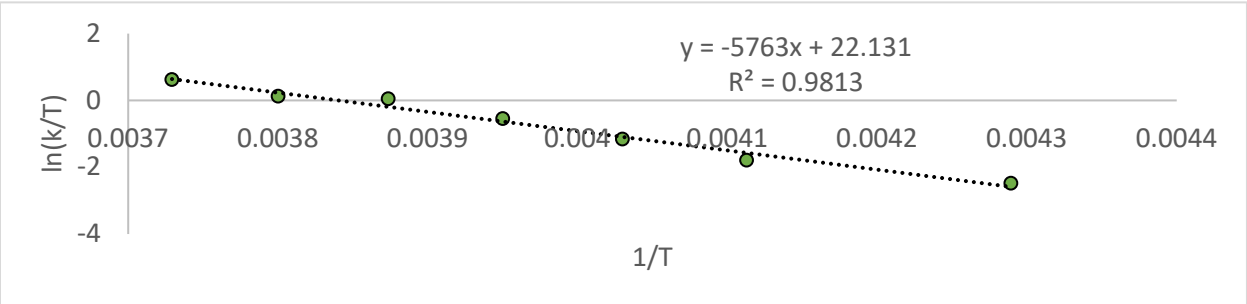

Figure S29. Stacked ^{1}H VT-NMR Spectra of **G^{NNHx}.**

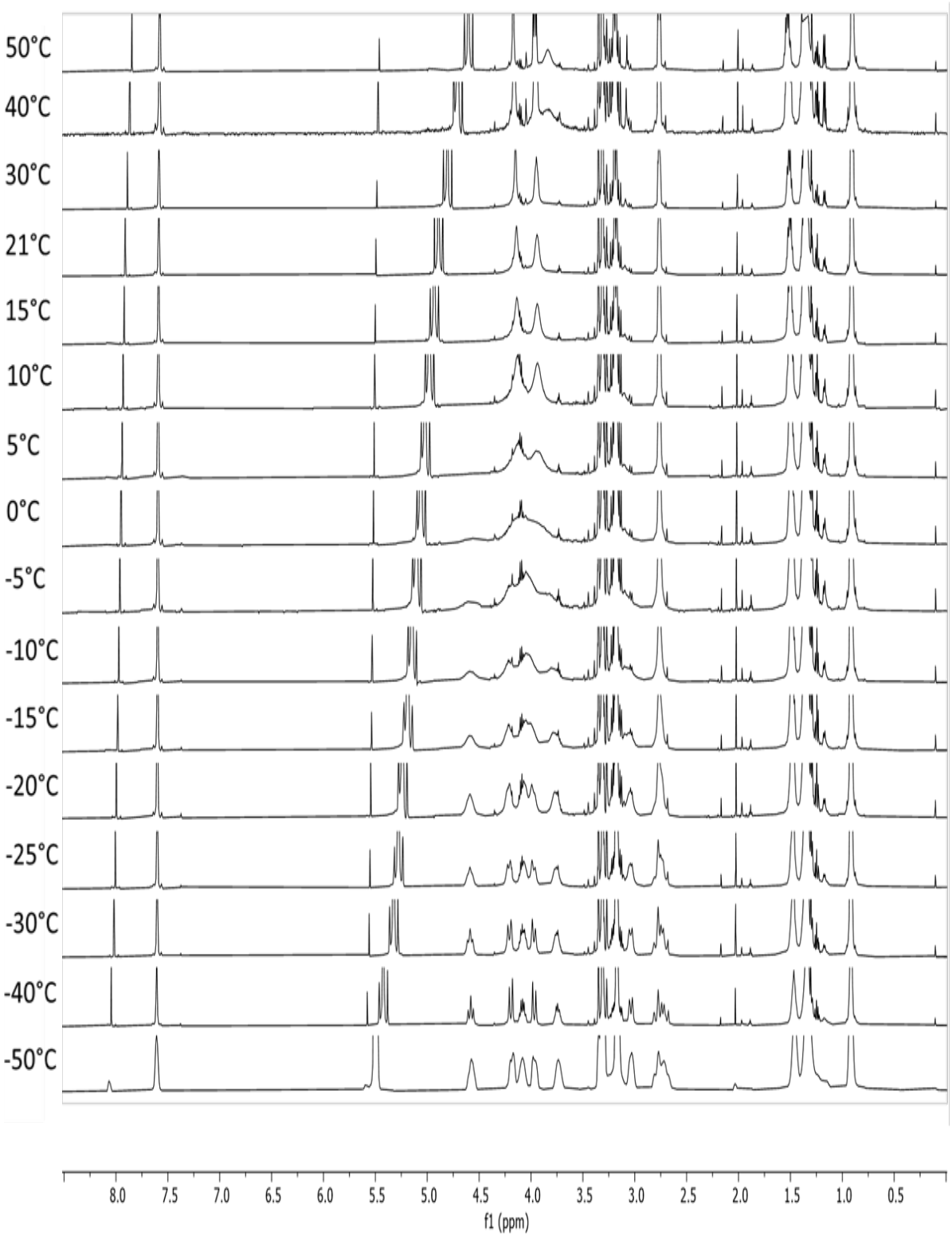

Figure S30. Annotated Stacked ^{1}H VT-NMR Spectra of $\mathbf{G^{NNHx}}$. The resonances corresponding to α are highlighted with red with a black border. The resonances corresponding to C are highlighted with blue without a border. The resonances corresponding to a are highlighted with green with a dashed border. The inlet highlights the temperatures around coalescence for C, with the resonances denoted by blue squares with a black border. The first spectrum post coalescence is denoted with the T_c in the respective resonance's color.

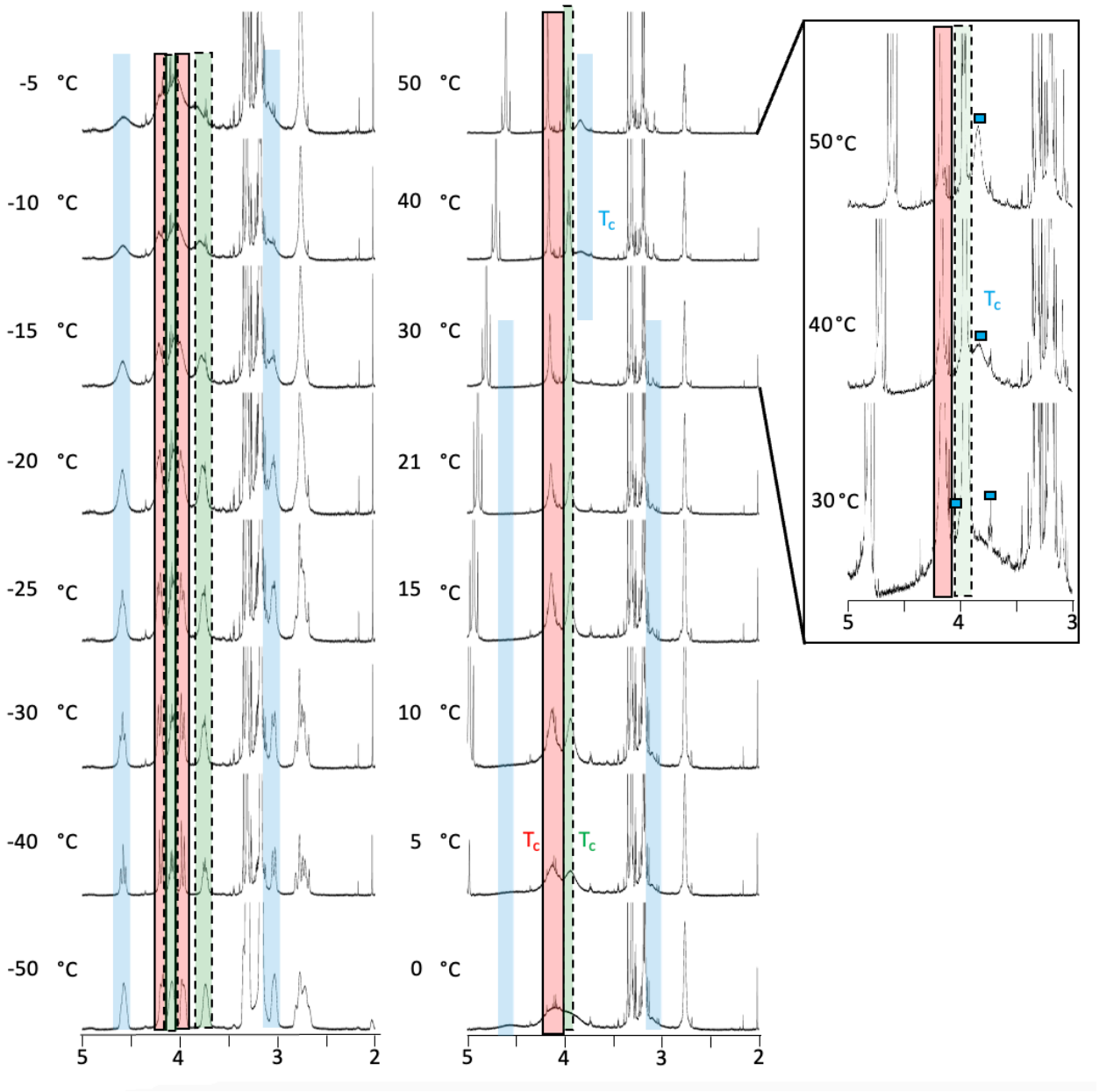

Figure S31. Chemical Shift Dependence on Temperature for $\mathbf{G^{NNHx}}$.

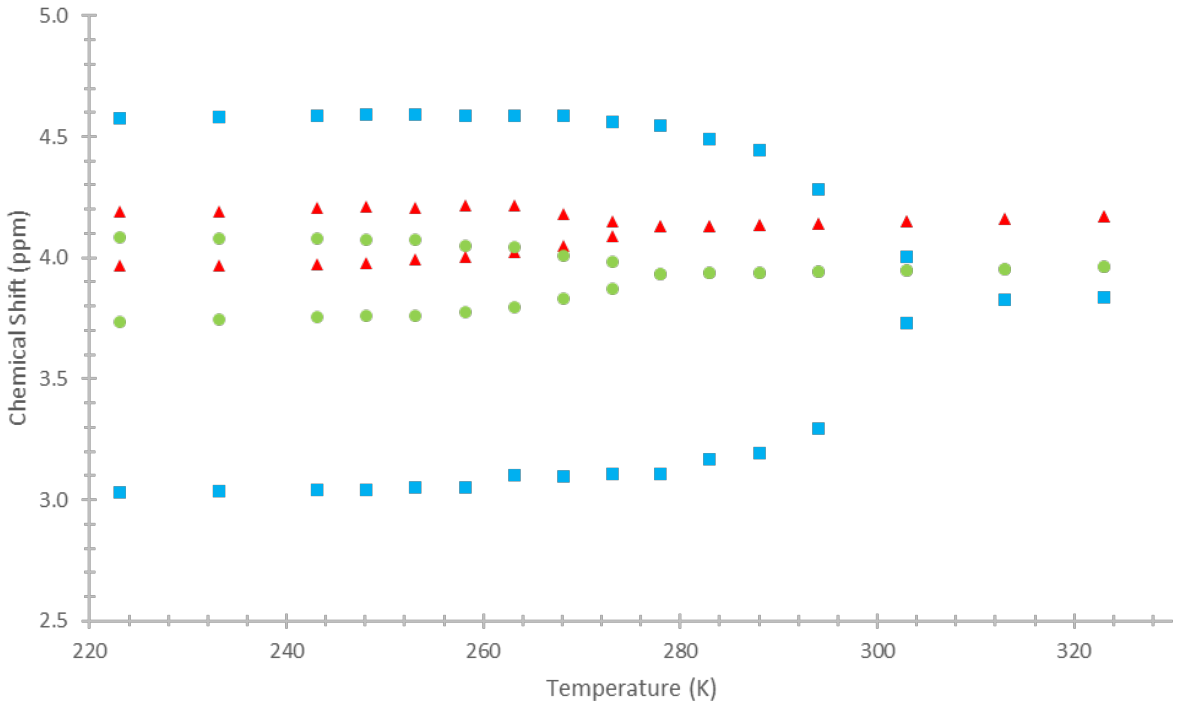

Figure S32. Log10 of the Difference in Chemical Shift with Temperature for $\mathbf{G^{NNHx}}$. Lines are derived from the linear sections of the graph.

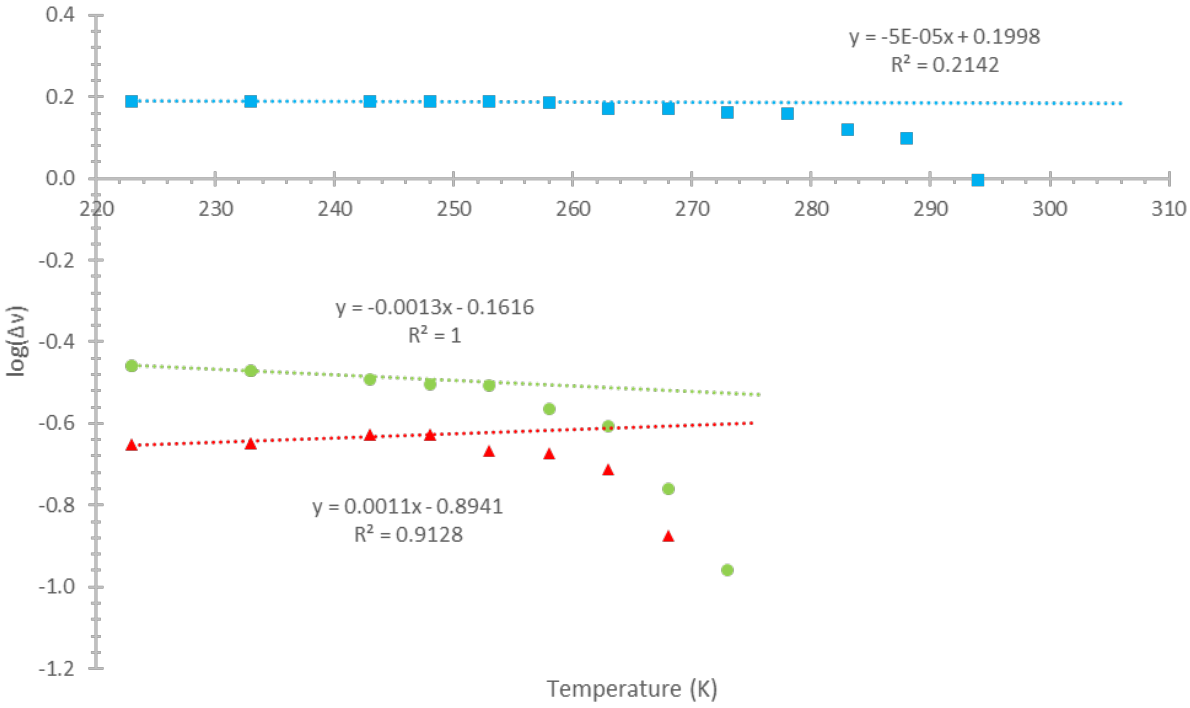

Table S12. Chemical Shift and Δν Dependence on Temperature for $\mathbf{G^{NNHx}}$.

	α				C				a			
T (K)	Chemical Shift (ppm)		Δν (ppm)	log(Δν)	Chemical Shift (ppm)		Δν (ppm)	log(Δν)	Chemical Shift (ppm)		Δν (ppm)	log(Δν)
323	4.1711	4.1711	-	-	3.8367	3.8367	-	-	3.9635	3.9635	-	-
313	4.1603	4.1603	-	-	3.8281	3.8281	-	-	3.9554	3.9554	-	-
303	4.1498	4.1498	-	-	4.0059	3.7278	0.2781	-0.5558	3.9480	3.9480	-	-
294	4.1420	4.1420	-	-	4.2820	3.2930	0.9890	-0.0048	3.9430	3.9430	-	-
288	4.1359	4.1359	-	-	4.4450	3.1945	1.2505	0.0971	3.9400	3.9400	-	-
283	4.1320	4.1320	-	-	4.4890	3.1683	1.3207	0.1208	3.9366	3.9366	-	-
278	4.1280	4.1280	-	-	4.5440	3.1080	1.4360	0.1572	3.9330	3.9330	-	-
273	4.1513	4.0898	-	-	4.5590	3.1070	1.4520	0.1620	3.9810	3.8710	0.1100	-0.9586
268	4.1821	4.0490	0.1331	-0.8758	4.5840	3.0980	1.4860	0.1720	4.0071	3.8330	0.1741	-0.7592
263	4.2180	4.0232	0.1948	-0.7104	4.5850	3.1000	1.4850	0.1717	4.0430	3.7952	0.2478	-0.6059
258	4.2170	4.0040	0.2130	-0.6716	4.5870	3.0507	1.5363	0.1865	4.0500	3.7770	0.2730	-0.5638
253	4.2084	3.9927	0.2157	-0.6661	4.5920	3.0520	1.5400	0.1875	4.0730	3.7618	0.3112	-0.5070
248	4.2116	3.9760	0.2356	-0.6278	4.5890	3.0410	1.5480	0.1898	4.0730	3.7590	0.3140	-0.5031
243	4.2074	3.9723	0.2351	-0.6288	4.5880	3.0398	1.5482	0.1898	4.0780	3.7556	0.3224	-0.4916
233	4.1934	3.9685	0.2250	-0.6479	4.5801	3.0371	1.5431	0.1884	4.0809	3.7432	0.3377	-0.4715
223	4.1890	3.9660	0.2230	-0.6517	4.5741	3.0294	1.5447	0.1888	4.0830	3.7348	0.3482	-0.4582

Table S13. Relevant Variables for the Determination of $\Delta G^{\ddagger}$ for $\mathbf{G^{NNHx}}$.

	T_c (K)	log(Δν)	Δν@T_c (ppm)	k (MHz)	$\Delta G^{\ddagger}$ (kcal/mol)
α	275.5	-0.5973	0.2527	280.7	13.00
C	308	0.1855	1.533	1702.4	13.50
a	275.5	-0.5280	0.2965	329.3	12.91
				Average	13.13

Figure S33. DNMR Traces for α and the Respective Fit for C for $\mathbf{G^{NNHx}}$. The original spectra are shown in black, while the simulated spectra are shown in green or mauve.

Temperature	k_α	k_C @ k_α
-40°C	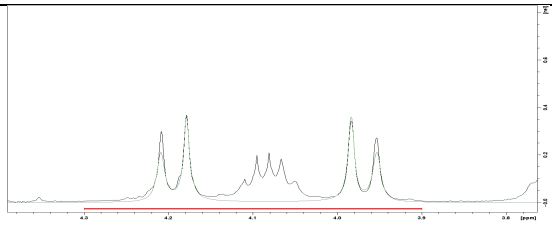	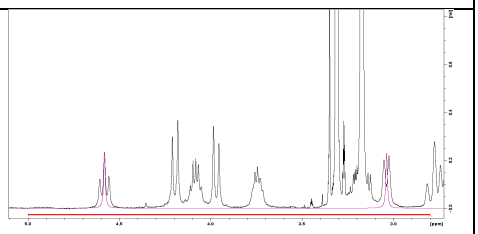
-30°C	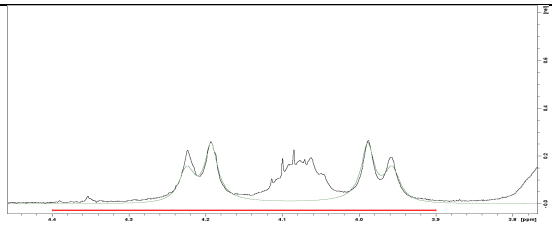	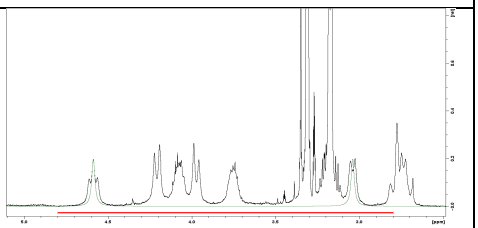
-25°C	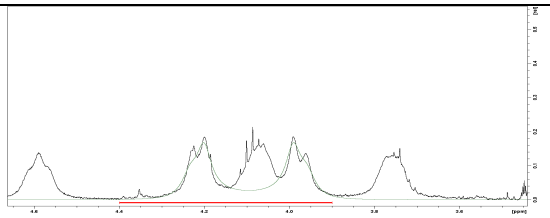	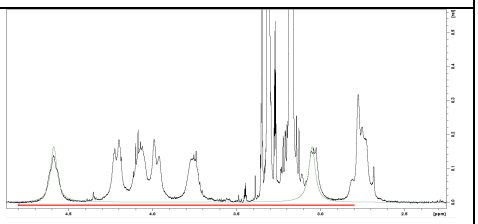
-20°C	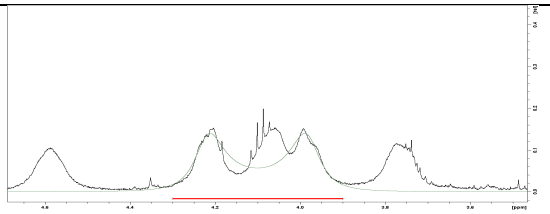	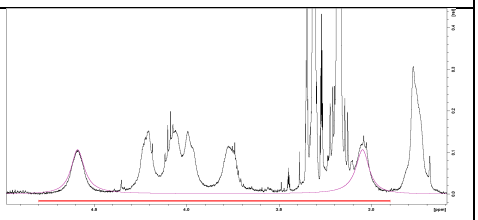
-15°C	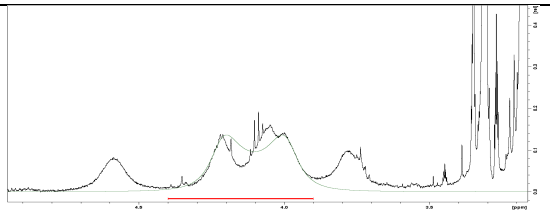	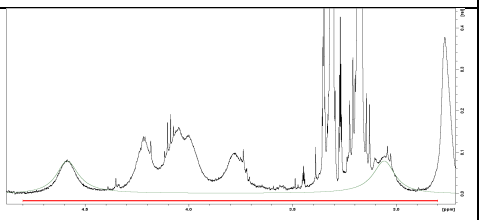
-10°C	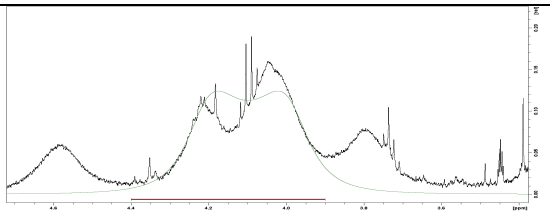	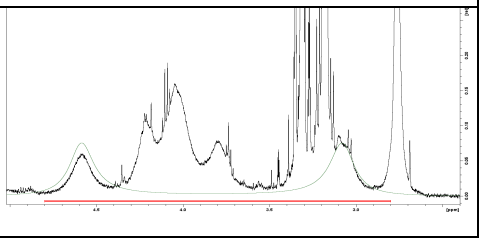

Figure S34. Thermodynamics Derived from DNMR for the α Resonance of $\mathbf{G^{NNHx}}$. a) Temperature dependent rate constant for the selected temperatures. b) Enthalpy, entropy, and free energy calculated from the Arrhenius and Eyring plots. c) The Arrhenius plot for α. d) The Eyring plot for α.

a)

T (°C)	T (K)	1/T	K	ln(k)	ln(k/T)
-40	233.15	0.00429	15.3783	2.733	-2.719
-30	243.15	0.00411	30.3078	3.411	-2.082
-25	248.15	0.00403	73.0843	4.292	-1.222
-20	253.15	0.00395	135.1340	4.906	-0.628
-15	258.15	0.00387	170.0070	5.136	-0.418
-10	263.15	0.00380	234.0780	5.456	-0.117

b)

Method	$\Delta H^{\ddagger}$	$\Delta S^{\ddagger}$	$\Delta G^{\ddagger}$
ln(k) vs 1/T	11.26	-0.0063	13.00
ln(k/T) vs 1/T	11.32	-0.0042	12.48

c)

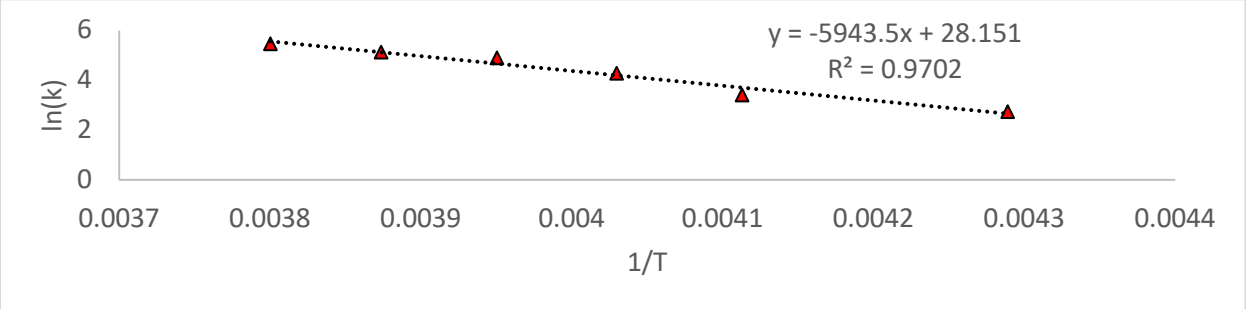

d)

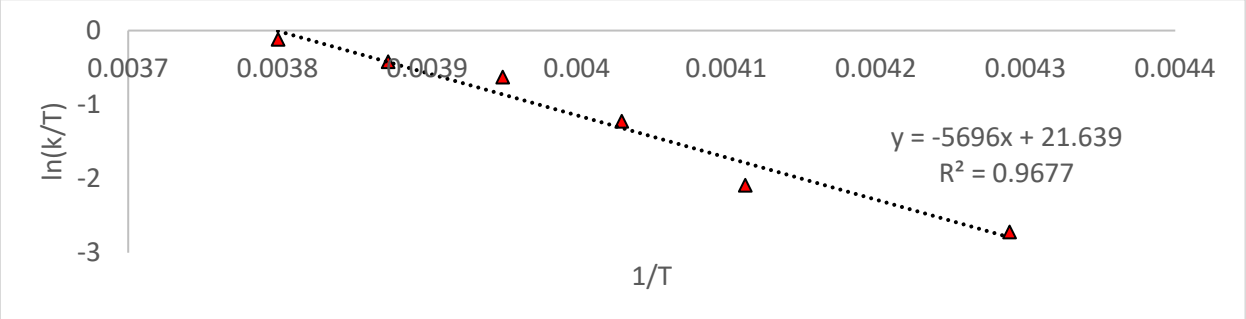

Figure S35. DNMR Traces for a and the Respective Fit for C for $\mathbf{G^{NNHx}}$. The original spectra are shown in black, while the simulated spectra are shown in green or mauve.

Temperature	k_a	k_C @ k_a
-30°C	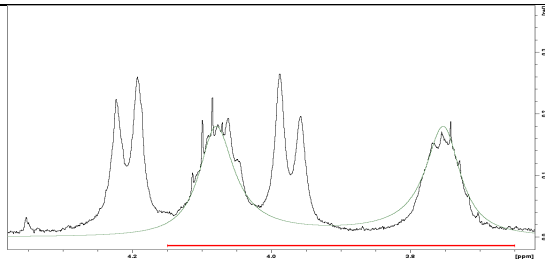	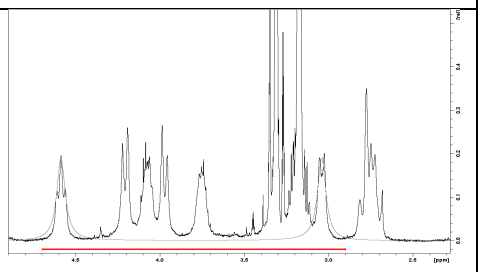
-25°C	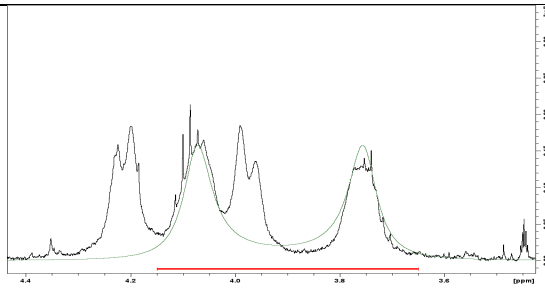	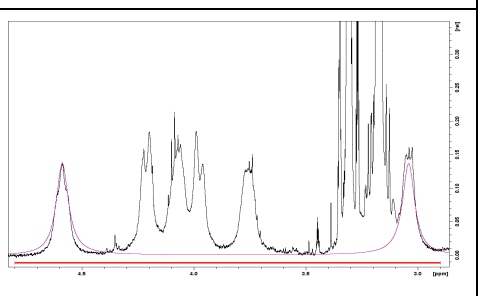
-20°C	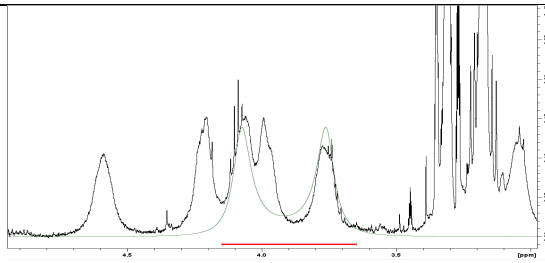	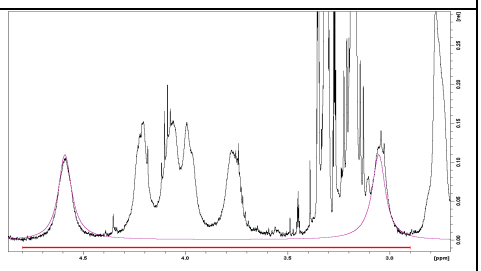
-15°C	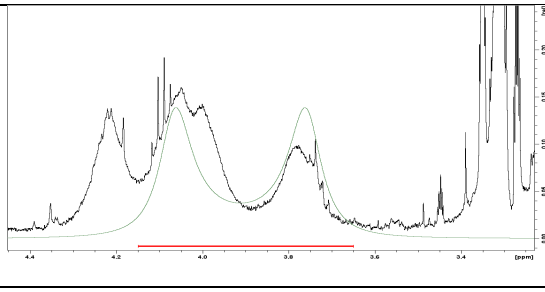	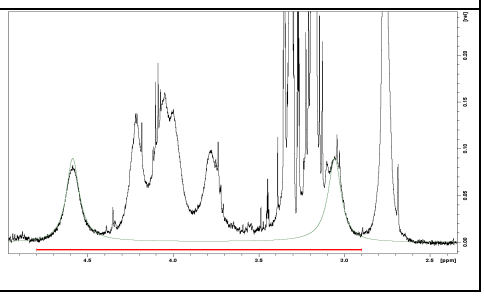

Figure S36. Thermodynamics Derived from DNMR for the a Resonance of $\mathbf{G}^{\mathbf{NNHx}}$. a) Temperature dependent rate constant for the selected temperatures. b) Enthalpy, entropy, and free energy calculated from the Arrhenius and Eyring plots. c) The Arrhenius plot for a. d) The Eyring plot for a.

a)

T (°C)	T (K)	1/T	K	ln(k)	ln(k/T)
-30	243.15	0.00411	63.4480	4.150	-1.343
-25	248.15	0.00403	71.6596	4.272	-1.242
-20	253.15	0.00395	91.6751	4.518	-1.016
-15	258.15	0.00387	113.6920	4.733	-0.820

b)

Method	$\Delta H^{\ddagger}$	$\Delta S^{\ddagger}$	$\Delta G^{\ddagger}$
ln(k) vs 1/T	4.42	-0.031	12.91
ln(k/T) vs 1/T	4.47	-0.032	13.17

c)

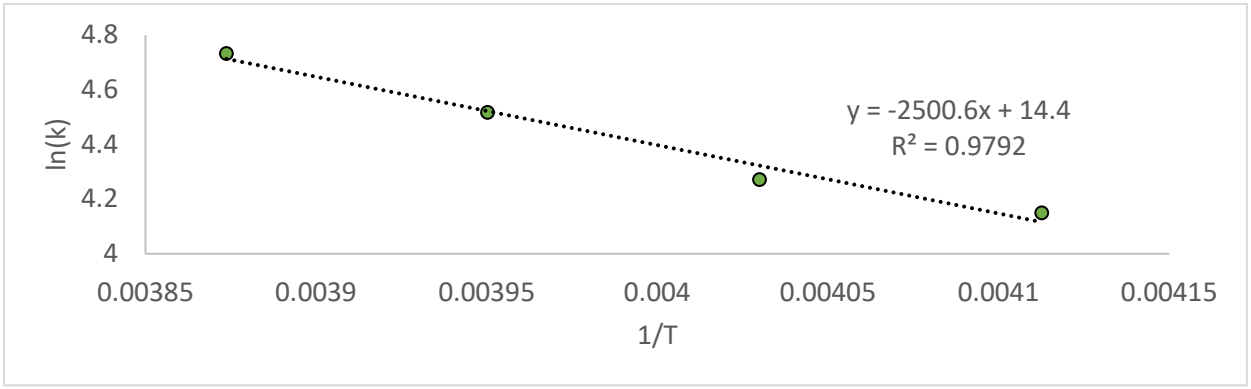

d)

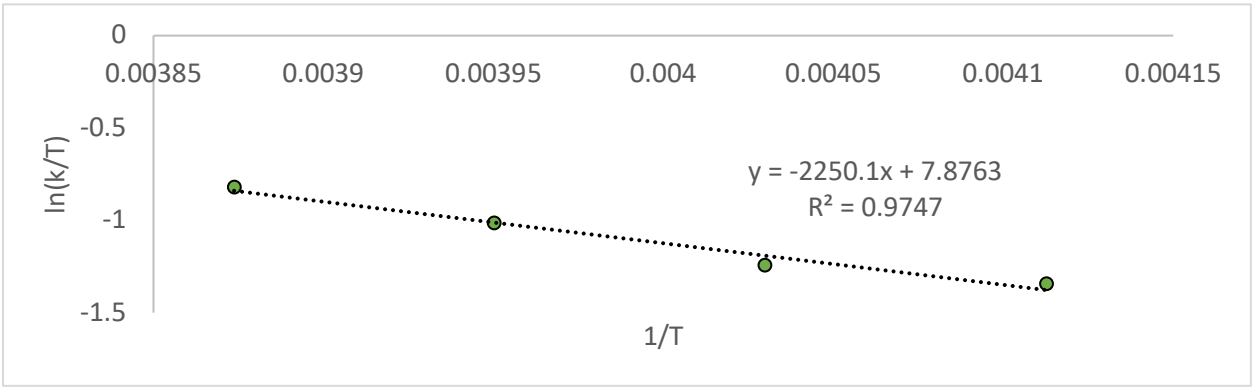

Figure S37. The 400 MHz ^{1}H NMR Spectrum of **G^{NNMe}** in DMSO.

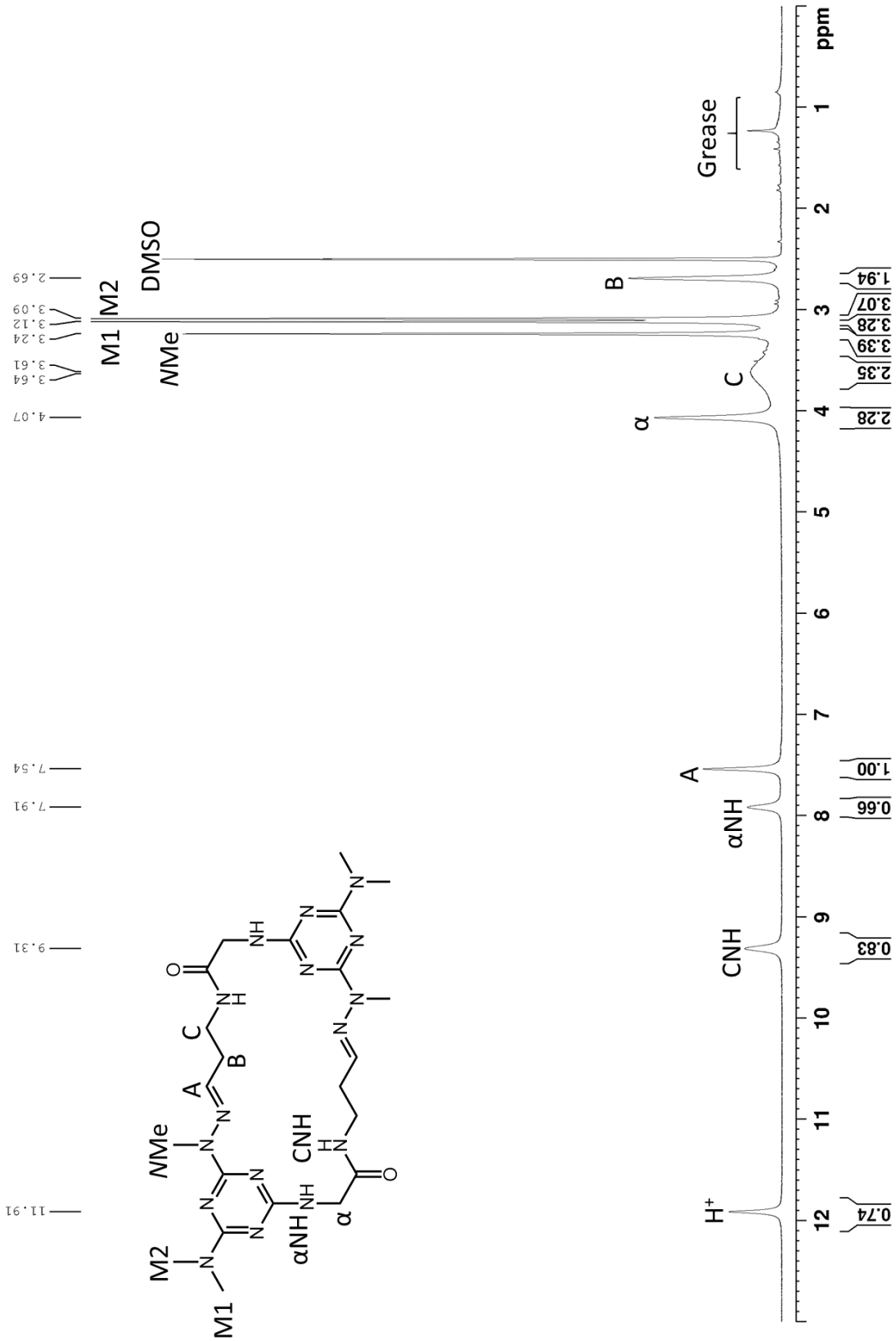

Figure S38. The 400 MHz ^{1}H NMR Spectrum of **G^{NNEt}** in DMSO.

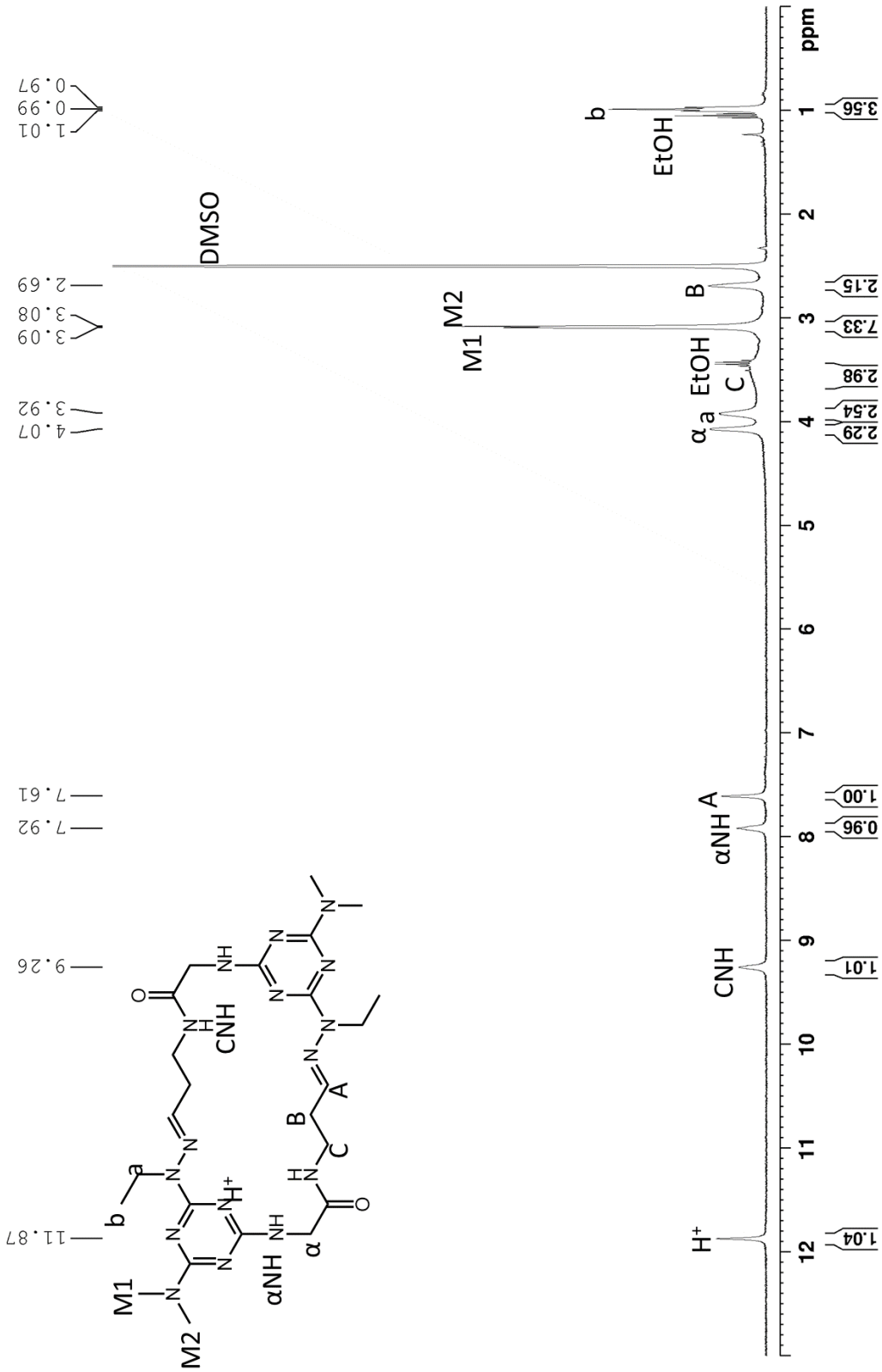

Figure S39. The 400 MHz ^{1}H NMR Spectrum of **G^{NNiPr}** in DMSO.

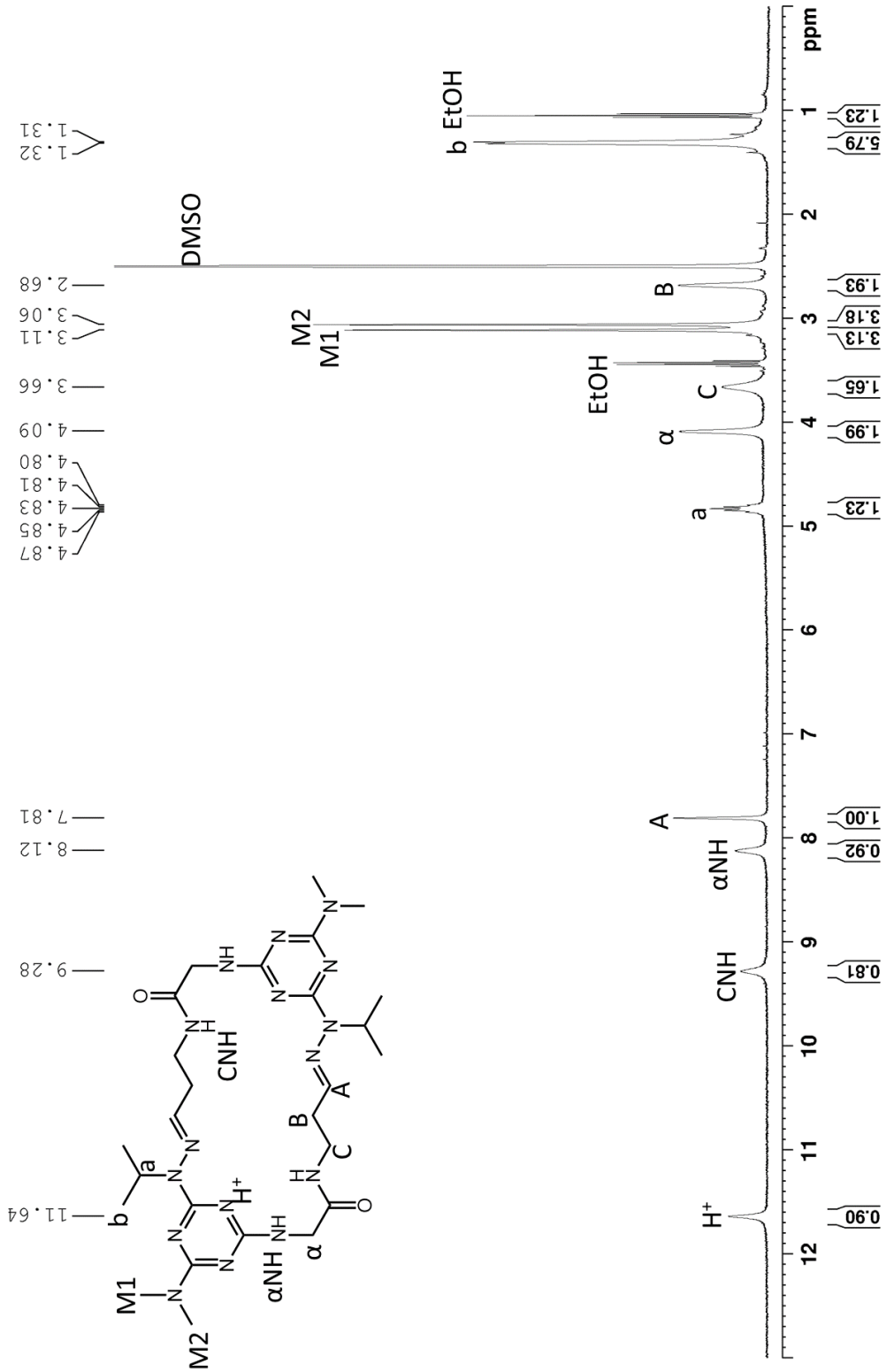

Figure S40. The 400 MHz ^{1}H NMR Spectrum of **G^{NNBn}** in DMSO.

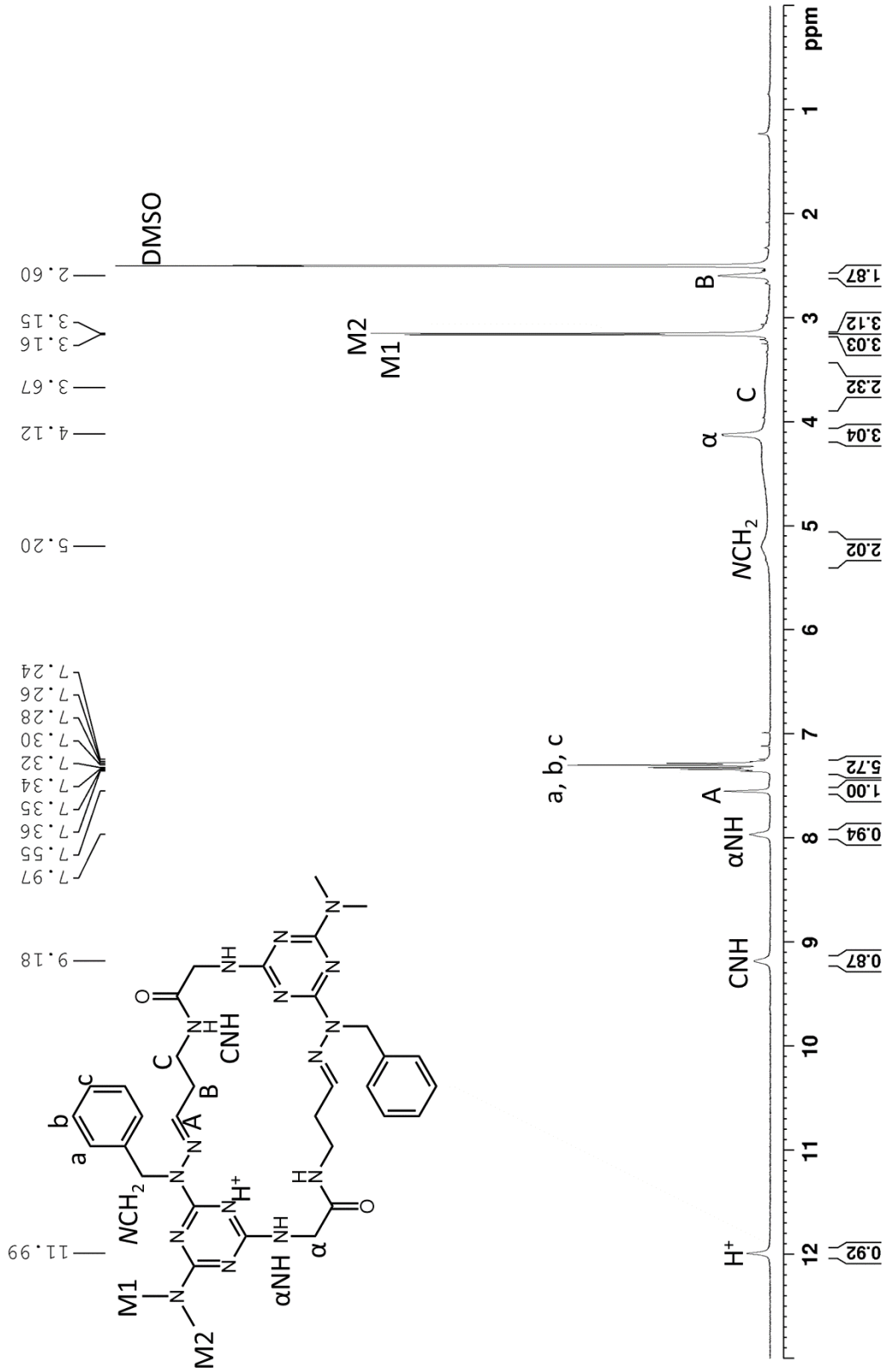

Figure S41. The 400 MHz ^{1}H NMR Spectrum of **G^{NNHx}** in DMSO.

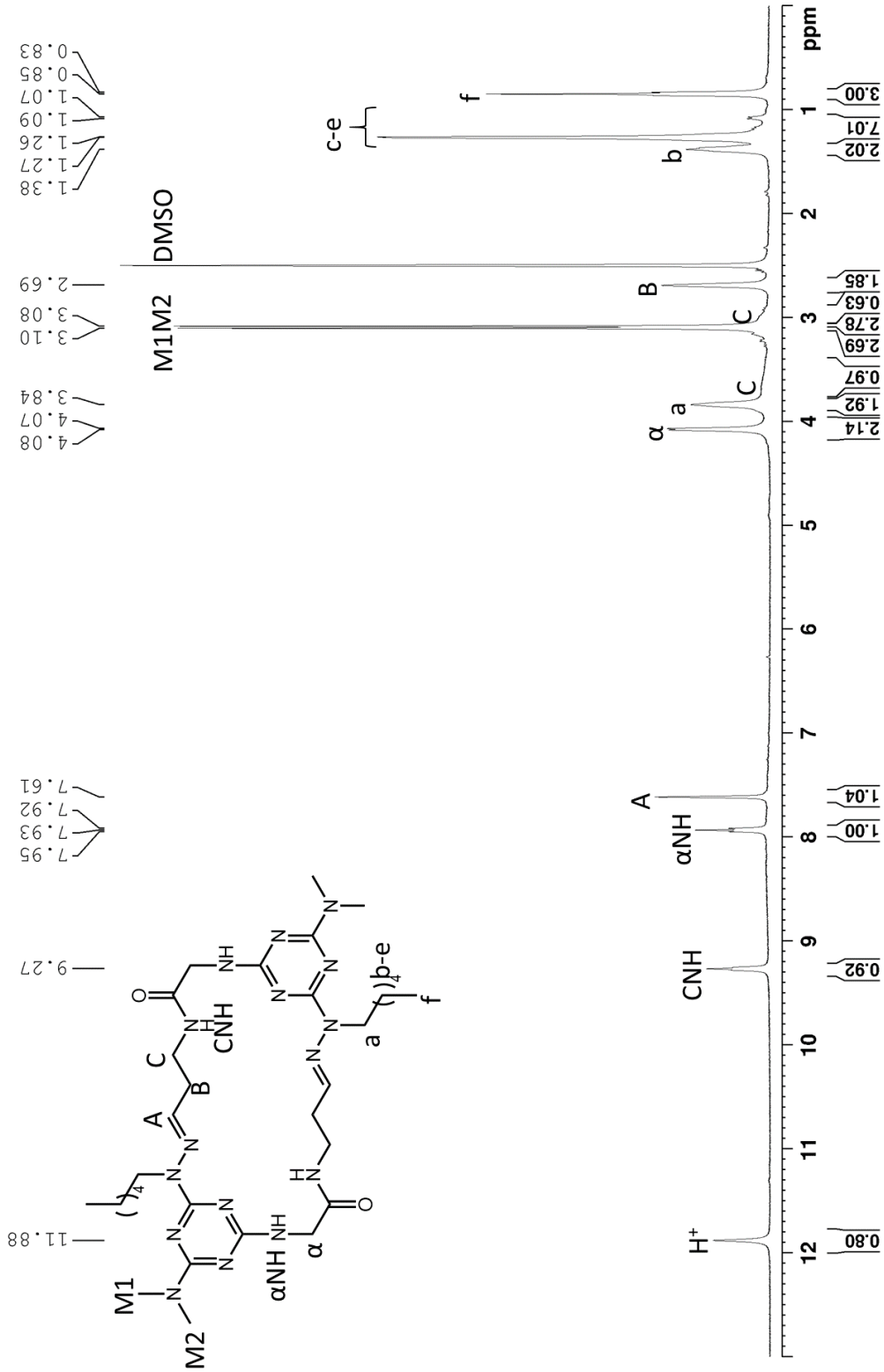

Figure S42. The 100 MHz ^{13}C NMR Spectrum of $\mathbf{G^{NNMe}}$ in DMSO.

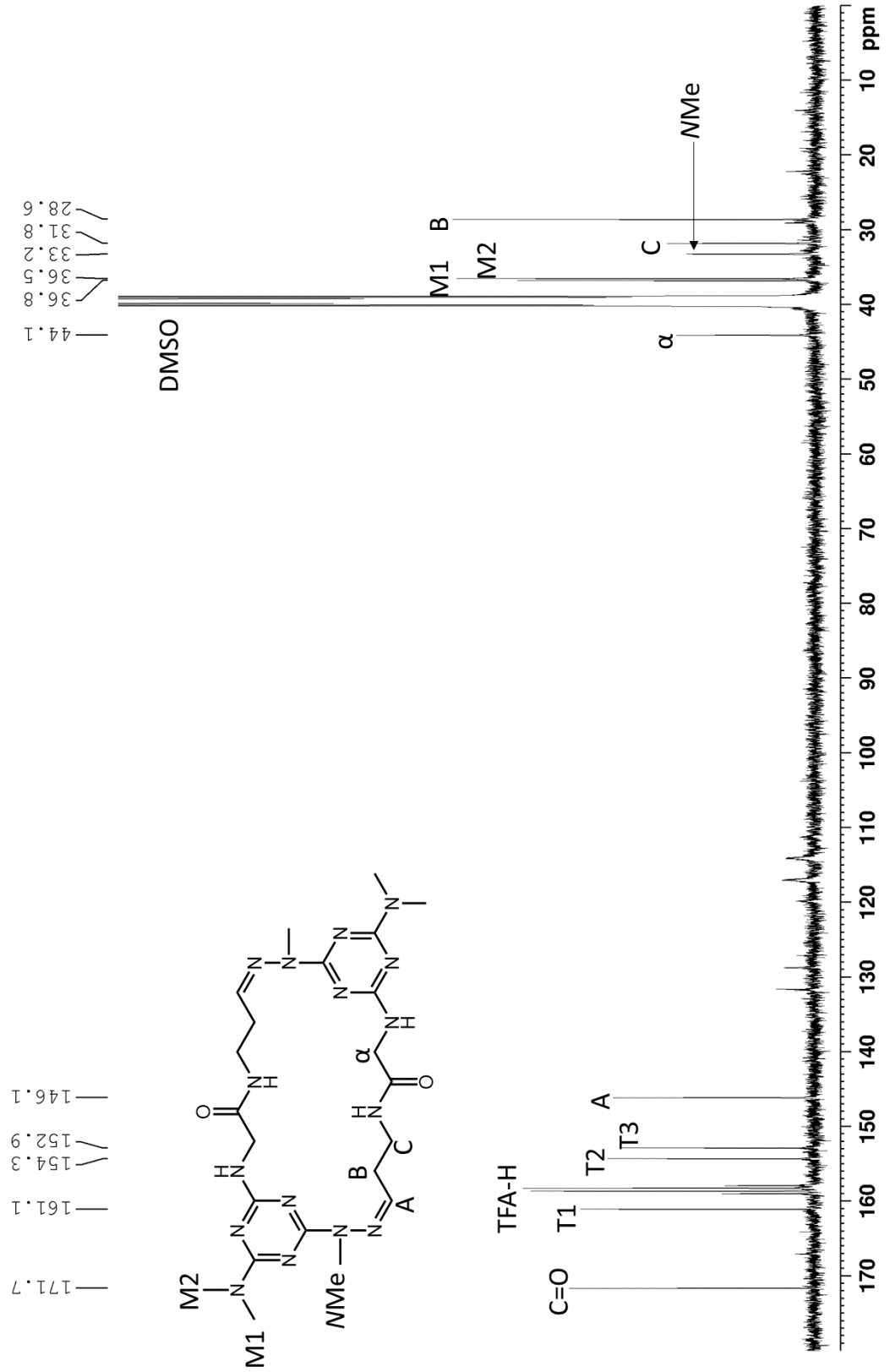

Figure S43. The 100 MHz ^{13}C NMR Spectrum of **G^{NNEt}** in DMSO.

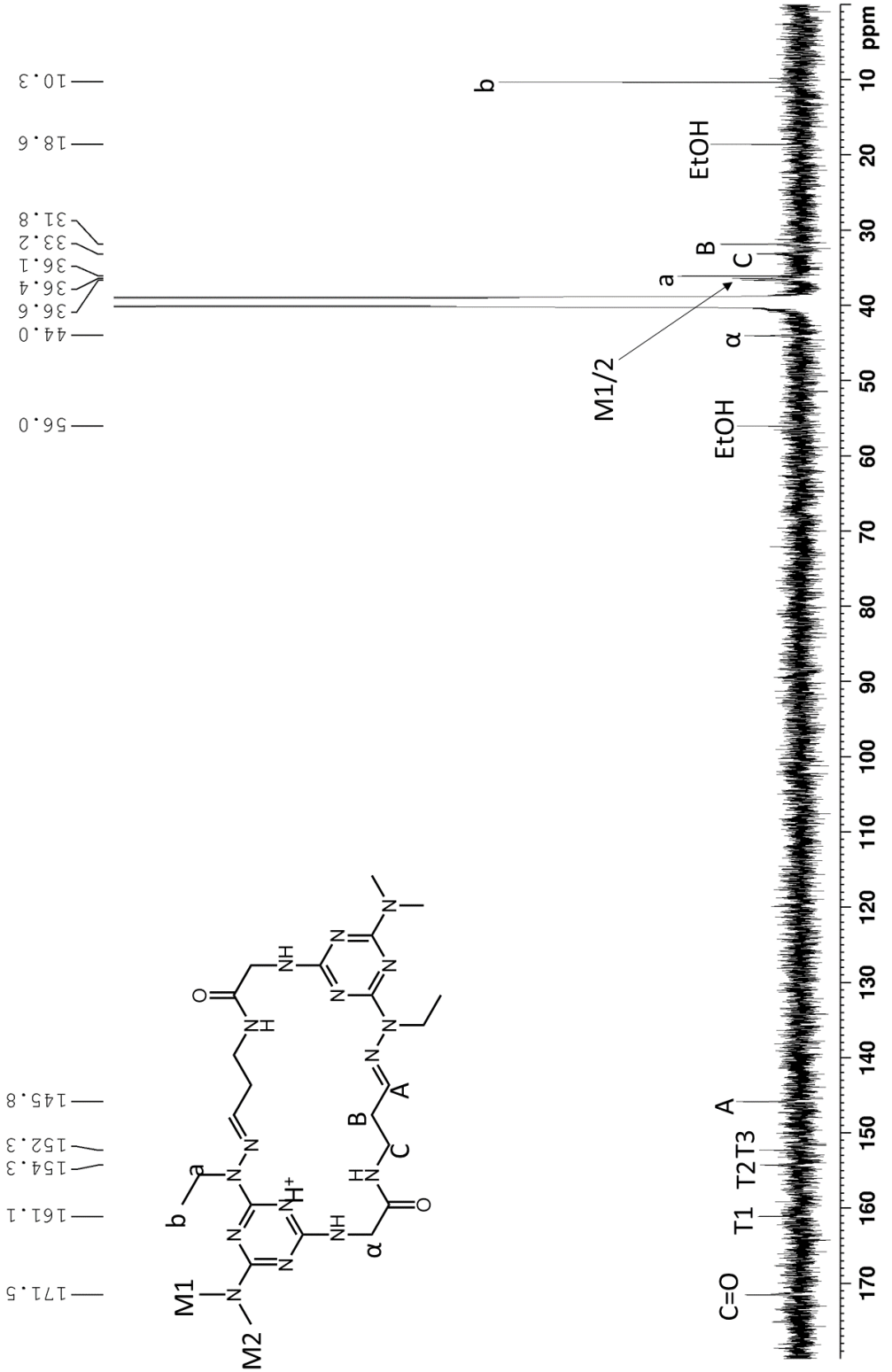

Figure S44. The 100 MHz ^{13}C NMR Spectrum of $\mathbf{G^{NNiPr}}$ in DMSO.

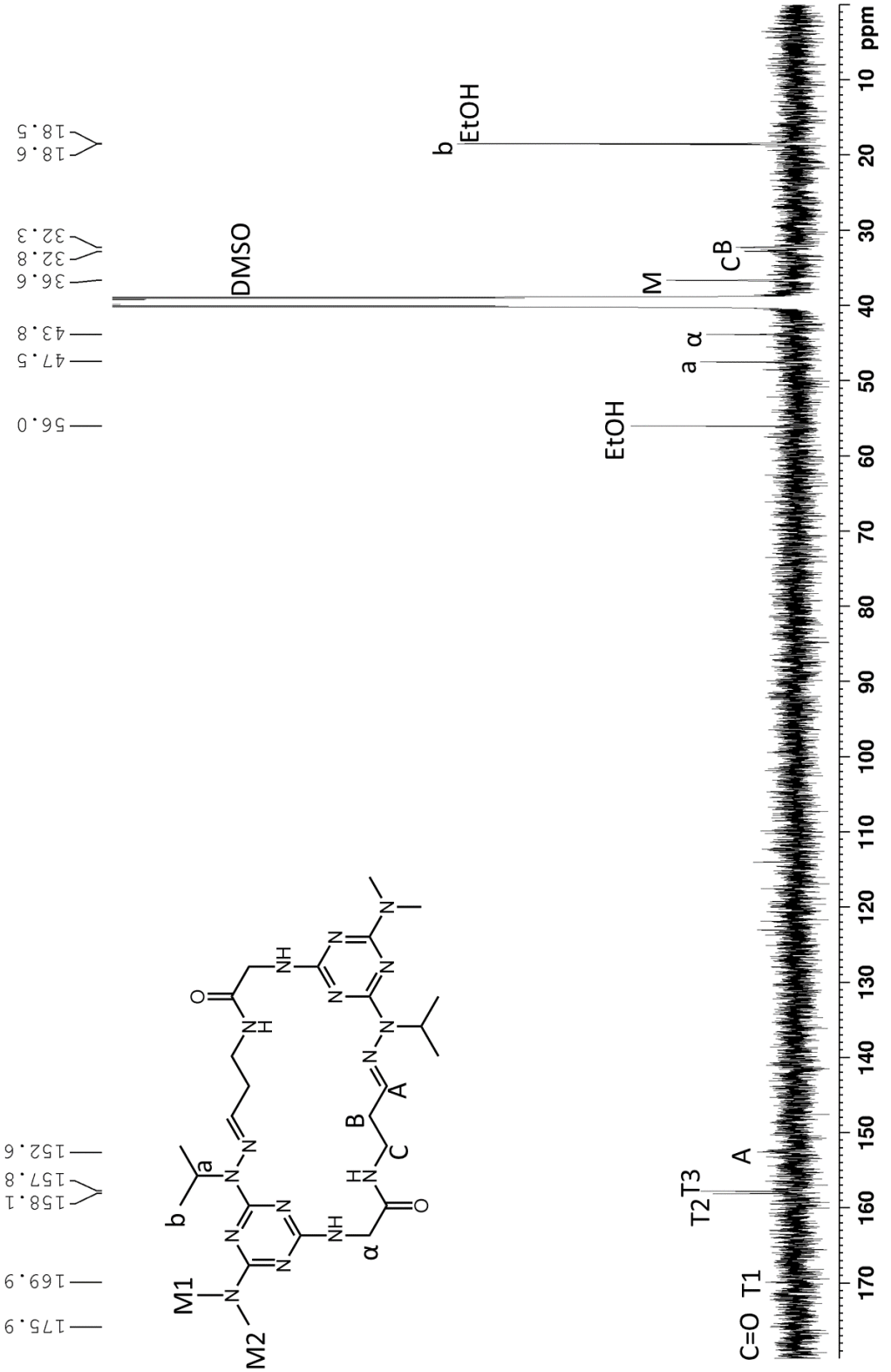

Figure S45. The 100 MHz ^{13}C NMR Spectrum of $\mathbf{G^{NNBn}}$ in DMSO.

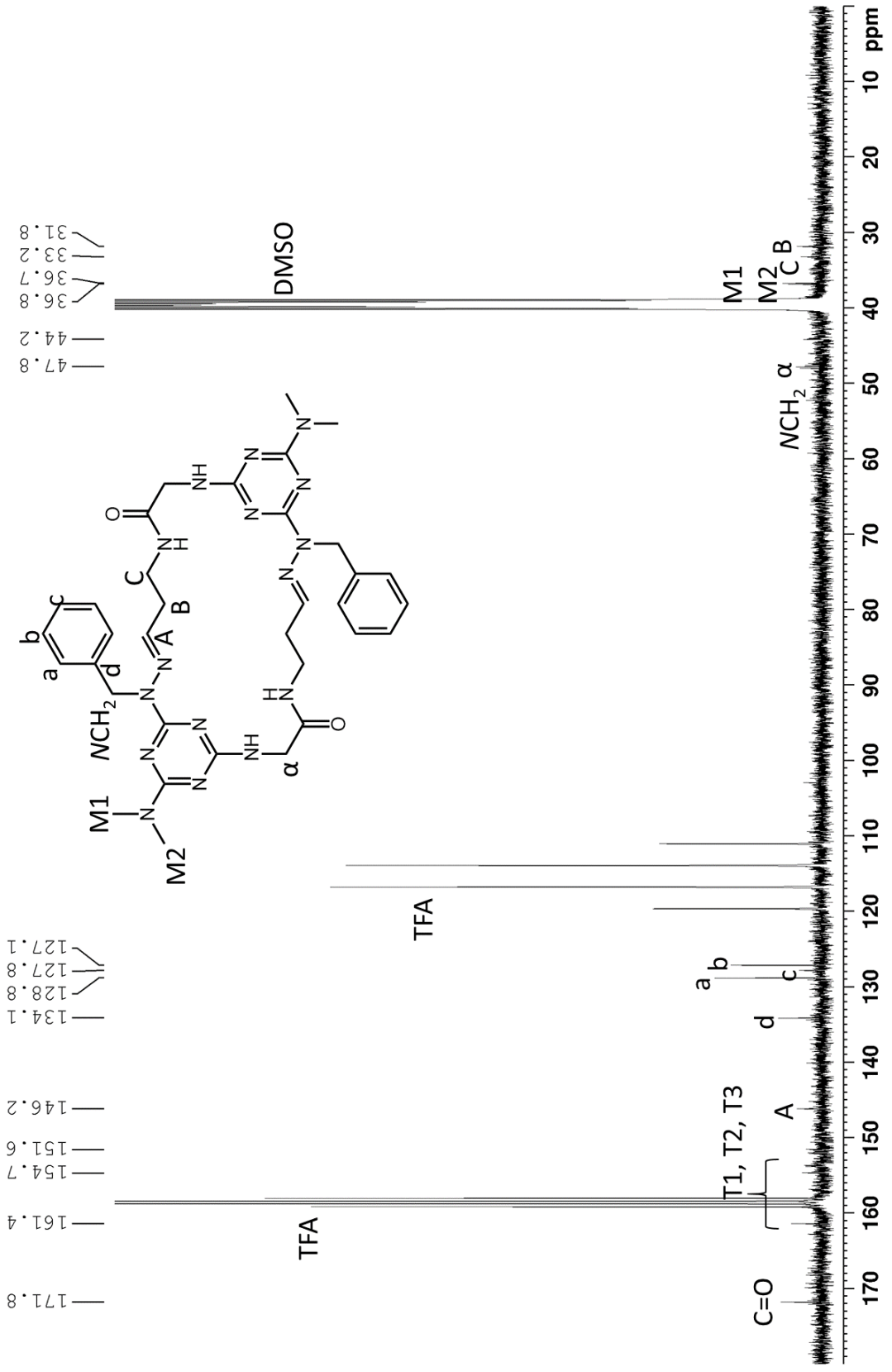

Figure S46. The 100 MHz ^{13}C NMR Spectrum of $\mathbf{G^{NNHx}}$ in DMSO

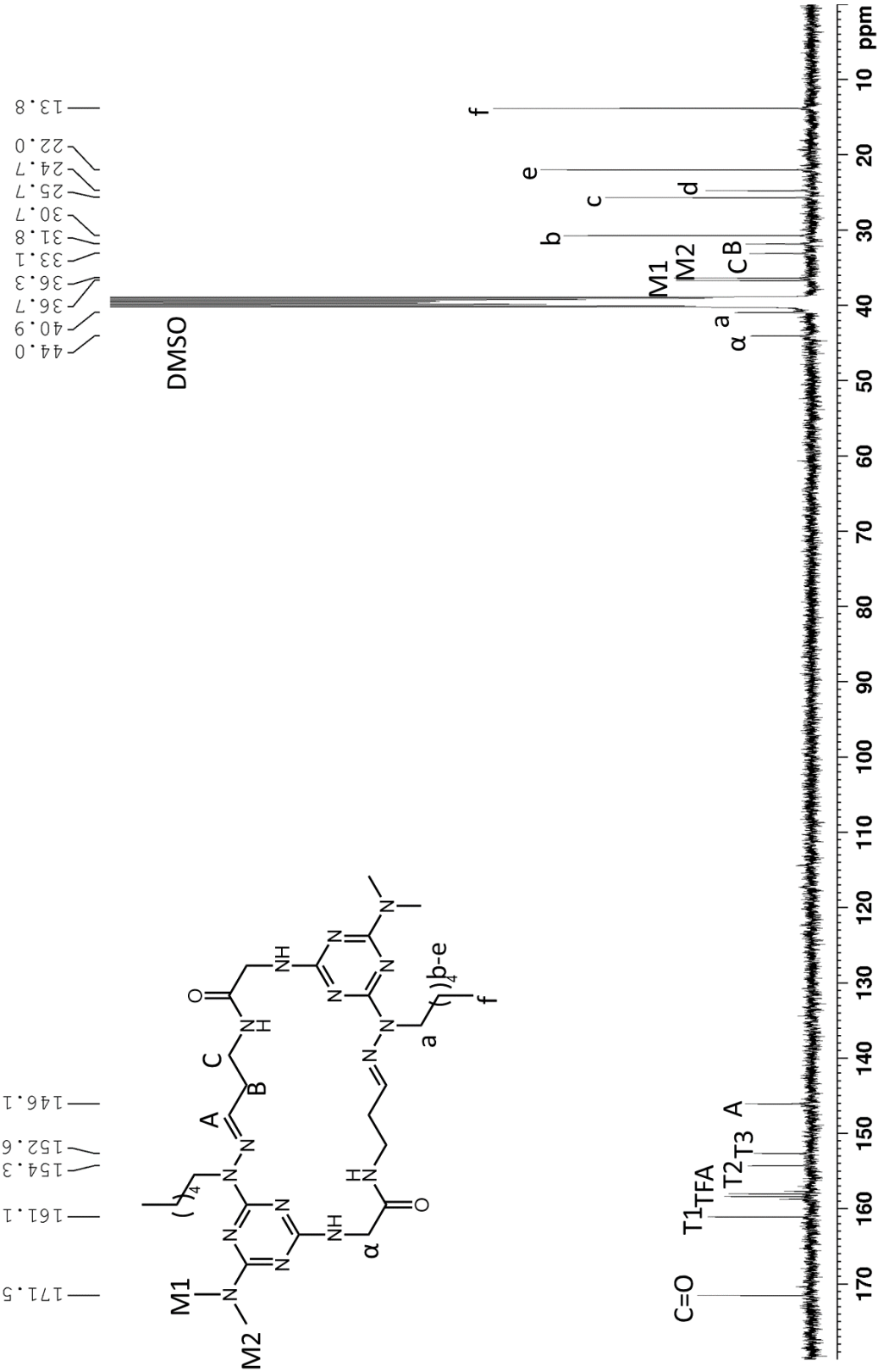

Figure S47. The 400 MHz rOesy and COSY NMR Spectrum of $\mathbf{G^{NNMe}}$ in DMSO.

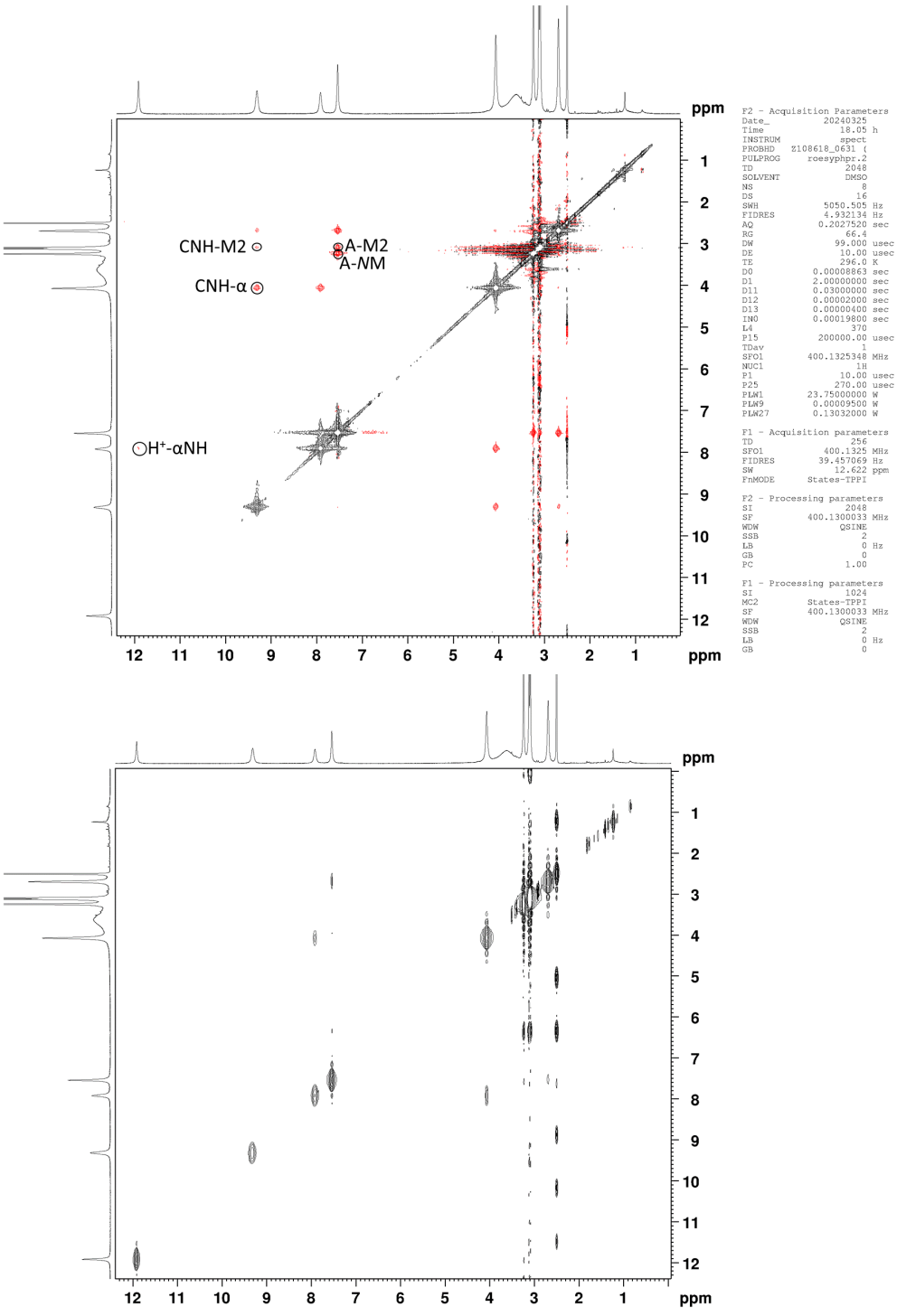

Figure S48. The 400 MHz rOesy and COSY NMR Spectrum of $\mathbf{G^{NNEt}}$ in DMSO.

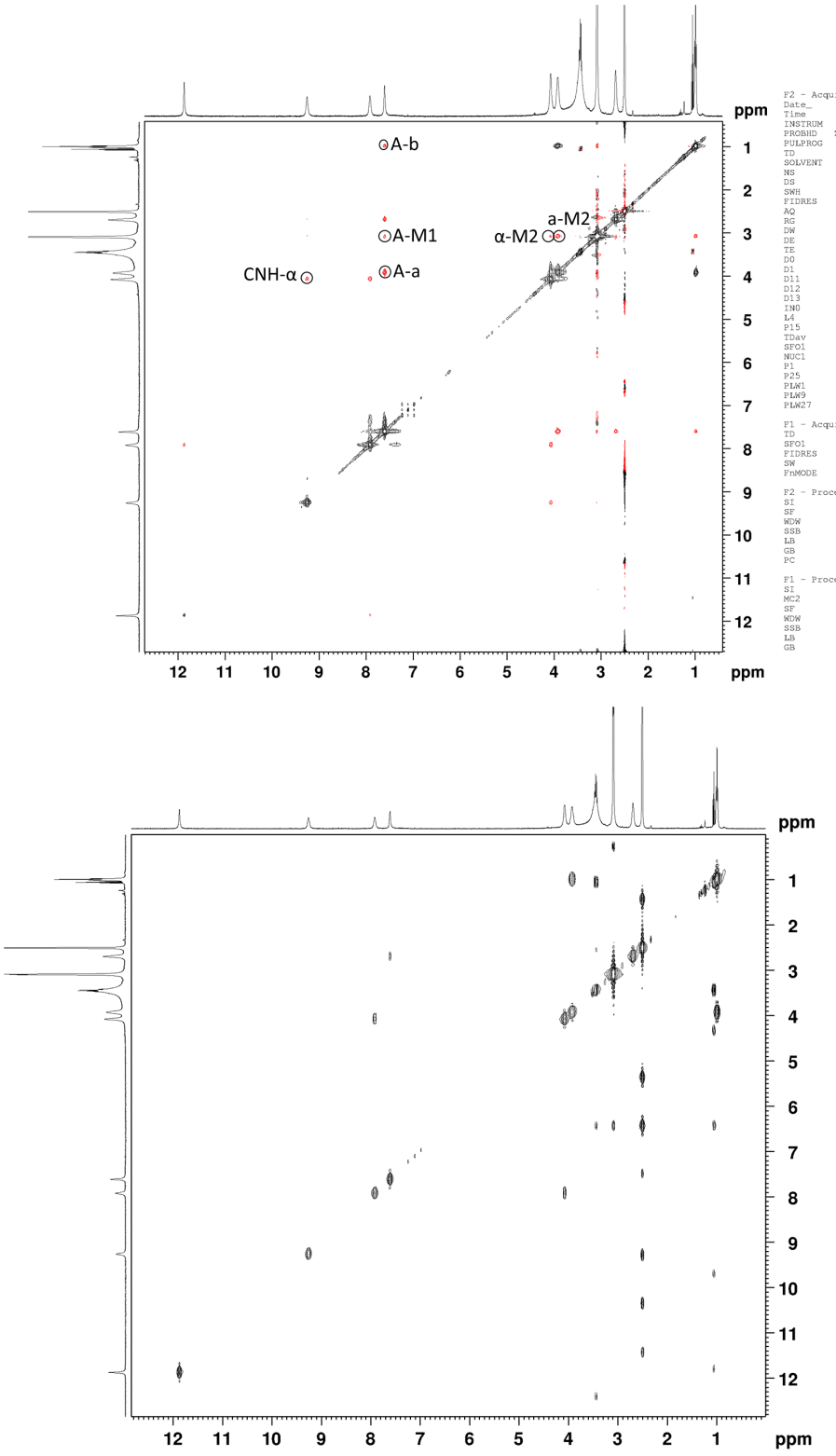

Figure S49. The 400 MHz rOesy and COSY NMR Spectrum of $\mathbf{G^{NNiPr}}$ in DMSO.

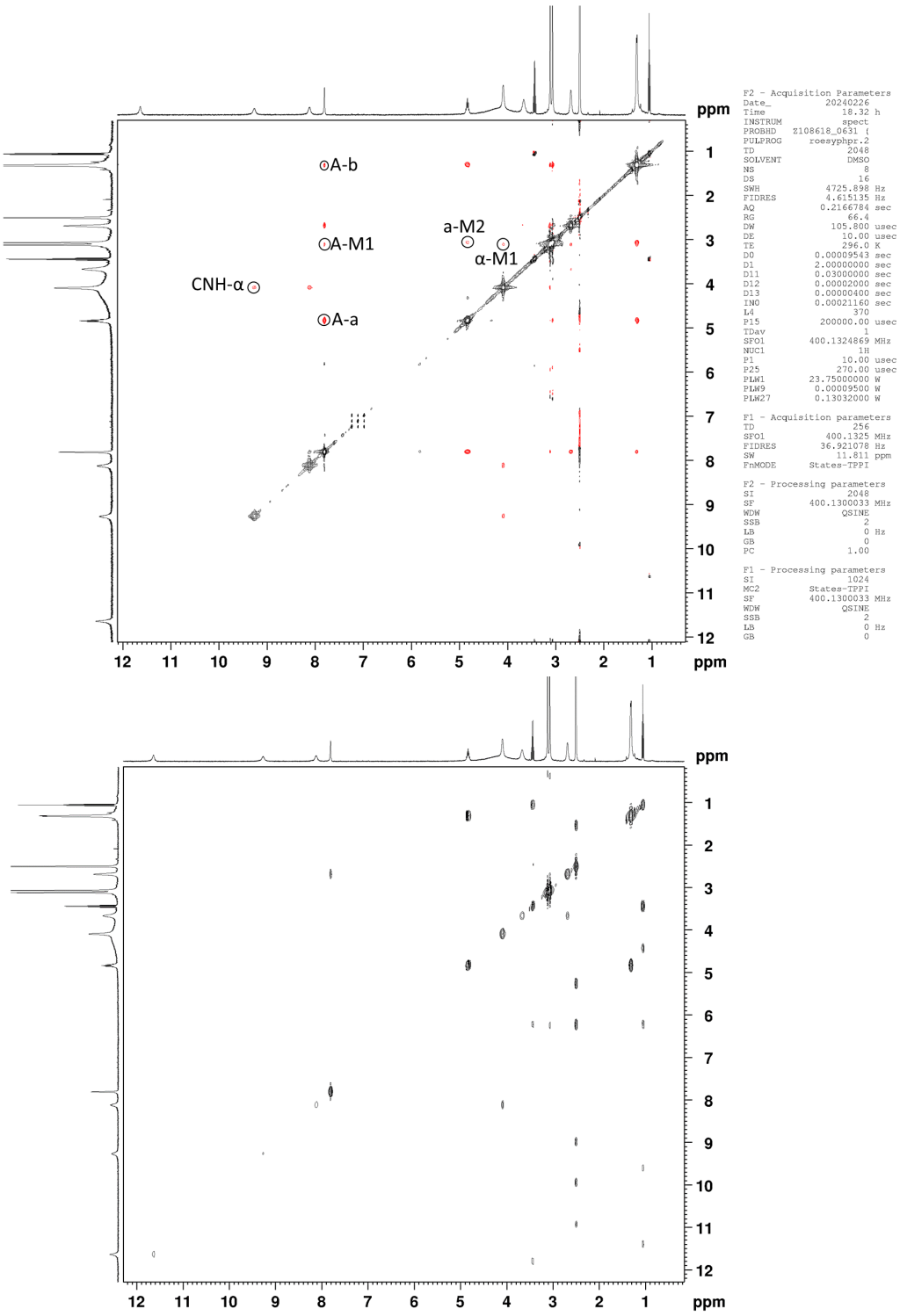

F2 - Acquisition Parameters
Date_ 20240226
Time 18.32 h
INSTRUM spect
PROBHD Z108618_0631 (
PULPROG roesyphpr.2
TD 2048
SOLVENT DMSO
NS 8
DS 16
SWH 4725.898 Hz
FIDRES 4.615135 Hz
AQ 0.2166784 sec
RG 66.4
DW 105.800 usec
DE 10.00 usec
TE 296.0 K
D0 0.00009543 sec
D1 2.00000000 sec
D11 0.03000000 sec
D12 0.00002000 sec
D13 0.00000400 sec
IN0 0.00021160 sec
L4 370
P15 200000.00 usec
TDav 1
SFO1 400.1324869 MHz
NUC1 1H
P1 10.00 usec
P25 270.00 usec
PLW1 23.75000000 W
PLW9 0.00009500 W
PLW27 0.13032000 W

F1 - Acquisition parameters
TD 256
SFO1 400.1325 MHz
FIDRES 36.921078 Hz
SW 11.811 ppm
FnMODE States-TPPI

F2 - Processing parameters
SI 2048
SF 400.1300033 MHz
WDW QSINE
SSB 2
LB 0 Hz
GB 0
PC 1.00

F1 - Processing parameters
SI 1024
MC2 States-TPPI
SF 400.1300033 MHz
WDW QSINE
SSB 2
LB 0 Hz
GB 0

Figure S50. The 400 MHz rOesy and COSY NMR Spectrum of $\mathbf{G^{NNBn}}$ in DMSO.

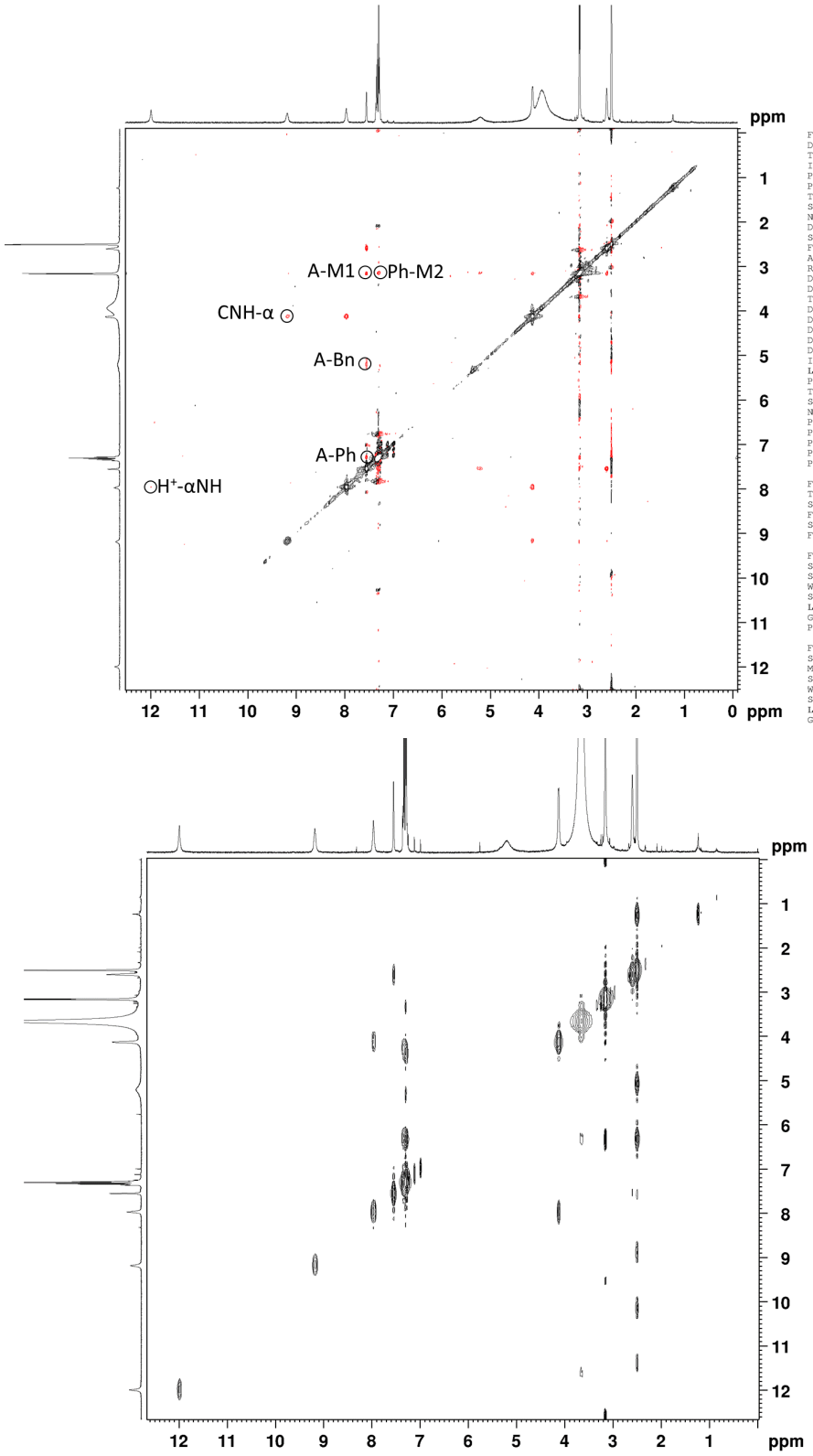

Figure S51. The 400 MHz rOesy and COSY NMR Spectra of **G**$^{\mathbf{NNHx}}$ in DMSO.

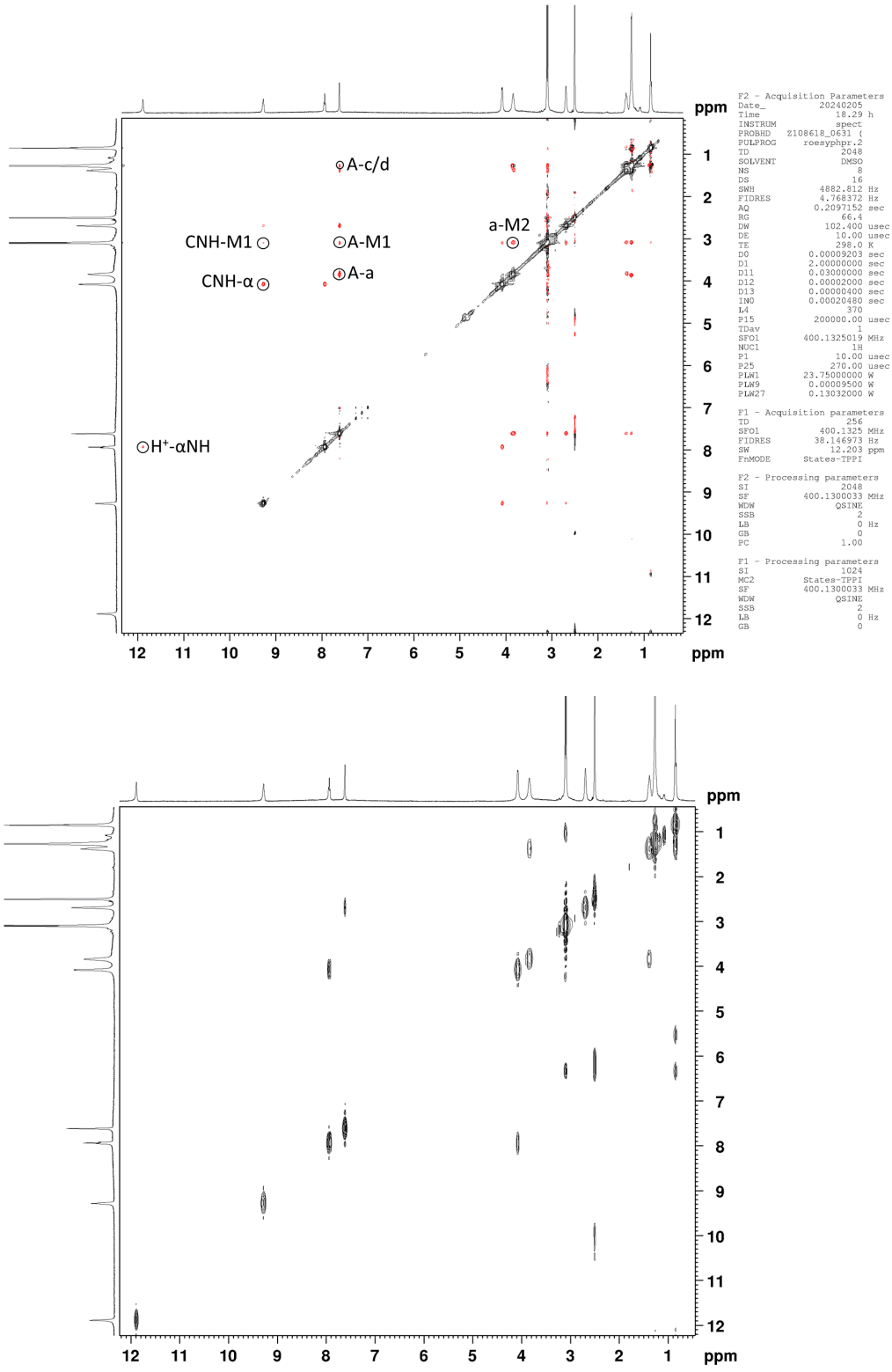

Figure S52. HRMS (ESI) of **G**^{NNMe}.

Elmt	Val.	Min	Max	Elmt	Val.	Min	Max	Elmt	Val.	Min	Max	Use Adduct
H	1	0	300	O	2	0	2	S	2	0	0	H
C	4	0	22	F	1	0	0	Cu	2	0	0	
N	3	0	16	Si	4	0	0					

Error Margin (ppm):	10	DBE Range:	-2.0 - 1000.0	Electron Ions:	both
HC Ratio:	unlimited	Apply N Rule:	yes	Use MSn Info:	no
Max Isotopes:	all	Isotope RI (%):	1.00	Isotope Res:	10000
MSn Iso RI (%):	75.00	MSn Logic Mode:	AND	Max Results:	500

Event#: 1 MS(E+) Ret. Time : 0.180 Scan# : 28

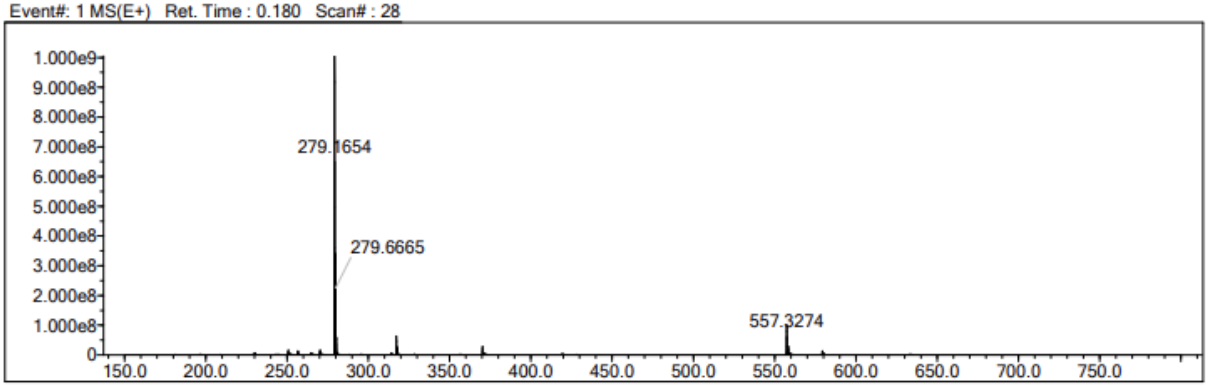

Measured region for 557.3274 m/z

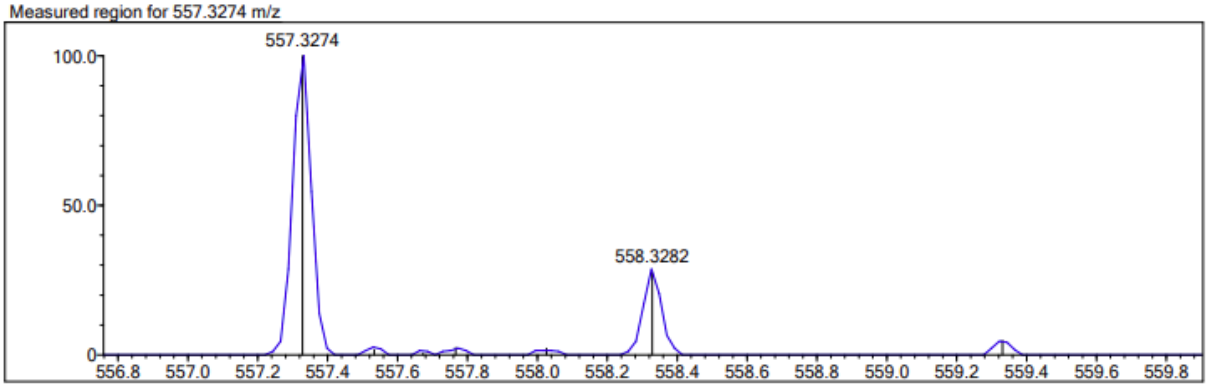

C22 H36 N16 O2 [M+H]+ : Predicted region for 557.3280 m/z

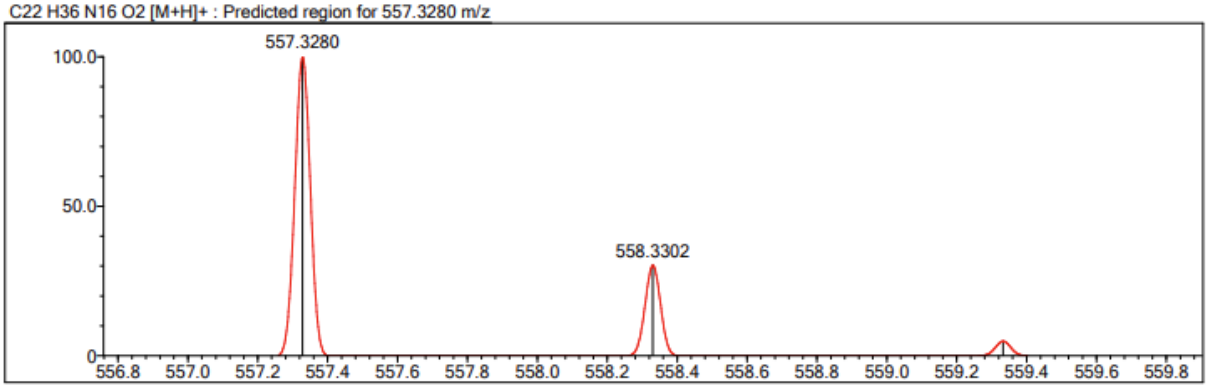

Rank	Score	Formula (M)	Ion	Meas. m/z	Pred. m/z	Df. (mDa)	Df. (ppm)	Iso	DBE
1	96.42	C22 H36 N16 O2	[M+H]+	557.3274	557.3280	-0.6	-1.08	96.62	13.0

Figure S53. HRMS (ESI) of **G^{NNEt}**.

Elmt	Val.	Min	Max	Elmt	Val.	Min	Max	Elmt	Val.	Min	Max	Use Adduct
H	1	0	300	O	2	0	2	S	2	0	0	H
C	4	0	24	F	1	0	0	Cu	2	0	0	
N	3	0	16	Si	4	0	0					

Error Margin (ppm):	10	DBE Range:	-2.0 - 1000.0	Electron Ions:	both
HC Ratio:	unlimited	Apply N Rule:	yes	Use MSn Info:	no
Max Isotopes:	all	Isotope RI (%):	1.00	Isotope Res:	10000
MSn Iso RI (%):	75.00	MSn Logic Mode:	AND	Max Results:	500

Event#: 1 MS(E+) Ret. Time : 0.287 Scan# : 44

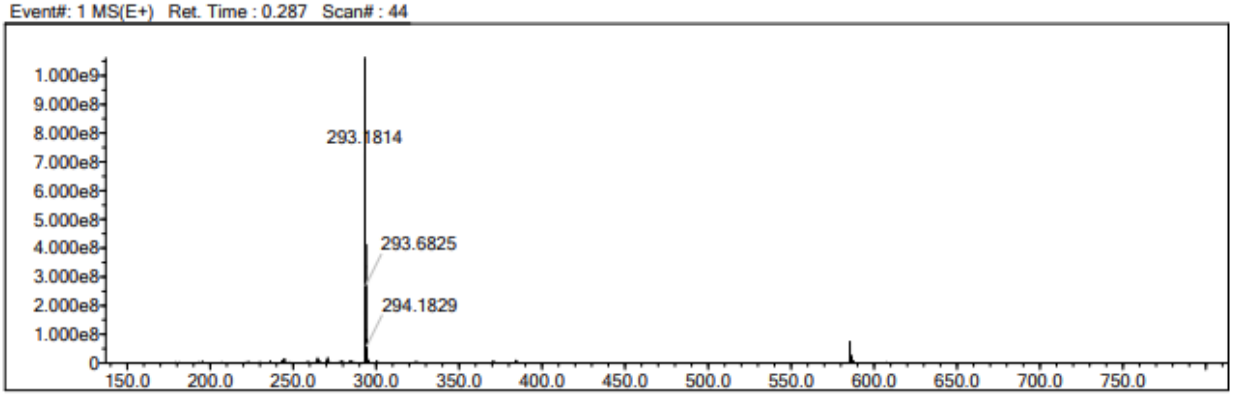

Measured region for 585.3572 m/z

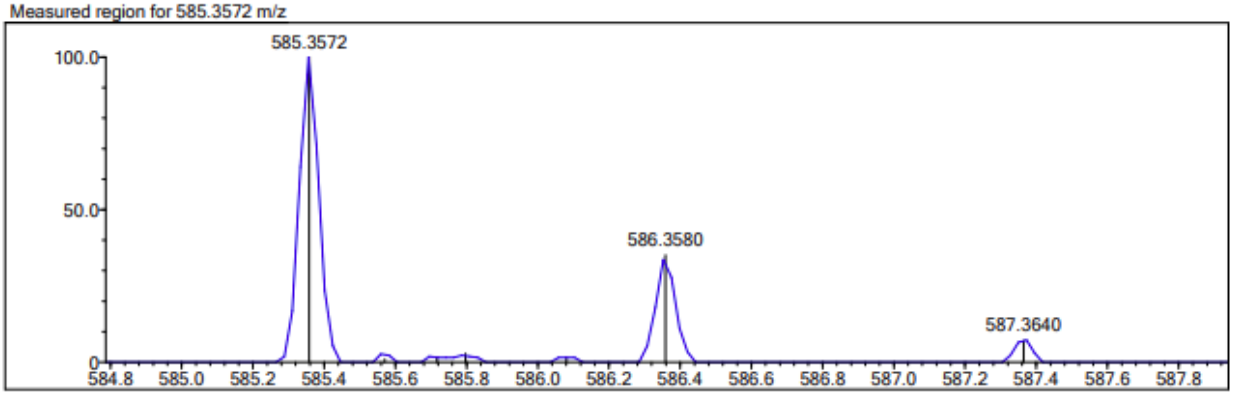

C24 H40 N16 O2 [M+H]+ : Predicted region for 585.3593 m/z

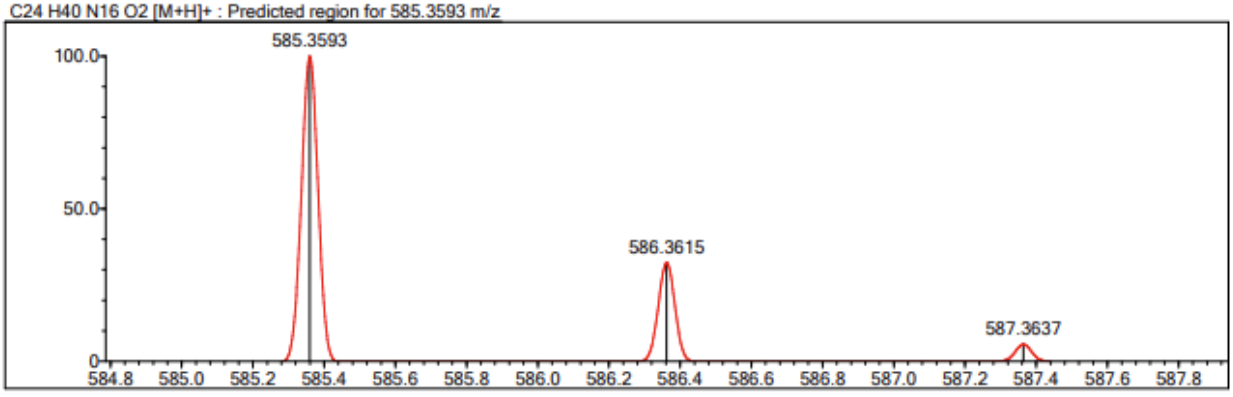

Rank	Score	Formula (M)	Ion	Meas. m/z	Pred. m/z	Df. (mDa)	Df. (ppm)	Iso	DBE
1	86.23	C24 H40 N16 O2	[M+H]+	585.3572	585.3593	-2.1	-3.59	92.20	13.0

Figure S54. HRMS (ESI) of **G**^{NNiPr}.

Elmt	Val.	Min	Max	Elmt	Val.	Min	Max	Elmt	Val.	Min	Max	Use Adduct
H	1	0	300	O	2	0	2	S	2	0	0	H
C	4	0	26	F	1	0	0	Cu	2	0	0	
N	3	0	16	Si	4	0	0					

Error Margin (ppm): 10
HC Ratio: unlimited
Max Isotopes: all
MSn Iso RI (%): 75.00

DBE Range: -2.0 - 1000.0
Apply N Rule: yes
Isotope RI (%): 1.00
MSn Logic Mode: AND

Electron Ions: both
Use MSn Info: no
Isotope Res: 10000
Max Results: 500

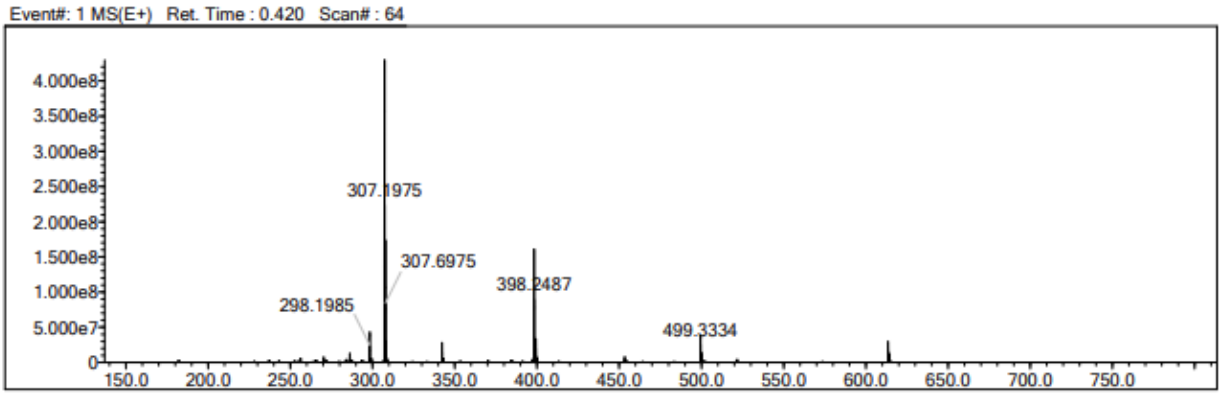

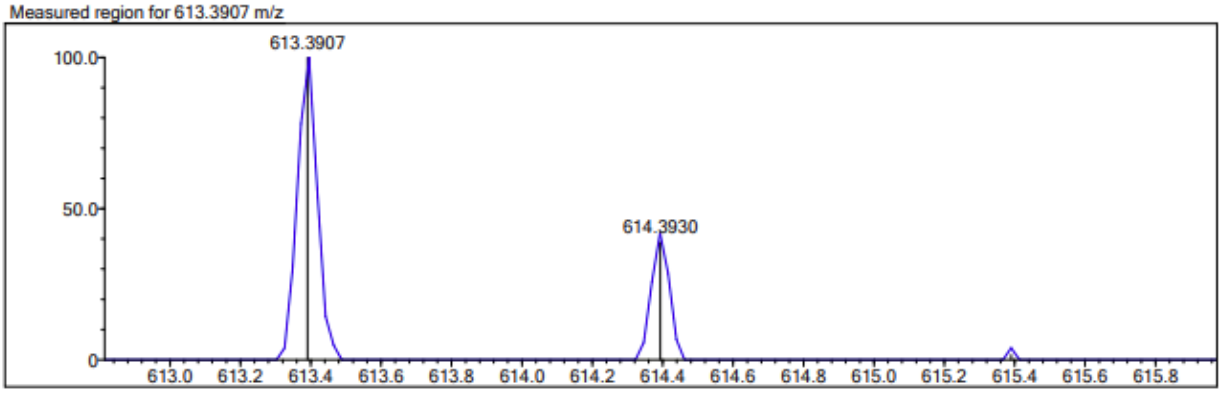

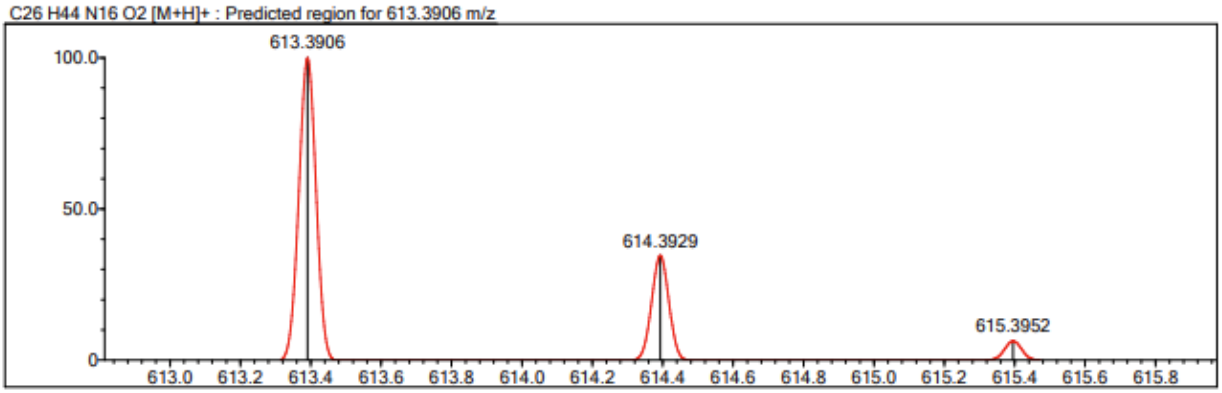

Rank	Score	Formula (M)	Ion	Meas. m/z	Pred. m/z	Df. (mDa)	Df. (ppm)	Iso	DBE
1	76.53	C26 H44 N16 O2	[M+H]+	613.3907	613.3906	0.1	0.16	76.53	13.0

Figure S55. HRMS (ESI) of $\mathbf{G}^{\mathbf{NNBn}}$.

Elmt	Val.	Min	Max	Elmt	Val.	Min	Max	Elmt	Val.	Min	Max	Use Adduct
H	1	0	300	O	2	0	2	S	2	0	0	H
C	4	0	34	F	1	0	0	Cu	2	0	0	
N	3	0	16	Si	4	0	0					

Error Margin (ppm): 10
HC Ratio: unlimited
Max Isotopes: all
MSn Iso RI (%): 75.00

DBE Range: -2.0 - 1000.0
Apply N Rule: yes
Isotope RI (%): 1.00
MSn Logic Mode: AND

Electron Ions: both
Use MSn Info: no
Isotope Res: 10000
Max Results: 500

Event#: 1 MS(E+) Ret. Time : 0.300 Scan# : 46

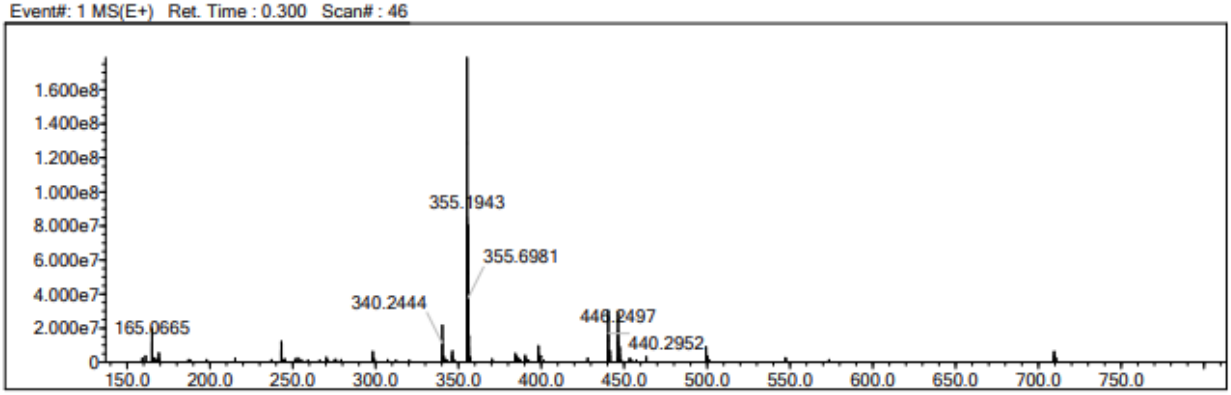

Measured region for 709.3896 m/z

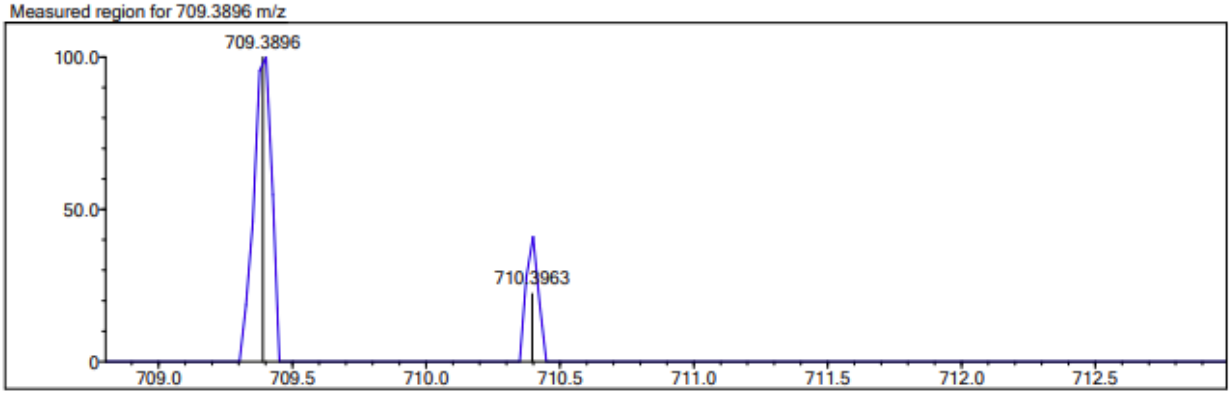

C34 H44 N16 O2 [M+H]+ : Predicted region for 709.3906 m/z

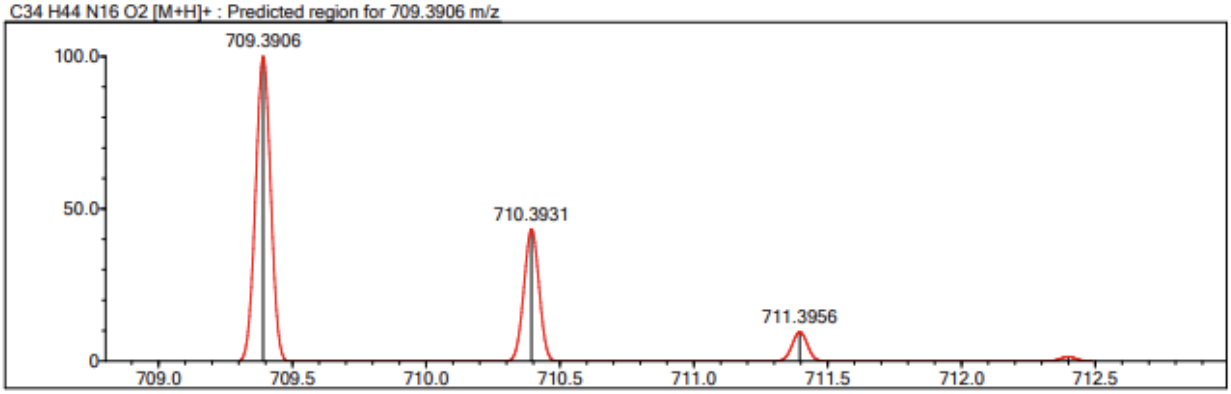

Rank	Score	Formula (M)	Ion	Meas. m/z	Pred. m/z	Df. (mDa)	Df. (ppm)	Iso	DBE
1	0.00	C34 H44 N16 O2	[M+H]+	709.3896	709.3906	-1.0	-1.41	0.00	21.0

Figure S56. HRMS (ESI) of $\mathbf{G}^{\mathbf{NNHx}}$.

Elmt	Val.	Min	Max	Elmt	Val.	Min	Max	Elmt	Val.	Min	Max	Use Adduct
H	1	0	300	O	2	0	2	S	2	0	0	H
C	4	0	32	F	1	0	0	Cu	2	0	0	
N	3	0	16	Si	4	0	0					

Error Margin (ppm): 10
HC Ratio: unlimited
Max Isotopes: all
MSn Iso RI (%): 75.00

DBE Range: -2.0 - 1000.0
Apply N Rule: yes
Isotope RI (%): 1.00
MSn Logic Mode: AND

Electron Ions: both
Use MSn Info: no
Isotope Res: 10000
Max Results: 500

Event#: 1 MS(E+) Ret. Time : 0.307 Scan# : 47

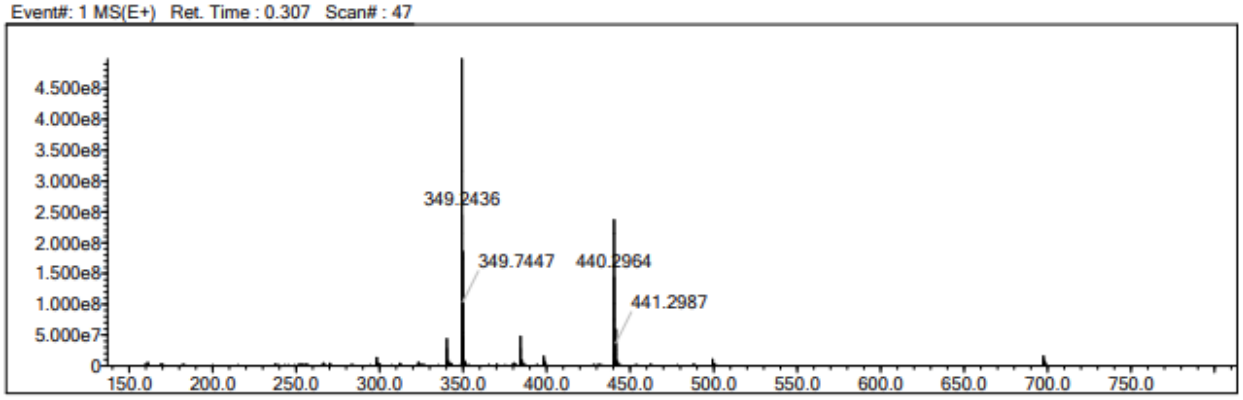

Measured region for 697.4863 m/z

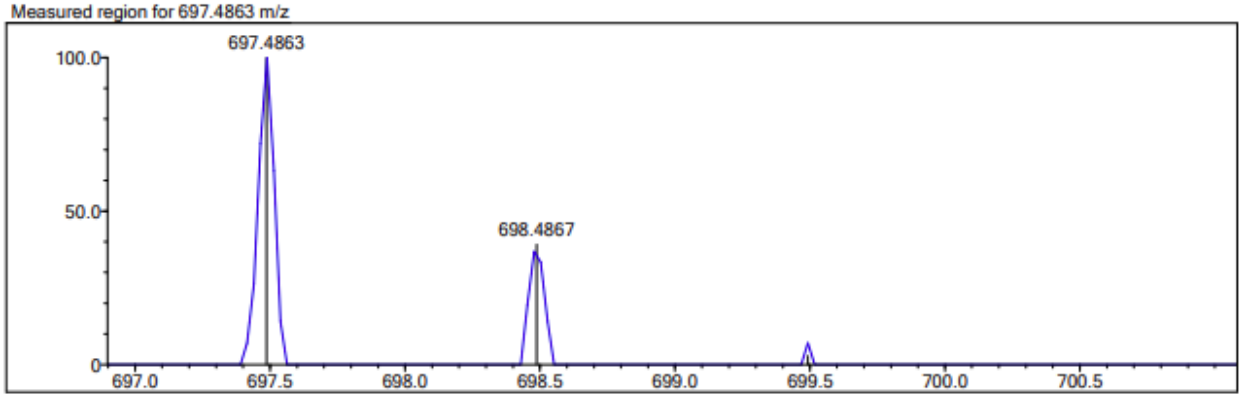

C32 H56 N16 O2 [M+H]+ : Predicted region for 697.4845 m/z

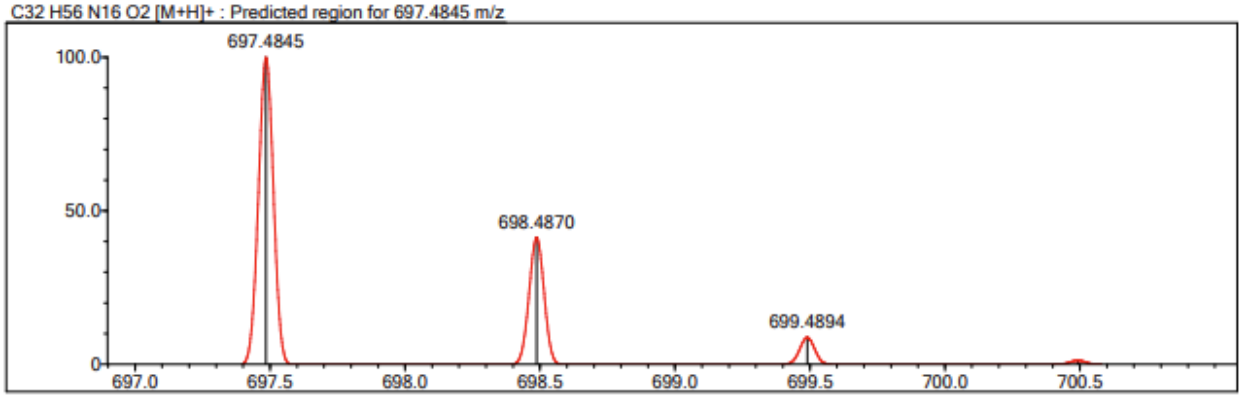

Rank	Score	Formula (M)	Ion	Meas. m/z	Pred. m/z	Df. (mDa)	Df. (ppm)	Iso	DBE
1	74.16	C32 H56 N16 O2	[M+H]+	697.4863	697.4845	1.8	2.58	77.21	13.0

GENERAL CHEMISTRY

Flash chromatography experiments were carried out on silica gel with a porosity of 60 Å, particle size 50–63 μm, surface area 500 – 600 m^2/g, a bulk density of 0.4 g/mL and a pH range of 6.5 – 7.5. Dichloromethane/methanol, chloroform/methanol, or ethyl acetate/hexanes were used as eluents for chromatographic purification. Thin-layer chromatography (TLC) was carried out in sealed chambers and visualized by UV absorption with following ninhydrin stain (1.5 g ninhydrin in 500 mL of isopropyl alcohol and 3.0 mL acetic acid) followed by heating. Excess solvent (e.g. post extraction, column chromatography, etc.) was removed *via* rotary evaporation on a Buchi Rotavapor R200 with a Welch Self-Cleaning Dry Vacuum System. All workup and purification procedures were carried out with reagent-grade solvents under ambient atmosphere. Abbreviations are as follows: BOC = *tert*-butyloxycarbonyl, TFA = trifluoroacetic acid, DCM = dichloromethane, THF = tetrahydrofuran, DMA = dimethylamine, HOBT = hydroxy benzotriazole, HBTU = hexafluorophosphate benzotriazole tetramethyl uronium, DIPEA = diisopropylethylamine, EDC = 1-ethyl-3-(3-dimethylaminopropyl)carbodiimide.

SYNTHESIS OF HYDRAZONES

General synthesis of non-commercially available hydrazones, deriving from the synthesis of **tert-butyl 2-benzylhydrazonecarboxylate**. Synthesis of the hydrazones was prepared by the imination of an aldehyde with tert-butyl carbazate as illustrated and described below.

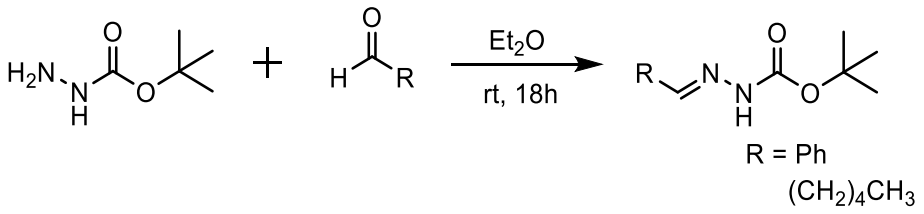

This procedure is a known synthesis.[C] Freshly distilled benzaldehyde (4.06 g, 38.3 mmol, 1.3 eq) was added to a solution of tert-butyl carbazate (3.6646 g, 27.7 mmol, 1 eq) in diethyl ether (18 mL, 1.5 M). The reaction was stirred for 18 hours and the precipitate was filtered and washed with cold diethyl ether. The precipitate then had excess solvent and ether removed *via* rotary evaporation, yielding pure **tert-butyl 2-benzylhydrazonecarboxylate** (5.573 g, 25.1 mmol, 90% yield) as a white powder.

HRMS (ESI) m/z: $[M + Na]^+$ Calculated for $C_{12}H_{16}N_2O_2$ 243.1104; Found 243.1089

^{1}H NMR ($CDCl_3$, 400 MHz): δ 8.04 (s, 1 H), 7.84 (s, 1 H), 7.68 (m, 2 H), 7.34 (m, 3 H), 1.53 (s, 9 H).

$^{13}C\{^1H\}$ NMR ($CDCl_3$, 100 MHz): δ 152.5, 143.7, 133.9, 129.8, 128.6, 127.2, 81.5, 28.3.

tert-Butyl 2-hexylhydrazonecarboxylate: Hexanal (2.0013 g, 20.0 mmol, 1.3 eq) was added to a solution of tert-butyl carbazate (2.0305 g, 15.4 mmol, 1 eq) in diethyl ether (10 mL, 1.5 M). The reaction was stirred for 11 hours and excess solvent was removed *via* rotary evaporation. The solid was then washed with cold diethyl ether over filter. The precipitate was isolated and residual diethyl ether was removed *via* rotary evaporation, affording pure **tert-butyl 2-hexylhydrazonecarboxylate** as a white flaky solid (3.111 g, 14.5 mmol, 94% yield).

HRMS (ESI) m/z: $[2M + H + Na]^{2+}$ Calculated for $C_{11}H_{22}N_2O_2$ 452.3327; Found 452.3262

^{1}H NMR ($CDCl_3$, 400 MHz): δ 7.62 (s, 1 H), 7.13 (t, *J* = 5.1 Hz, 1 H), 2.27 (td, *J* = 9.4, 5.1 Hz, 2 H), 1.53 – 1.45 (m, 11 H), 1.35 – 1.25 (m, 4 H), 0.88 (m, 3 H).

$^{13}C\{^1H\}$ NMR ($CDCl_3$, 100 MHz): δ 152.5, 147.5, 81.0, 32.2, 31.4, 28.3, 26.4, 22.4, 14.0.

Synthesis of **tert-butyl 2-benzylhydrazinecarboxylate** by palladium on carbon catalyzed reduction of the hydrazone.

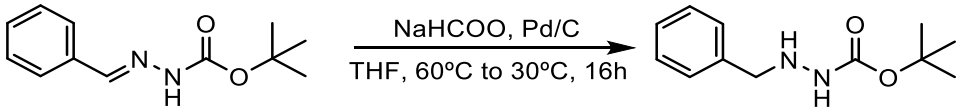

This procedure is a known synthesis.[D] **tert-Butyl 2-benzylhydrazonecarboxylate** (2.0392, 9.26 mmol, 1 eq) was added to a round-bottom flask along with 10% Pd/C (0.1972 g, 1.85 mmol, 0.2 eq) and sodium formate (1.1333 g, 16.64 mmol, 1.8 eq) along with 9.2 mL of 17% water in ethanol (1 M). The reaction was heated to 60°C and stirred for 1.5 hours. The temperature was then lowered to 30°C and stirred for 17 hours. The reaction was then filtered and washed with 50 mL EtOAc and 50 mL water. The solvent was then extracted twice with 50 mL EtOAc. The organic layer was dried with magnesium sulfate and filtered. Solvent was removed *via* rotary evaporation, yielding **tert-butyl 2-benzylhydrazinecarboxylate** along with a small amount of the hydrazone. The hydrazine/hydrazone mixture was utilized without further purification (1.649 g, 7.42 mmol, 80% crude yield), afforded as a flakey white powder.

HRMS (ESI) m/z: $[M + Na]^+$ Calculated for $C_{12}H_{18}N_2O_2$ 245.1266; Found 245.1241

^{1}H NMR ($CDCl_3$, 400 MHz): δ 7.39 – 7.31 (m, 6 H), 6.08 (m, 1 H), 4.00 (m, 2 H), 1.47 (s, 9 H).

$^{13}C\{^1H\}$ NMR ($CDCl_3$, 100 MHz): δ 152.5, 133.9, 129.0, 128.5, 127.5, 81.5, 55.8, 28.3.

Synthesis of **tert-butyl 2-hexylhydrazinecarboxylate** by TsOH catalyzed $NaCNBH_3$ reduction of the hydrazone.

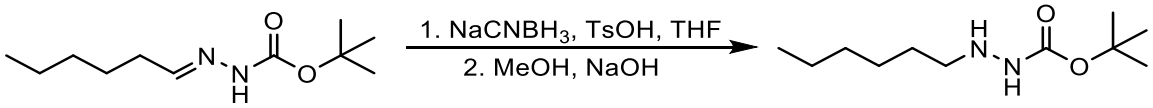

This procedure follows a known synthesis.[E] **tert-Butyl 2-hexylhydrazonecarboxylate** (2.5038, 11.7 mmol, 1 eq) in THF (75 mL, 0.16 M) was charged to a round-bottom flask. Sodium cyanoborohydride (0.750 g, 11.9 mmol, 1 eq) and bromocresol green were then added to the round-bottom flask with stirring, with an immediate dark blue color developing. *p*-Toluenesulfonic acid (2.0469 g, 11.9 mmol, 1 eq) in THF (75 mL, 0.16 M) was then carefully dripped in to the round-bottom flask over the course of an hour in order to maintain a pH between 3 – 5 (as evidenced by a light green color from the bromocresol green). Not all of the *p*-toluenesulfonic acid was added as the pH held steadily acidic after ~70mL of the acid solution was added. After 2 hours (1 hour since finishing adding the *p*-toluenesulfonic acid), saturated sodium carbonate in water was added to the round-bottom to turn the solution basic (development of a dark blue color) to prevent evolution of HCN gas. Solvent was then removed *via* rotary evaporation. The remaining solid was then extracted twice with 100 mL ethyl acetate and 100 mL saturated bicarbonate in water. The organic layer was isolated and ethyl acetate was removed *via* rotary evaporation. The resulting crude mixture was redissolved in methanol (35 mL) and 1M NaOH (15 mL, 0.2 M) and stirred for 2.5 hours. The solvent was removed *via* rotary evaporation. The resulting crude mixture was extracted twice with 100 mL ethyl acetate and 100 mL water. The organic layer was collected and dried with sodium sulfate and filtered. Ethyl acetate was then removed *via* rotary evaporation, and the crude reaction was purified with

column chromatography (275 mL silica, 15% ethyl acetate in hexanes to 25% ethyl acetate in hexanes), affording pure **tert-butyl 2-hexylhydrazinecarboxylate** (1.403 g, 6.5 mmol, 56% yield) as a clear oil.

HRMS (ESI) m/z: $[M + H]^+$ Calculated for $C_{11}H_{24}N_2O_2$ 217.1911; Found 217.1896

^1H NMR ($CDCl_3$, 400 MHz): δ 6.06 (m, 1 H), 3.92 (m, 1 H), 2.83 (m, 2 H), 1.69 – 1.39 (m, 2 H), 1.46 (s, 9 H), 1.37 – 1.24 (m, 6 H), 0.88 (m, 3 H).

$^{13}C\{^1H\}$ NMR ($CDCl_3$, 100 MHz): δ 156.8, 80.3, 52.1, 31.8, 28.4, 27.8, 26.8, 22.6, 14.0.

Figure S57. The 400 MHz ^{1}H and 100 MHz ^{13}C NMR Spectra of **tert-butyl 2-benzylhydrazonecarboxylate** in $CDCl_3$.

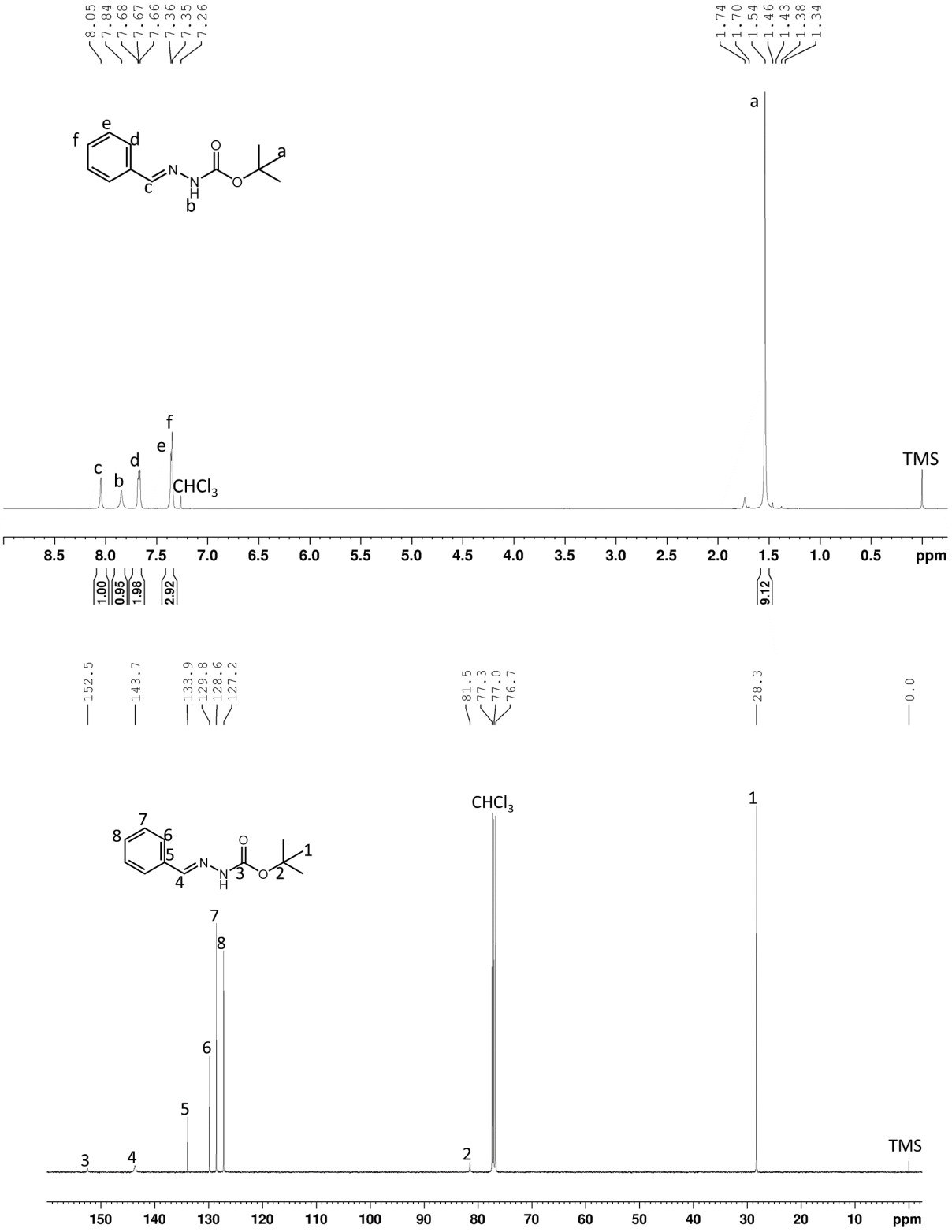

Figure S58. The 400MHz ^{1}H and 100 MHz ^{13}C NMR Spectra of **tert-butyl 2-hexylhydrazonecarboxylate** in $CDCl_3$.

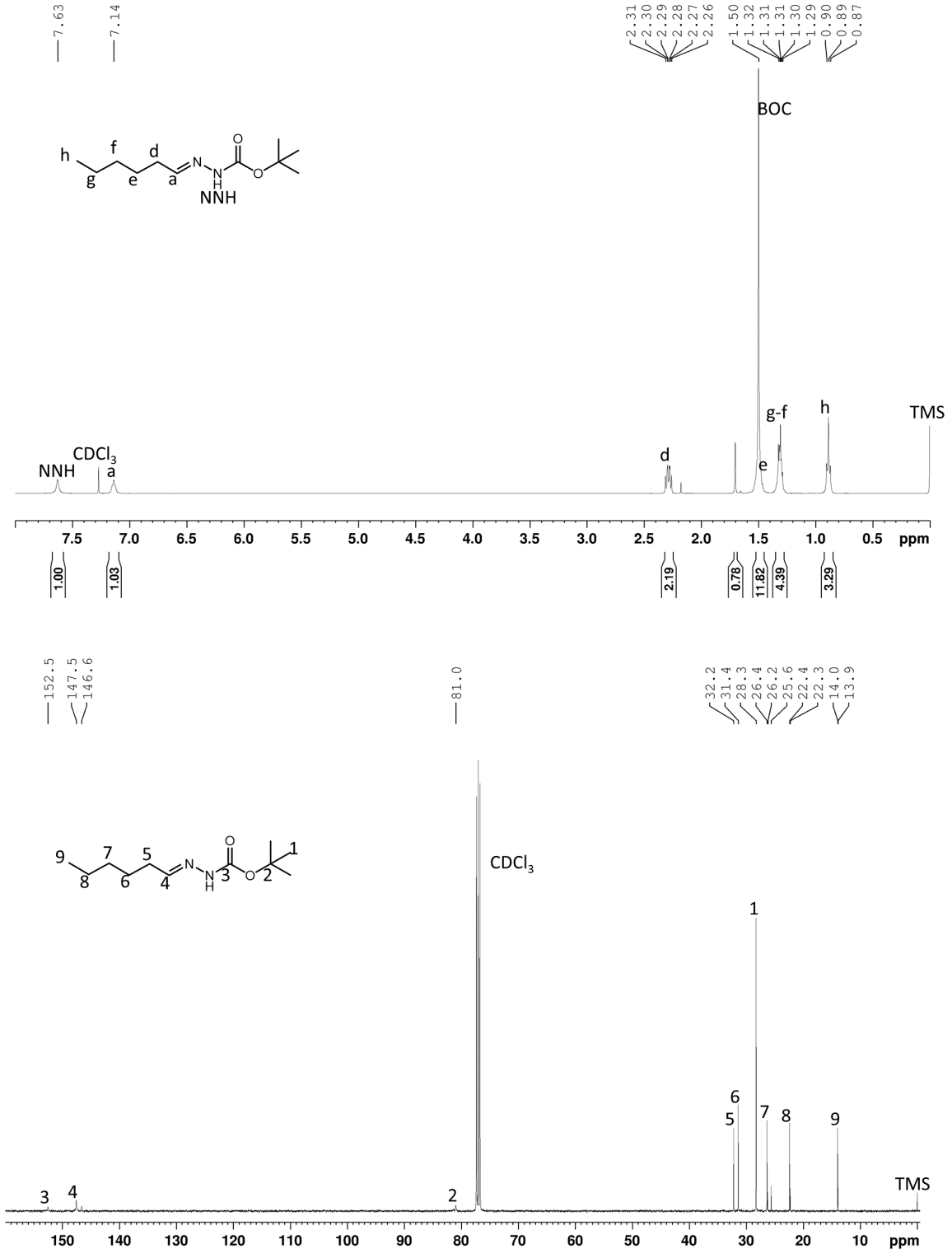

Figure S59. The 400 MHz ^{1}H and 100 MHz ^{13}C NMR Spectra of **tert-butyl 2-benzylhydrazinecarboxylate** in $CDCl_3$.

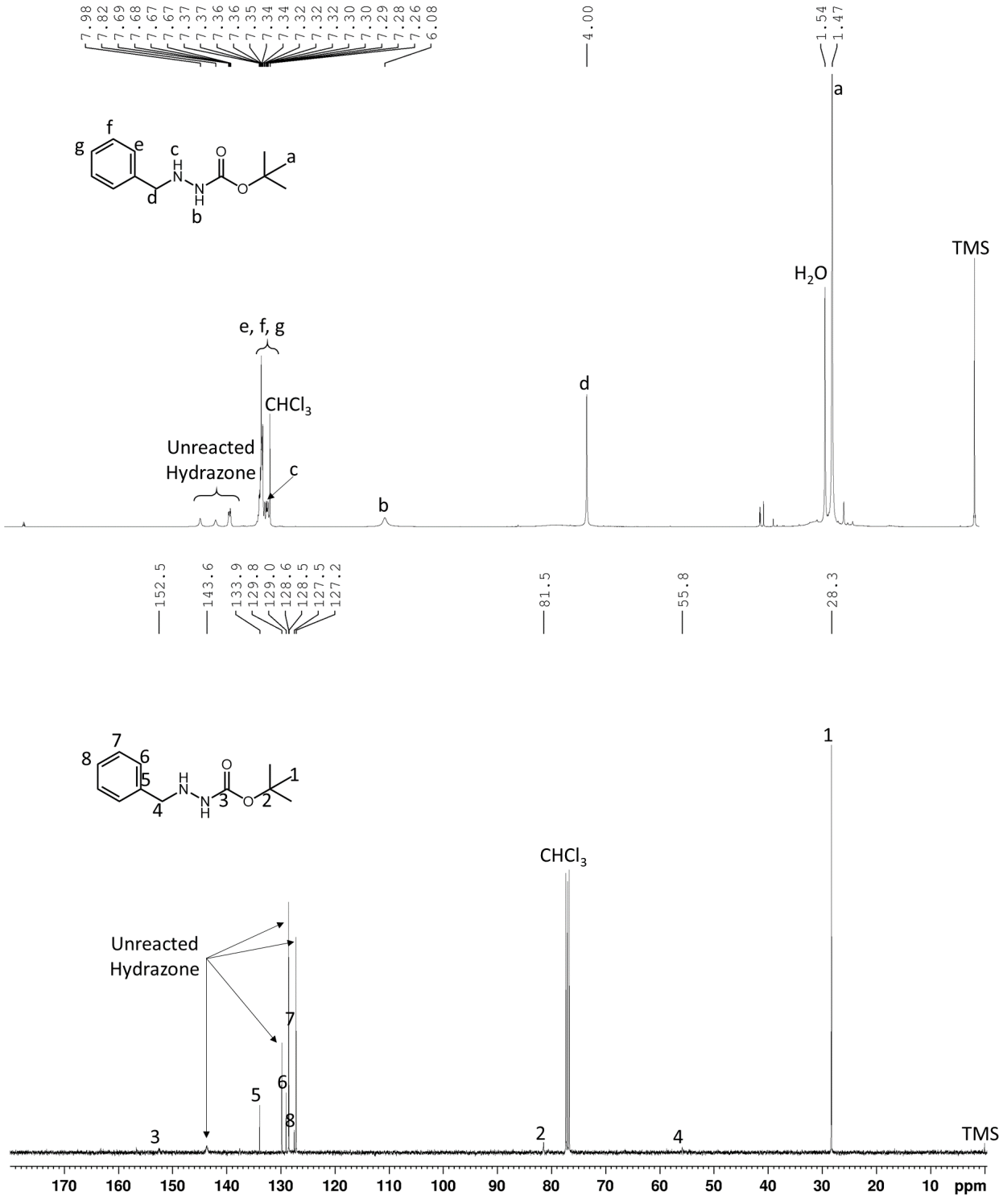

Figure S60. The 400 MHz ^{1}H and 100 MHz ^{13}C Spectra of **tert-Butyl 2-hexylhydrazinecarboxylate** in $CDCl_3$.

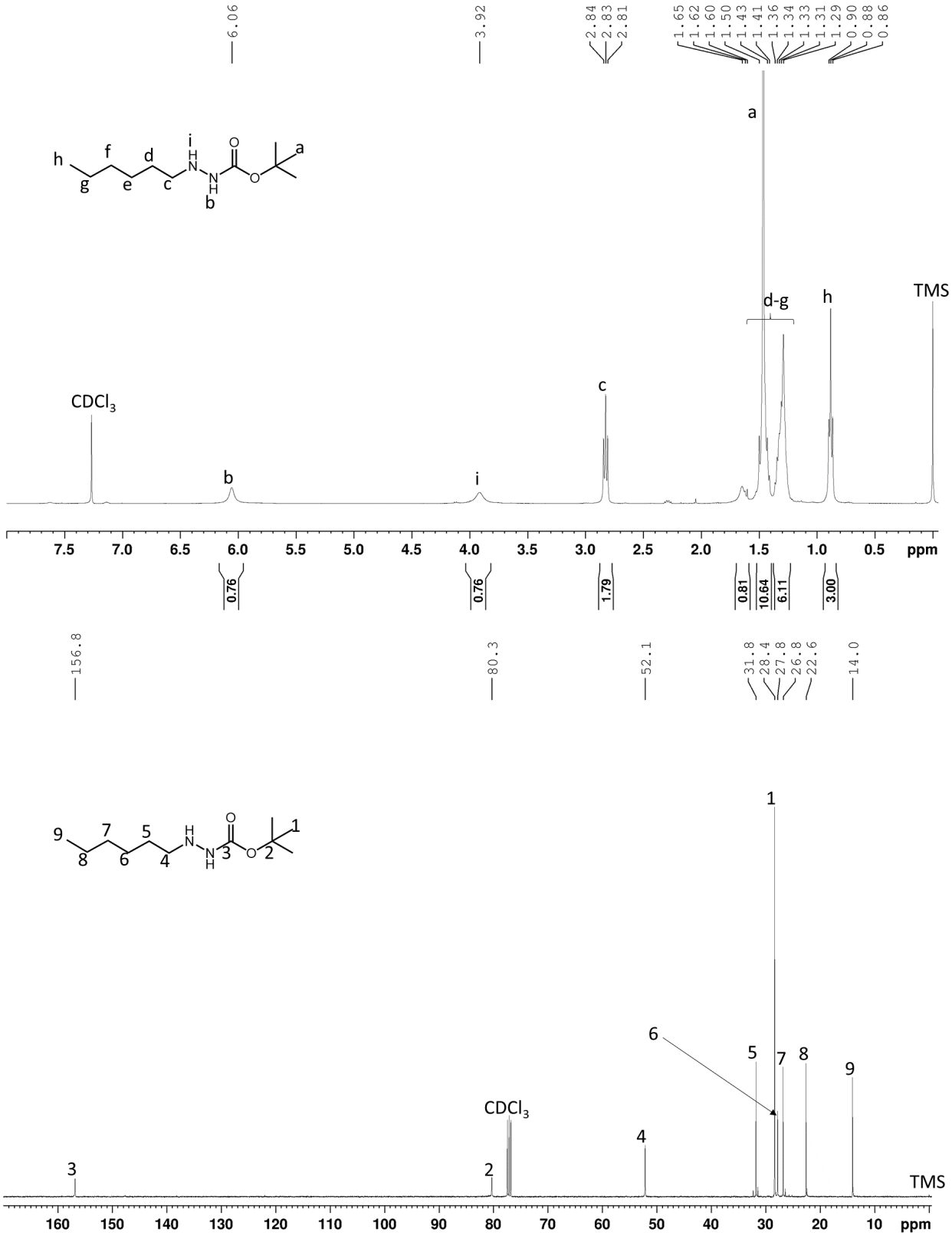

Figure S61. HRMS (ESI) of **tert-butyl 2-hexylhydrazonecarboxylate**.

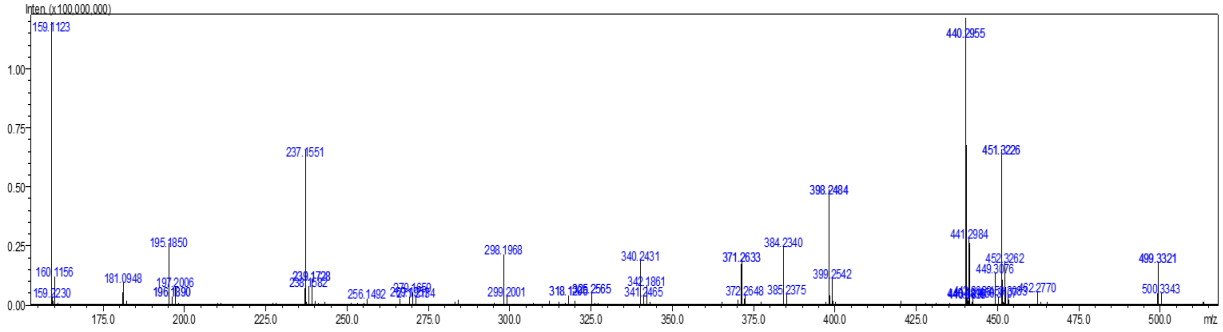

Figure S62. HRMS (ESI) of **tert-butyl 2-hexylhydrazinecarboxylate**.

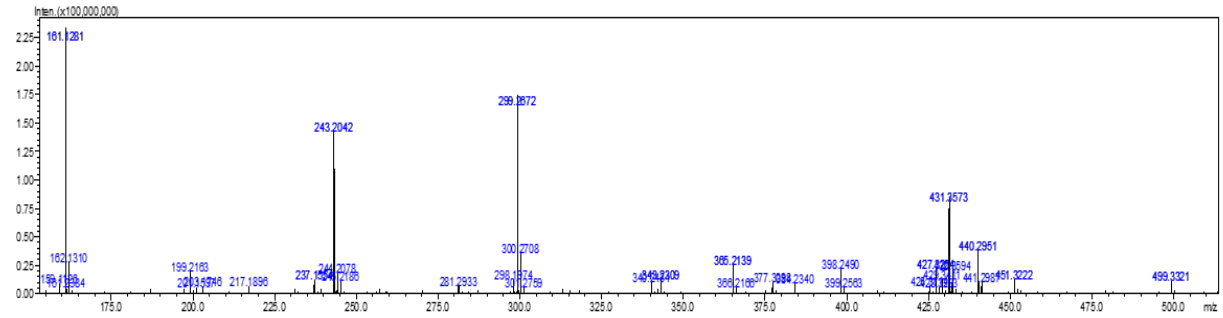

Figure S63. HRMS (ESI) of **tert-Butyl 2-benzylhydrazinecarboxylate**.

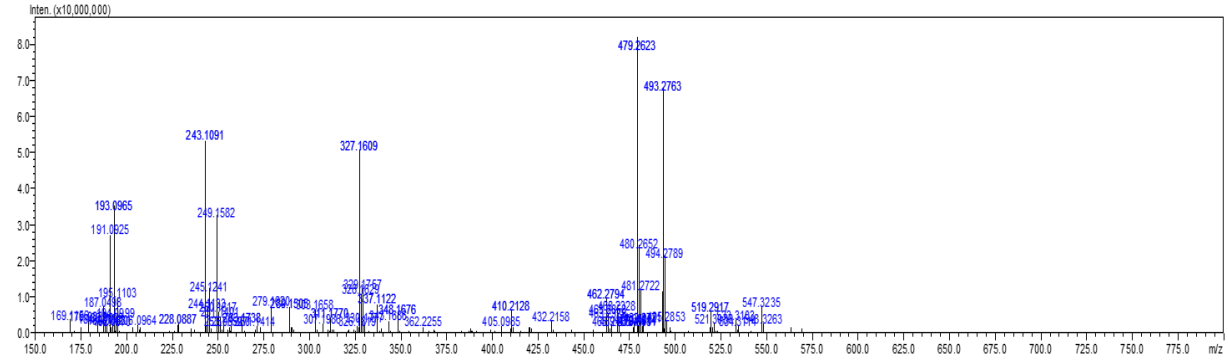

Figure S64. HRMS (ESI) of **tert-butyl 2-benzylhydrazonecarboxylate**.

Elmt	Val.	Min	Max	Elmt	Val.	Min	Max	Elmt	Val.	Min	Max	Use Adduct
H	1	0	300	O	2	0	2	S	2	0	0	H
C	4	0	12	F	1	0	0	Cu	2	0	0	Na
N	3	0	2	Si	4	0	0					

Error Margin (ppm):	10	DBE Range:	-2.0 - 1000.0	Electron Ions:	both
HC Ratio:	unlimited	Apply N Rule:	yes	Use MSn Info:	no
Max Isotopes:	all	Isotope RI (%):	1.00	Isotope Res:	10000
MSn Iso RI (%):	75.00	MSn Logic Mode:	AND	Max Results:	500

Event#: 1 MS(E+) Ret. Time : 0.100 Scan# : 16

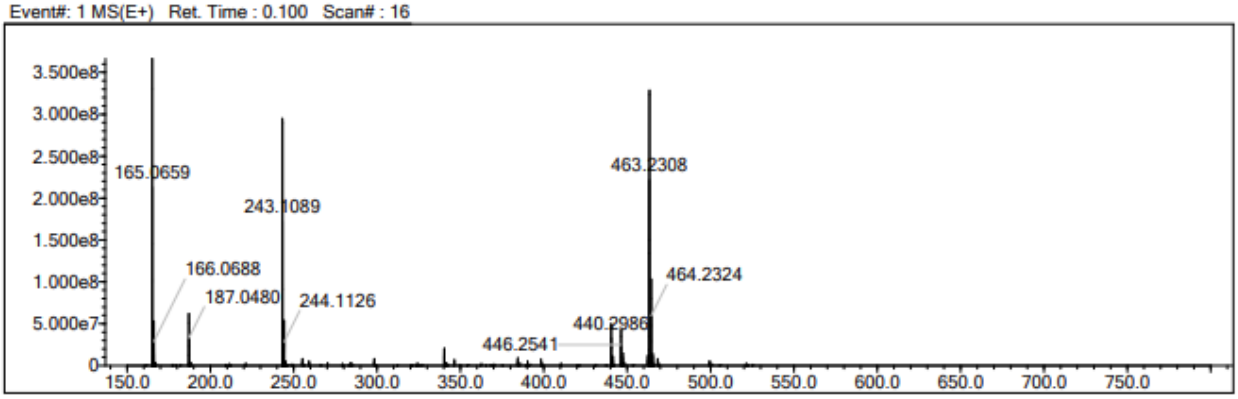

Measured region for 243.1089 m/z

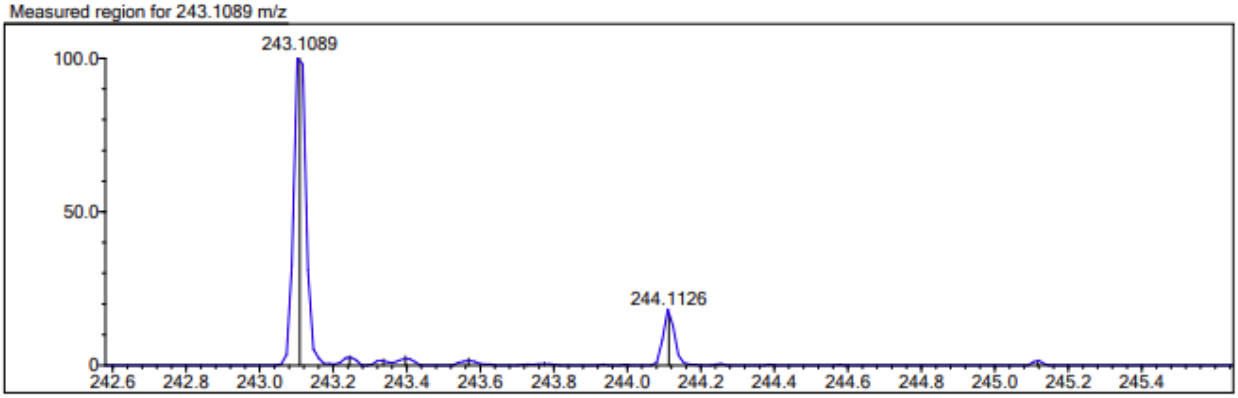

C12 H16 N2 O2 [M+Na]+ : Predicted region for 243.1104 m/z

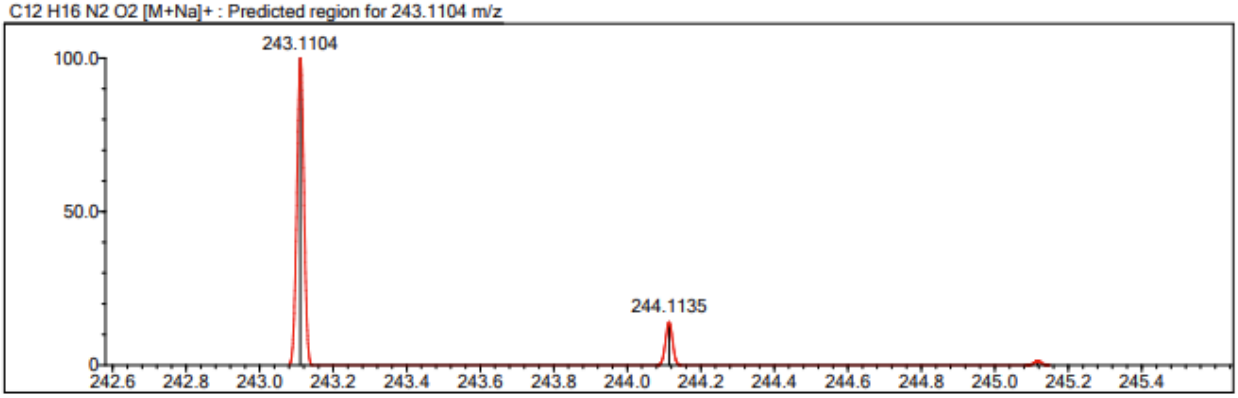

Rank	Score	Formula (M)	Ion	Meas. m/z	Pred. m/z	Df. (mDa)	Df. (ppm)	Iso	DBE
1	74.81	C12 H16 N2 O2	[M+Na]+	243.1089	243.1104	-1.5	-6.17	95.54	6.0

SYNTHESIS OF ESTERS

General synthesis of ester products derived from the synthesis of **G^{NNHx}-Ester**. Synthesis of the esters was conducted by a one-pot sequential addition to the starting cyanuric chloride as illustrated and described below.

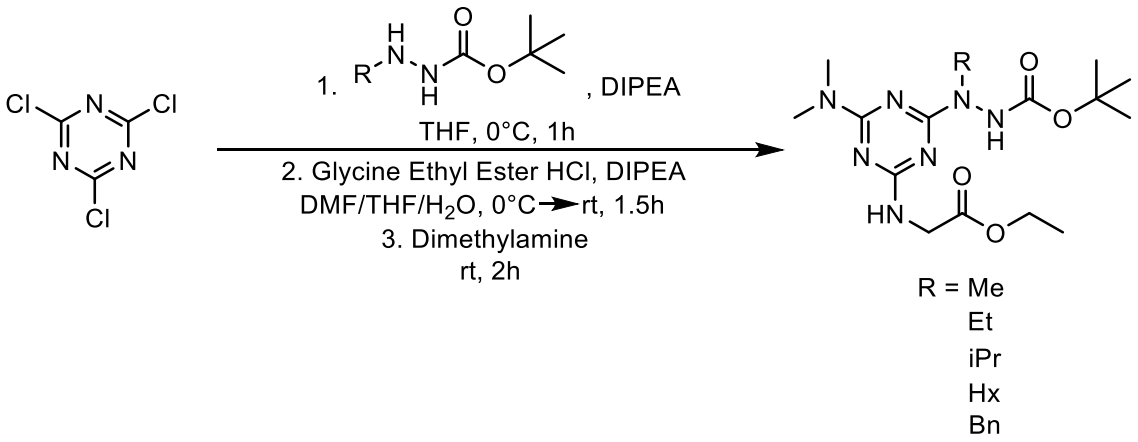

A round-bottom flask was charged with cyanuric chloride (0.2435 g, 1.3 mmol, 1 eq) in THF (13 mL, 0.1 M). The solution was cooled to 0°C with an ice/water bath. tert-Butyl 2-hexylhydrazinecarboxylate (0.2857 g, 1.3 mmol, 1 eq) in THF (13 mL, 0.1 M) and DIPEA (0.3426 g, 2.7 mmol, 2 eq) was then dripped in to the round-bottom flask at 1 drop/second. After the tert-butyl 2-hexylhydrazinecarboxylate had fully dripped in, the ice/water bath was removed. The reaction had finished after 2.5 hours. The reaction was then concentrated *via* rotary evaporation and resuspended in 6 mL of DMF (0.2 M) and cooled to 0°C with an ice/water bath. Glycine ethyl ester hydrochloride (0.1844 g, 1.3 mmol, 1 eq) in DMF (6 mL, 0.2 M) and DIPEA (0.3526 g, 2.7 mmol, 2 eq) was then dripped into the round-bottom flask at 1 drop/second. Deionized water was dripped in to the reaction to solubilize the glycine ethyl ester hydrochloride (~1.5 mL). Once the glycine ethyl ester hydrochloride solution had fully dripped in, the ice/water bath was removed. After an hour of reaction time, extra DIPEA (0.3891 g, 3.0 mmol, 2.3 eq) was added to the reaction to bring the pH to 10. The reaction finished after 1.5 hours. Dimethylamine 40% in water (0.1693 g of the 40% solution, 1.5 mmol, 1.1 eq) was then added to the round-bottom flask. After 40 minutes of stirring, DIPEA (0.1875 g, 1.5 mmol, 1.1 eq) was added to bring the pH from 7 to 8. Extra dimethylamine (0.1081 g of the 40% solution, 1.0 mmol, 0.7 eq) was added after 1.5 hours of reacting. The reaction finished after 2 hours of stirring. The solvent was removed by rotary evaporation and extracted thrice with 75 mL of ethyl acetate and 70 mL of brine. The organic layer was collected and dried with magnesium sulfate and filtered. The ethyl acetate was then removed *via* rotary evaporation, affording crude **G^{NNHx}-Ester**. The crude mixture was purified *via* column chromatography with 75 mL SiO_2 and 25% ethyl acetate in hexanes, affording pure **G^{NNHx}-Ester** (0.479 g, 1.1 mmol, 83% yield).

HRMS (ESI) m/z: $[M + H]^+$ Calculated for $C_{20}H_{37}N_7O_4$ 440.2980; Found 440.2961

^{1}H NMR (DMSO, 400 MHz): δ 8.92 – 8.31 (s, 1 H), 7.30 – 6.85 (m, 1 H), 4.07 (m, 2 H), 3.85 (d, *J* = 5.6 Hz, 2 H), 3.63 – 3.46 (m, 2 H), 3.00 (s, 6 H), 1.54 – 1.37 (m, 2 H), 1.40 (s, 9 H), 1.32 – 1.21 (m, 6 H), 1.17 (m, 3 H), 0.85 (m, 3 H).

^{13}C{^{1}H} NMR (DMSO, 100 MHz): δ 170.8, 166.6, 165.9, 165.1, 155.5, 78.8, 60.0, 48.7, 42.4, 35.4, 35.2, 31.1, 30.9, 28.1, 27.0, 25.8, 14.2, 14.1.

G^{NNEt}-Ester: A round-bottom flask was charged with cyanuric chloride (0.1964 g, 1.1 mmol, 1 eq) in THF (12 mL, 0.1 M). The solution was cooled to 0°C with an ice/water bath. tert-Butyl 2-ethylhydrazinecarboxylate (0.1706 g, 1.1 mmol, 1 eq) in THF (12 mL, 0.1 M) and DIPEA (0.3031 g, 2.4 mmol, 2.2 eq) was then dripped into the round-bottom flask at 1 drop/second. 15 minutes after the tert-butyl 2-ethylhydrazinecarboxylate had fully dripped in, the ice/water bath was removed. The reaction had finished after 1 hour. The reaction was then concentrated *via* rotary evaporation and resuspended in 5.5 mL of DMF (0.2 M) and cooled to 0°C with an ice/water bath. Glycine ethyl ester hydrochloride (0.1486 g, 1.1 mmol, 1 eq) in DMF (5.5 mL, 0.2 M) and DIPEA (0.5585 g, 4.3 mmol, 4.1 eq) was then dripped into the round-bottom flask at 1 drop/second. The ice/water bath was removed an hour after the glycine ethyl ester solution had dripped in. The reaction finished after 1.5 hours. Dimethylamine 40% in water (0.2489 g of the 40% solution, 2.2 mmol, 2 eq) was then added to the round-bottom flask. The reaction finished after 1.5 hours of stirring. The solvent was removed by rotary evaporation and extracted thrice with 75 mL of ethyl acetate and 75 mL of brine. The organic layer was collected and dried with magnesium sulfate and filtered. The ethyl acetate was then removed *via* rotary evaporation, affording crude **G^{NNEt}-Ester**. The crude mixture was purified *via* column chromatography with 75 mL SiO_2 and 25% to 50% ethyl acetate in hexanes, affording pure **G^{NNEt}-Ester** (0.325 g, 0.85 mmol, 80% yield).

HRMS (ESI) m/z: $[M + H]^+$ Calculated for $C_{16}H_{29}N_7O_4$ 384.2354; Found 384.2337

^{1}H NMR (DMSO, 400 MHz): δ 8.92 – 8.28 (s, 1 H), 7.30 – 6.91 (m, 1 H), 4.07 (m, 2 H), 3.85 (d, *J* = 5.2 Hz, 2 H), 3.66 – 3.51 (m, 2 H), 3.00 (s, 6 H), 1.45 – 1.22 (s, 9 H), 1.17 (m, 3 H), 1.11 – 0.80 (m, 3 H).

^{13}C{^{1}H} NMR (DMSO, 100 MHz): δ 170.4, 166.1, 165.7, 165.1, 155.6, 78.8, 60.0, 42.6, 35.4, 35.2, 28.2, 14.2, 12.5.

G^{NNMe}-Ester: A round-bottom flask was charged with cyanuric chloride (0.2495 g, 1.4 mmol, 1 eq) in THF (14 mL, 0.1 M) and cooled to 0°C with an ice/water bath. tert-Butyl 2-methylhydrazinecarboxylate (0.1978, 1.4 mmol, 1 eq) and DIPEA (0.4203 g, 3.3 mmol, 2.4 eq) in THF (14 mL, 0.1 M) was then added dropwise *via* a pressure-equalized addition funnel at a rate of 1 drop/second. The reaction finished 15 minutes after the hydrazine finished dripping in. Excess THF was then removed *via* rotary evaporation, and the reaction was then resuspended in THF (7 mL, 0.2 M). Glycine ethyl ester hydrochloride (0.1890 g, 1.4 mmol, 1 eq) and DIPEA (1.0470 g, 8.1 mmol, 6 eq) in methanol (7 mL, 0.2 M) was then added dropwise to the initial reaction in a 10°C water bath. The ice bath was removed 20 minutes after the glycine finished dripping in. The reaction finished after another 2 hours. Dimethylamine 40% in water (0.4410 g of the 40% solution, 3.9 mmol, 2.9 eq) was then added to the round-bottom flask. The reaction finished after 1.5 hours. The reaction was then concentrated down *via* rotary evaporation and was extracted with 50 mL ethyl acetate and 100 mL of water, followed by 50 mL of brine. The organic layer was collected and dried with

magnesium sulfate and filtered. The filtrate was collected and crude **G^{NNMe}-Ester** was obtained after rotary evaporation. The crude reaction was then purified with column chromatography using 50 mL of SiO_2 and 5% methanol in chloroform, affording pure **G^{NNMe}-Ester** (0.468 g, 1.3 mmol, 94% yield).

HRMS (ESI) m/z: $[M + H]^+$ Calculated for $C_{15}H_{27}N_7O_4$ 370.2197; Found 370.2182

^{1}H NMR (DMSO, 400 MHz): δ 8.99 – 8.42 (s, 1 H), 7.28 – 6.97 (m, 1 H), 4.08 (q, *J* = 7.0 Hz, 2 H), 3.85 (m, 2 H), 3.18 – 3.07 (s, 3 H), 3.00 (s, 6 H), 1.43 – 1.26 (s, 9 H), 1.17 (t, *J* = 7.0 Hz, 3 H).

^{13}C{^{1}H} NMR (DMSO, 100 MHz): δ 170.8, 166.9, 165.5, 165.1, 155.3, 79.0, 60.0, 42.6, 37.4, 35.2, 28.2, 14.2.

G^{NNiPr}-Ester: Cyanuric chloride (0.5293 g, 2.9 mmol, 1 eq) in THF (30 mL, 0.1 M) was charged to a round-bottom flask and cooled to 0°C with an ice/water bath. tert-Butyl 2-isopropylhydrazinecarboxylate (0.5005 g, 2.9 mmol, 1 eq) and DIPEA (0.8247 g, 6.4 mmol, 2.2 eq) in THF (30 mL, 0.1 M) was then dripped in to the round-bottom flask at a rate of 1 drop/second. The water/ice bath was removed after the tert-Butyl 2-isopropylhydrazinecarboxylate solution finished adding. The reaction was left to go for 2 hours, after which the reaction had finished. The solution was then concentrated *via* rotary evaporation and then resuspended in DMF (15 mL, 0.2 M). Glycine ethyl ester hydrochloride (0.4008 g, 2.9 mmol, 1 eq) and DIPEA (1.1247 g, 8.7 mmol, 3 eq) in 2:1 DMF:MeOH (15 mL, 0.2 M) was then added dropwise to the round-bottom flask. The reaction finished after 1.5 hours of stirring. Dimethylamine 40% in water (0.6600 g of the 40% solution, 5.9 mmol, 2 eq) was then added to the round-bottom flask *via* pipette. The reaction had finished by TLC after 1.5 hours of stirring. The reaction was then concentrated down to 10 mL *via* rotary evaporation and extracted thrice with 50 mL ethyl acetate and 50 mL water. The organic layer was collected and dried with magnesium sulfate and then filtered. Solvent from the dried organic layer was then removed *via* rotary evaporation, affording crude **G^{NNiPr}-Ester**. The crude product was purified with column chromatography, using 200 mL SiO_2 and 7:2 hexanes:ethyl acetate, affording pure **G^{NNiPr}-Ester** (0.620 g, 1.6 mmol, 54% yield). Some fractions were contaminated with the monochlorotriazine (i.e., the intermediate that precedes the addition of dimethylamine), which upon inclusion with the pure **G^{NNiPr}-Ester** gives an adjusted crude yield of 1.108 g (2.8 mmol, 97% yield)

HRMS (ESI) m/z: $[M + H]^+$ Calculated for $C_{17}H_{31}N_7O_4$ 398.2483; Found 398.2465

^{1}H NMR (DMSO, 400 MHz): δ 8.56 – 8.03 (s, 1 H), 7.24 – 6.83 (m, 1 H), 4.88 – 4.64 (m, 1 H), 4.11 – 4.02 (m, 2 H), 3.85 (m, 2 H), 3.00 (s, 6 H), 1.44 – 1.22 (s, 9 H), 1.21 – 0.80 (m, 9 H).

^{13}C{^{1}H} NMR (DMSO, 100 MHz): δ 170.8, 170.4, 165.7, 165.5, 156.2, 78.6, 60.0, 46.8, 42.7, 35.4, 28.2, 19.4, 14.2.

G^{NNBn}-Ester: Cyanuric chloride (0.4547 g, 2.5 mmol, 1 eq) in THF (25 mL, 0.1 M) was charged to a round-bottom flask and cooled to 0°C with an ice/water bath. tert-Butyl 2-benzylhydrazinecarboxylate (0.5466 g, 2.5 mmol, 1 eq) in THF (25 mL, 0.1 M) and DIPEA (0.9526 g, 7.4 mmol, 3 eq) was then added dropwise to the round-bottom flask at a rate of 1 drop/second. The ice/water bath was removed after the hydrazine had finished dripping in, was left to stir for another 45 minutes. The reaction was then concentrated down *via* rotary evaporation and then resuspended in 12 mL of THF (0.2 M). The reaction was cooled to 0°C with

an ice/water bath. Glycine ethyl ester hydrochloride (0.3443 g, 2.5 mmol, 1 eq) in methanol (12 mL, 0.2 M) and DIPEA (0.9630, 7.5 mmol, 3 eq) was then added dropwise to the round-bottom flask. The ice/water bath was removed after 15 minutes of stirring. The reaction had finished after 40 minutes of stirring. Dimethylamine 40% in water (0.5609 g of the 40% solution, 4.9 mmol, 2 eq) was then added to the round-bottom flask at room temperature. The reaction finished after 1.25 hours of stirring. The reaction was concentrated *via* rotary evaporation and was extracted thrice with 50 mL of water and 50 mL of ethyl acetate. The organic layer was collected and dried with magnesium sulfate and concentrated down *via* rotary evaporation, affording crude **G^{NNBn}-Ester**. Column chromatography with 75 mL SiO_2 and 25% ethyl acetate in hexanes afforded pure **G^{NNBn}-Ester** (0.2952 g, 0.66 mmol, 27% yield) as a clear oil.

HRMS (ESI) m/z: $[M + H]^+$ Calculated for $C_{21}H_{31}N_7O_4$ 446.2510; Found 446.2494

^{1}H NMR (CD_3OD, 400 MHz): δ 7.39 – 7.19 (m, 5 H), 4.22 – 3.96 (m, 6 H), 3.08 (s, 6 H), 1.51 – 1.27 (s, 9 H), 1.24 (m, 3 H).

$^{13}C\{^1H\}$ NMR (CD_3OD, 100 MHz): δ 173.0, 167.7, 166.9, 163.1, 158.5, 139.4, 129.8, 129.3, 128.1, 81.5, 62.0, 53.7, 43.9, 36.4, 36.2, 30.8, 14.5.

Figure S65. The 400 MHz ^{1}H and 100 MHz ^{13}C NMR Spectra of **G^{NNMe}-Ester** in DMSO.

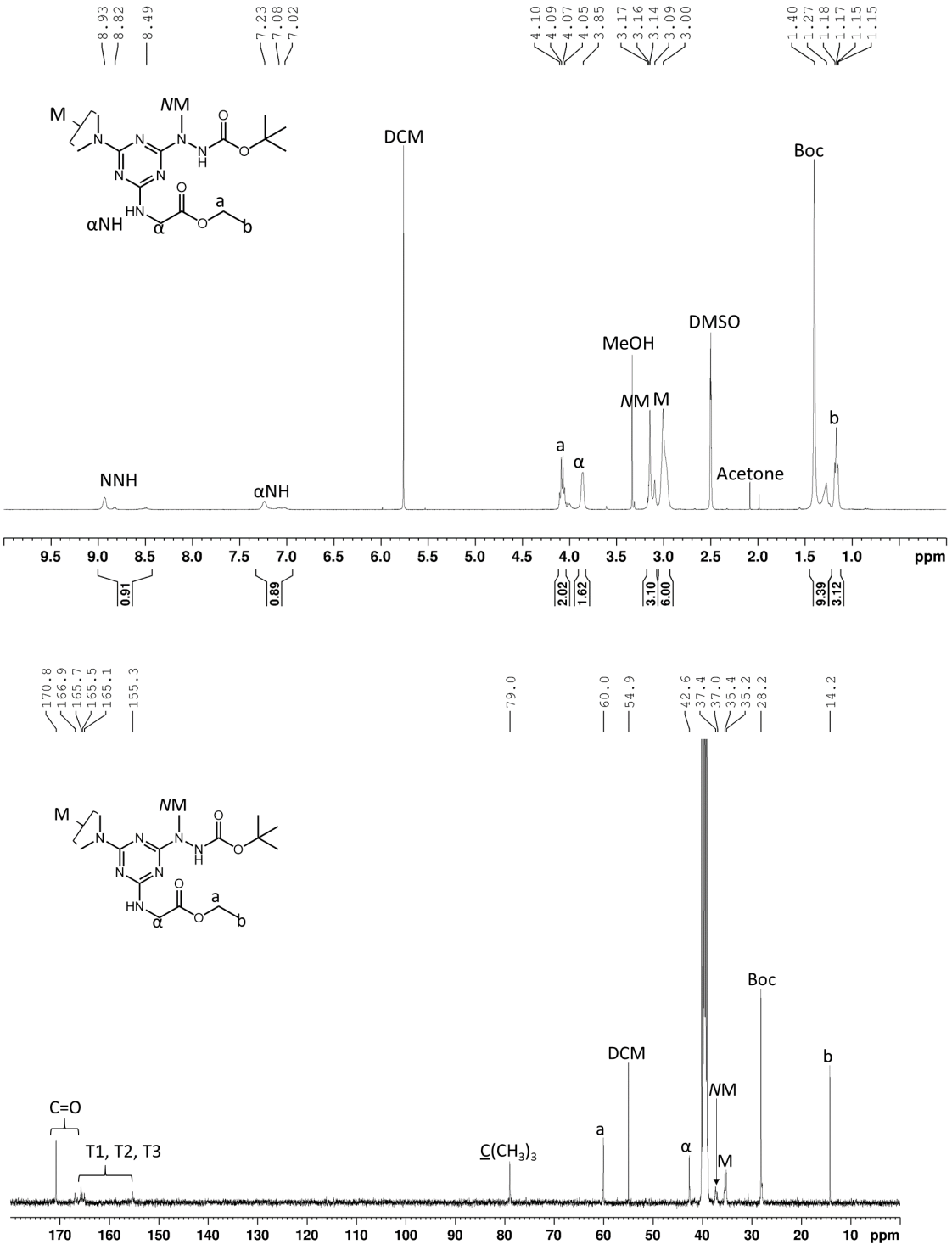

Figure S66. The 400 MHz ^{1}H and 100 MHz ^{13}C NMR Spectra of **G^{NNEt}-Ester** in DMSO.

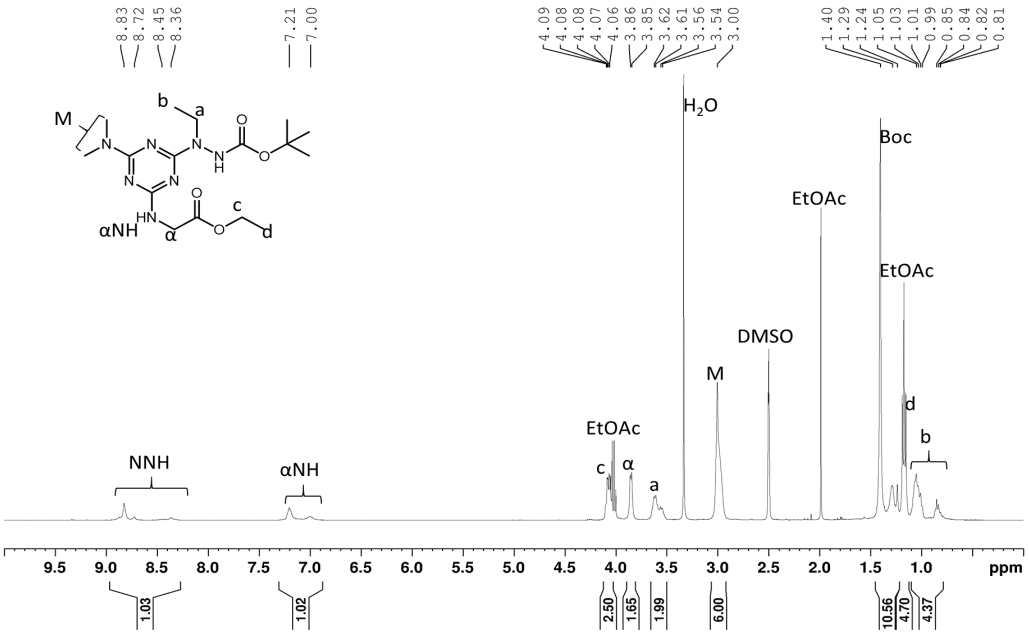

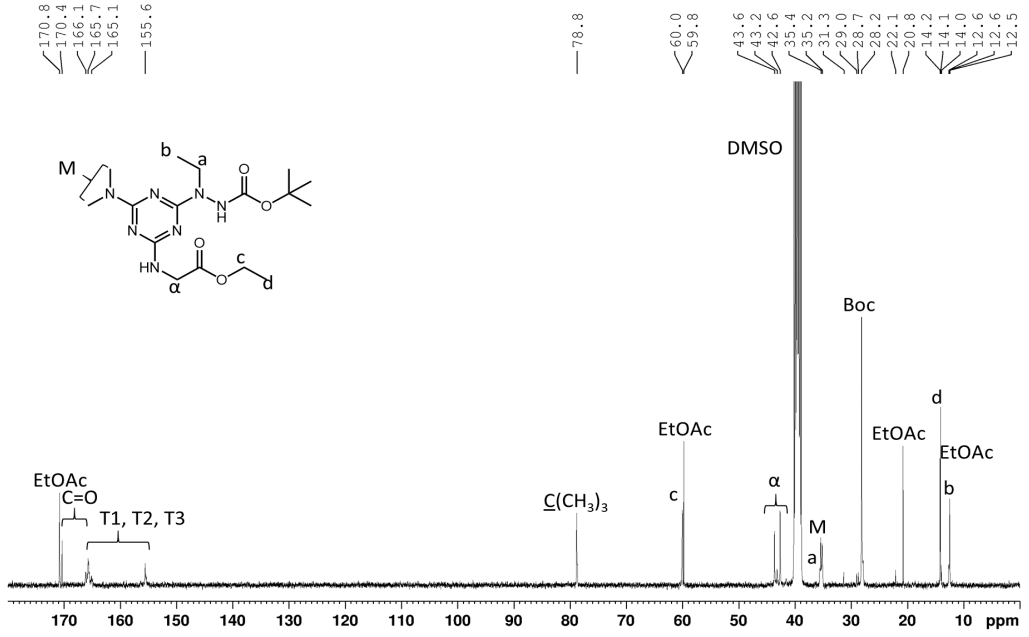

Figure S67. The 400 MHz ^{1}H and 100 MHz ^{13}C NMR Spectra of **G^{NNiPr}-Ester** in DMSO.

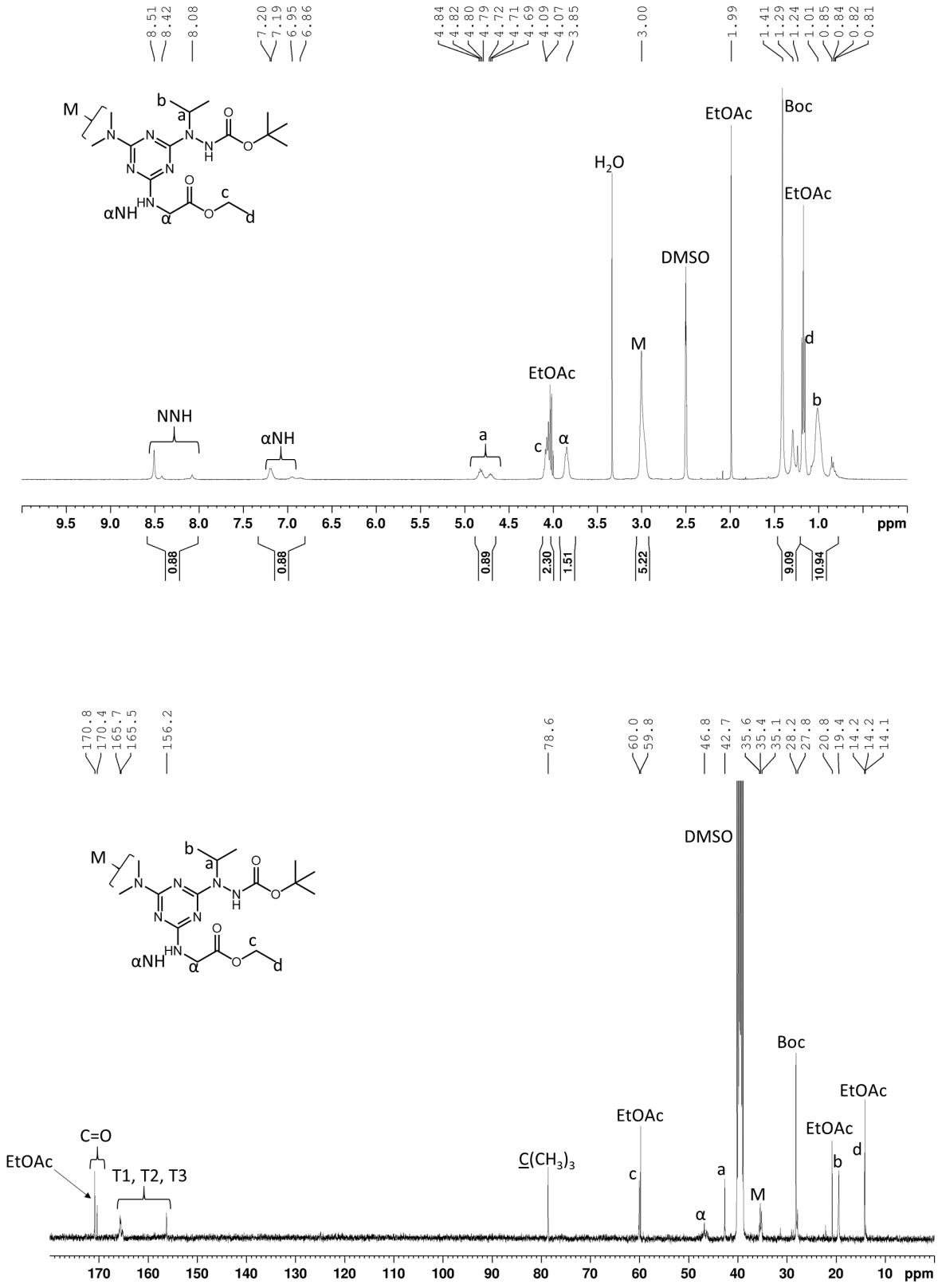

Figure S68. The 400 MHz ^{1}H and 100 MHz ^{13}C NMR Spectra of **G^{NNBn}-Ester** in CD_3OD.

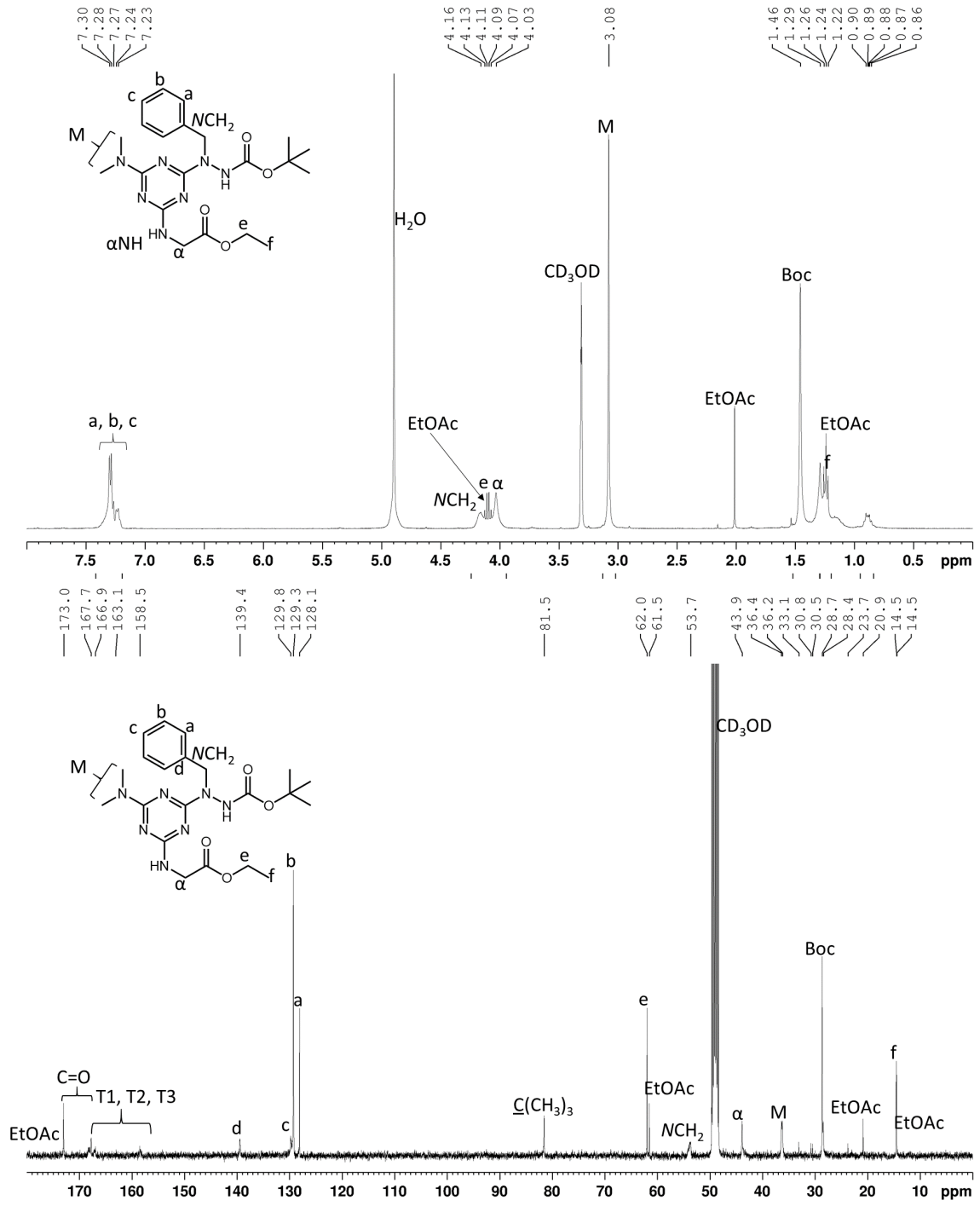

Figure S69. The 400 MHz ^{1}H and 100 MHz ^{13}C NMR Spectra of **G^{NNHx}-Ester** in DMSO.

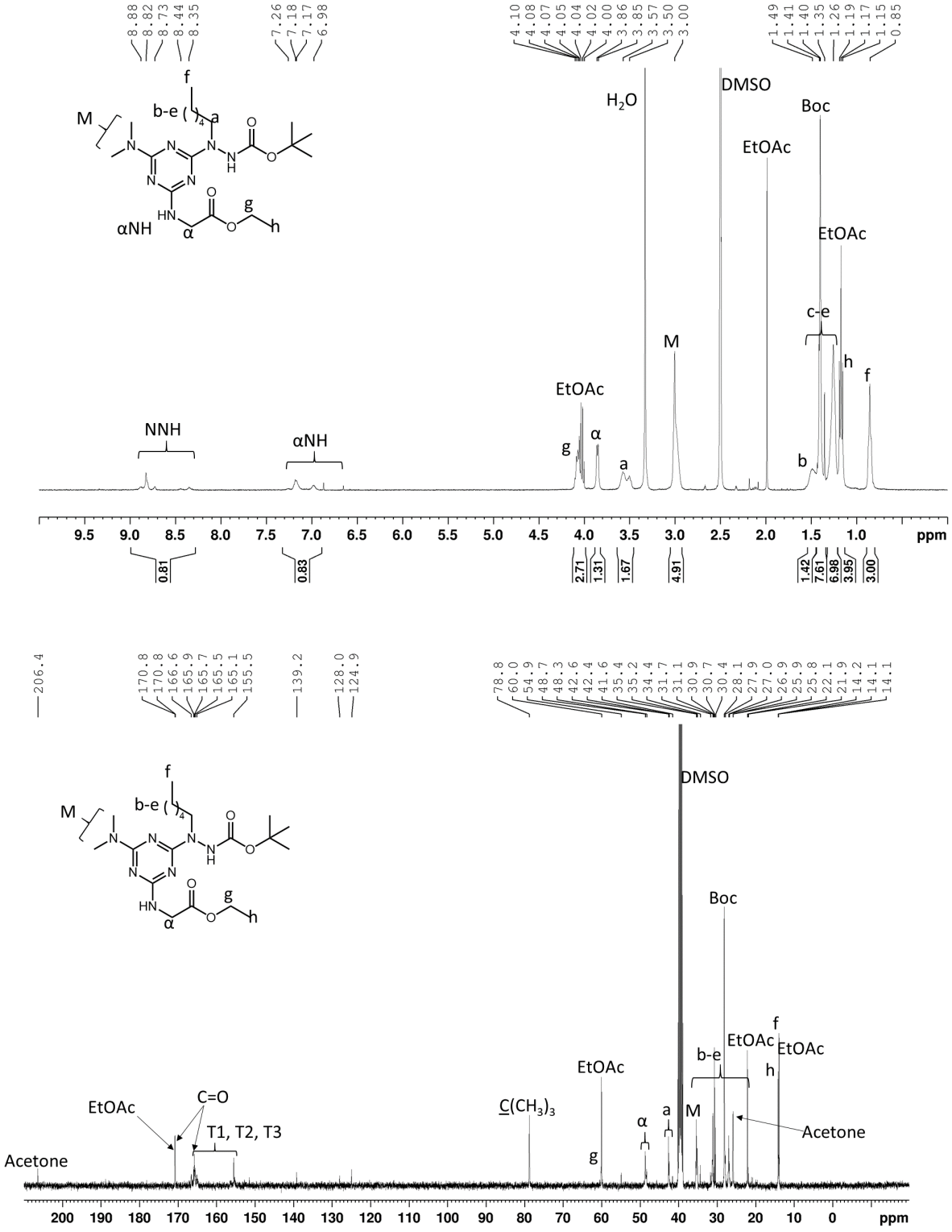

Figure S70. HRMS (ESI) of **G^{NNMe}-Ester**.

Elmt	Val.	Min	Max	Elmt	Val.	Min	Max	Elmt	Val.	Min	Max	Use Adduct
H	1	0	300	O	2	0	4	S	2	0	0	H
C	4	0	15	F	1	0	0	Cu	2	0	0	
N	3	0	7	Si	4	0	0					

Error Margin (ppm): 10
HC Ratio: unlimited
Max Isotopes: all
MSn Iso RI (%): 75.00

DBE Range: -2.0 - 1000.0
Apply N Rule: yes
Isotope RI (%): 1.00
MSn Logic Mode: AND

Electron Ions: both
Use MSn Info: no
Isotope Res: 10000
Max Results: 500

Event#: 1 MS(E+) Ret. Time : 0.587 Scan# : 89

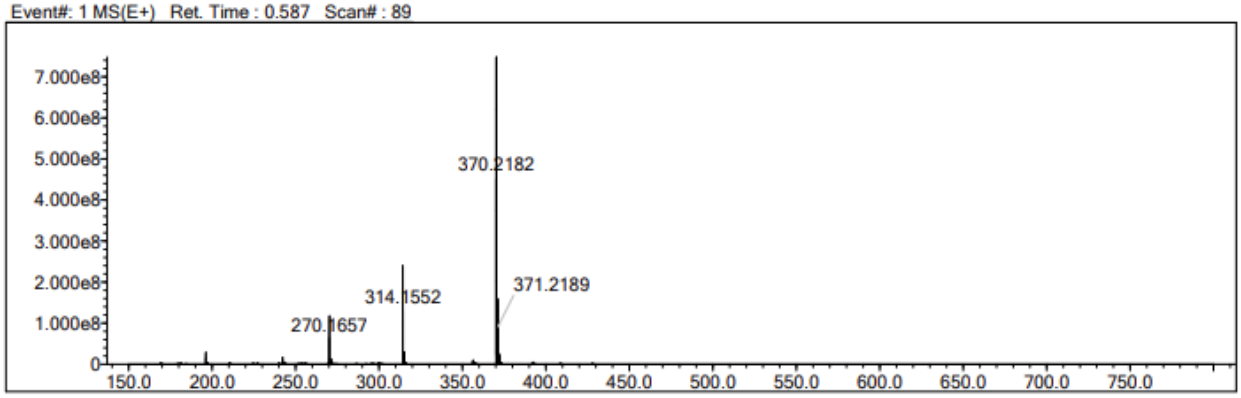

Measured region for 370.2182 m/z

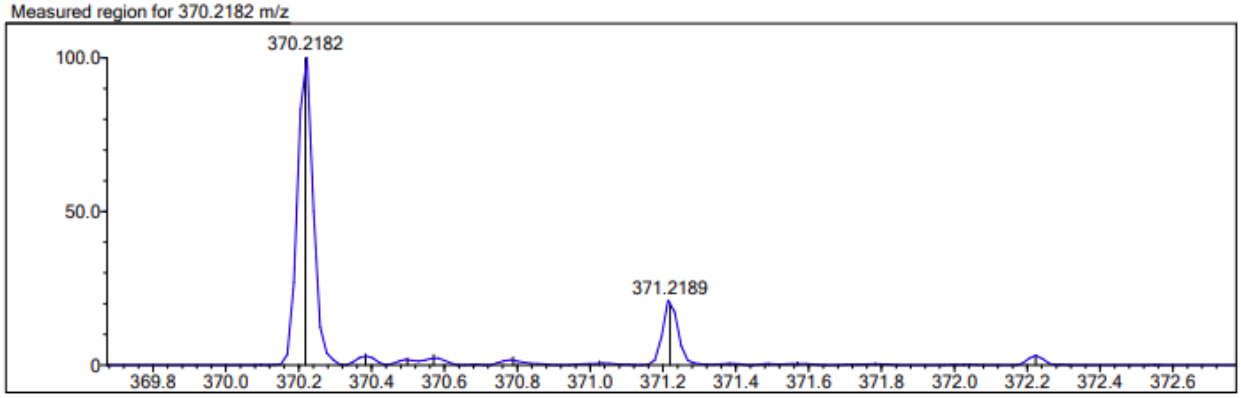

C15 H27 N7 O4 [M+H]+ : Predicted region for 370.2197 m/z

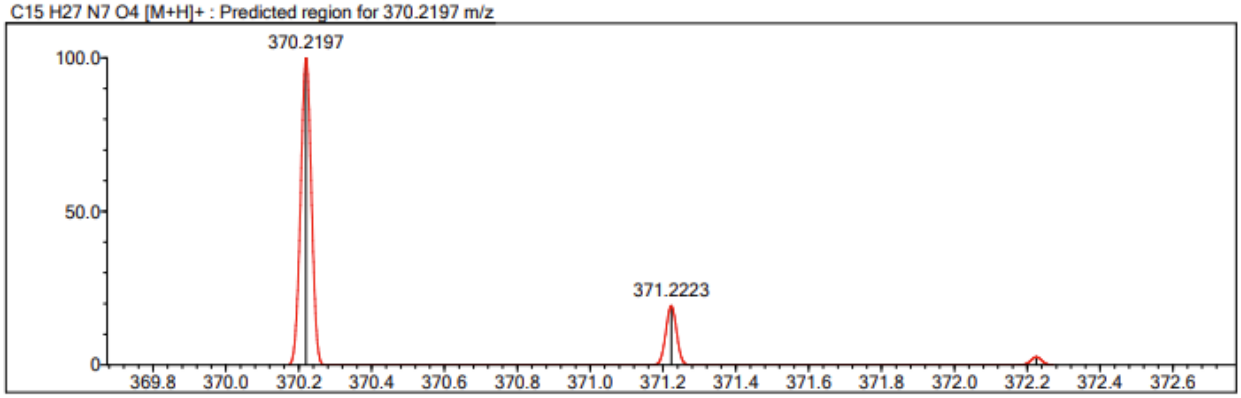

Rank	Score	Formula (M)	Ion	Meas. m/z	Pred. m/z	Df. (mDa)	Df. (ppm)	Iso	DBE
1	89.86	C15 H27 N7 O4	[M+H]+	370.2182	370.2197	-1.5	-4.05	97.28	6.0

Figure S71. HRMS (ESI) of **G^{NNEt}-Ester**.

Elmt	Val.	Min	Max	Elmt	Val.	Min	Max	Elmt	Val.	Min	Max	Use Adduct
H	1	0	300	O	2	0	4	S	2	0	0	H
C	4	0	16	F	1	0	0	Cu	2	0	0	
N	3	0	7	Si	4	0	0					

Error Margin (ppm): 10
HC Ratio: unlimited
Max Isotopes: all
MSn Iso RI (%): 75.00

DBE Range: -2.0 - 1000.0
Apply N Rule: yes
Isotope RI (%): 1.00
MSn Logic Mode: AND

Electron Ions: both
Use MSn Info: no
Isotope Res: 10000
Max Results: 500

Event#: 1 MS(E+) Ret. Time : 0.420 Scan# : 64

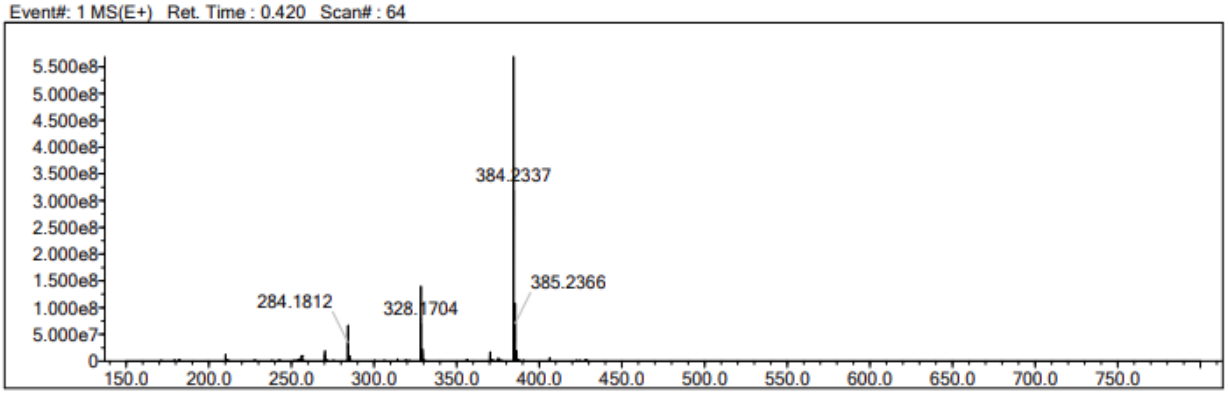

Measured region for 384.2337 m/z

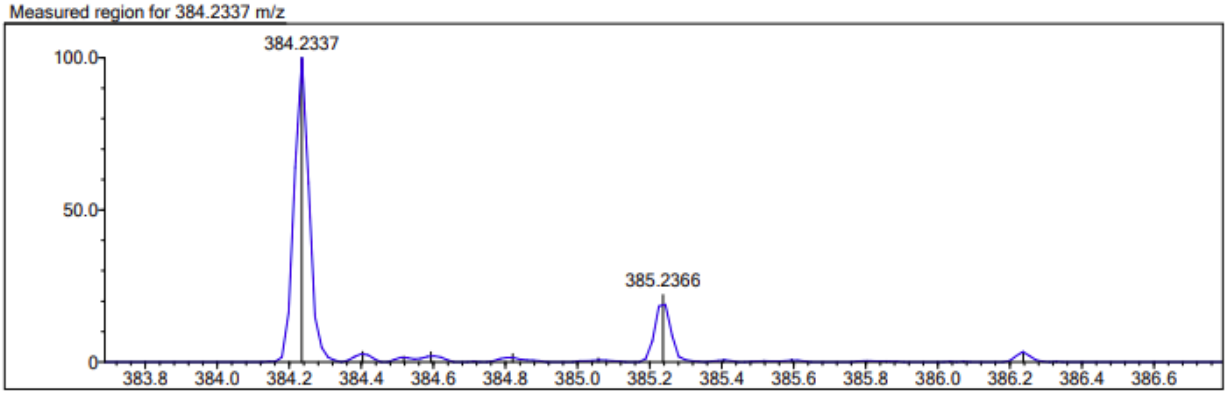

C16 H29 N7 O4 [M+H]+ : Predicted region for 384.2354 m/z

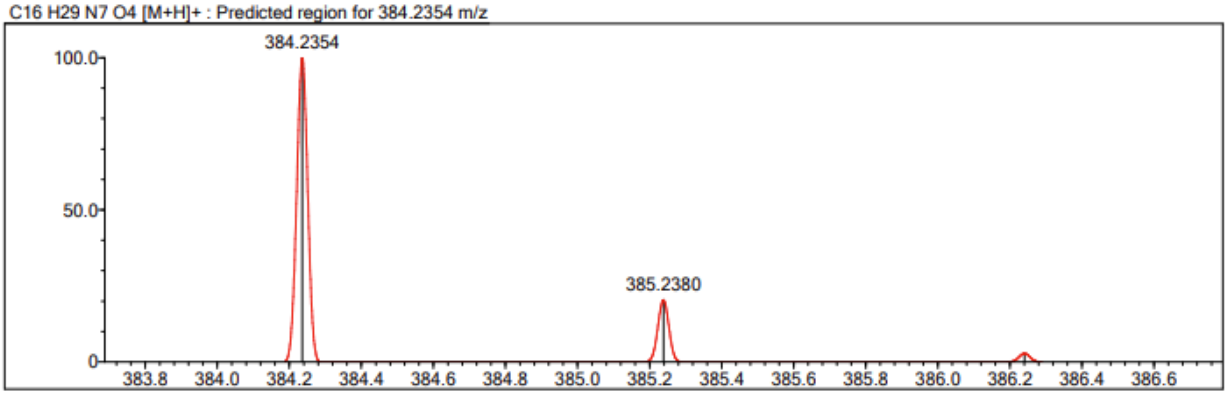

Rank	Score	Formula (M)	Ion	Meas. m/z	Pred. m/z	Df. (mDa)	Df. (ppm)	Iso	DBE
1	85.68	C16 H29 N7 O4	[M+H]+	384.2337	384.2354	-1.7	-4.42	93.69	6.0

Figure S72. HRMS (ESI) of **G^{NNiPr}-Ester**.

Elmt	Val.	Min	Max	Elmt	Val.	Min	Max	Elmt	Val.	Min	Max	Use Adduct
H	1	0	300	O	2	0	4	S	2	0	0	H
C	4	0	24	F	1	0	0	Cu	2	0	0	
N	3	0	16	Si	4	0	0					

Error Margin (ppm): 10
HC Ratio: unlimited
Max Isotopes: all
MSn Iso RI (%): 75.00

DBE Range: -2.0 - 1000.0
Apply N Rule: yes
Isotope RI (%): 1.00
MSn Logic Mode: AND

Electron Ions: both
Use MSn Info: no
Isotope Res: 10000
Max Results: 500

Event#: 1 MS(E+) Ret. Time : 0.207 Scan# : 32

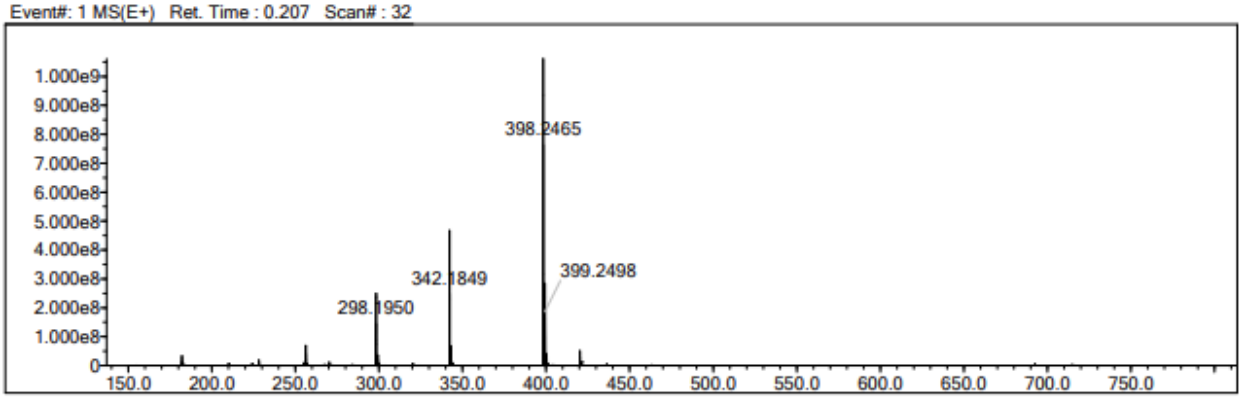

Measured region for 398.2465 m/z

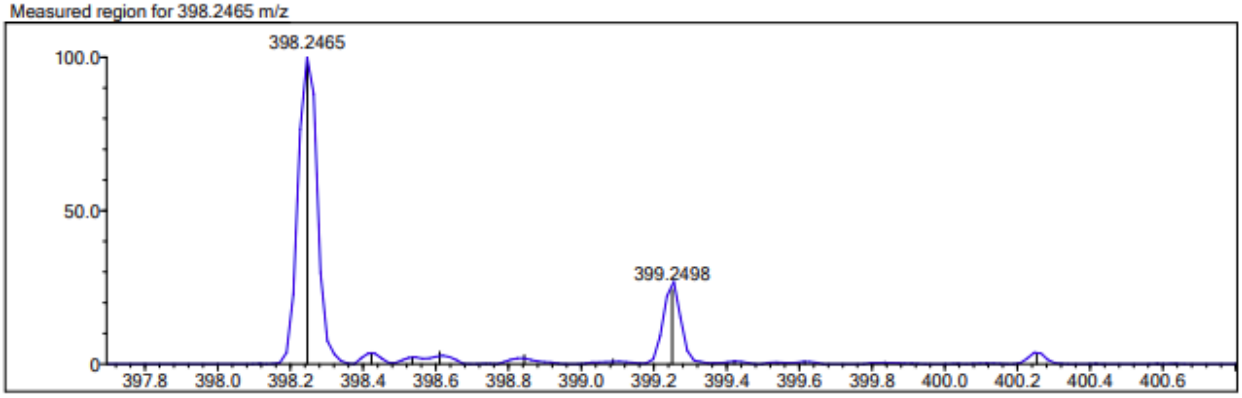

C13 H27 N13 O2 [M+H]+ : Predicted region for 398.2483 m/z

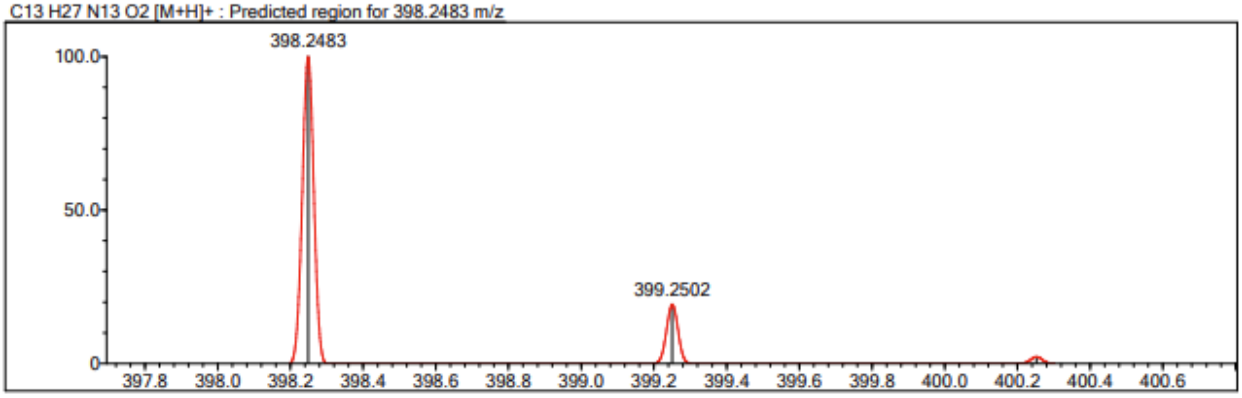

Rank	Score	Formula (M)	Ion	Meas. m/z	Pred. m/z	Df. (mDa)	Df. (ppm)	Iso	DBE
1	78.13	C13 H27 N13 O2	[M+H]+	398.2465	398.2483	-1.8	-4.52	85.66	7.0

Figure S73. HRMS (ESI) of **G^{NNBn}-Ester**.

Elmt	Val.	Min	Max	Elmt	Val.	Min	Max	Elmt	Val.	Min	Max	Use Adduct
H	1	0	300	O	2	0	4	S	2	0	0	H
C	4	0	21	F	1	0	0	Cu	2	0	0	
N	3	0	7	Si	4	0	0					

Error Margin (ppm): 10
HC Ratio: unlimited
Max Isotopes: all
MSn Iso RI (%): 75.00

DBE Range: -2.0 - 1000.0
Apply N Rule: yes
Isotope RI (%): 1.00
MSn Logic Mode: AND

Electron Ions: both
Use MSn Info: no
Isotope Res: 10000
Max Results: 500

Event#: 1 MS(E+) Ret. Time : 0.193 Scan# : 30

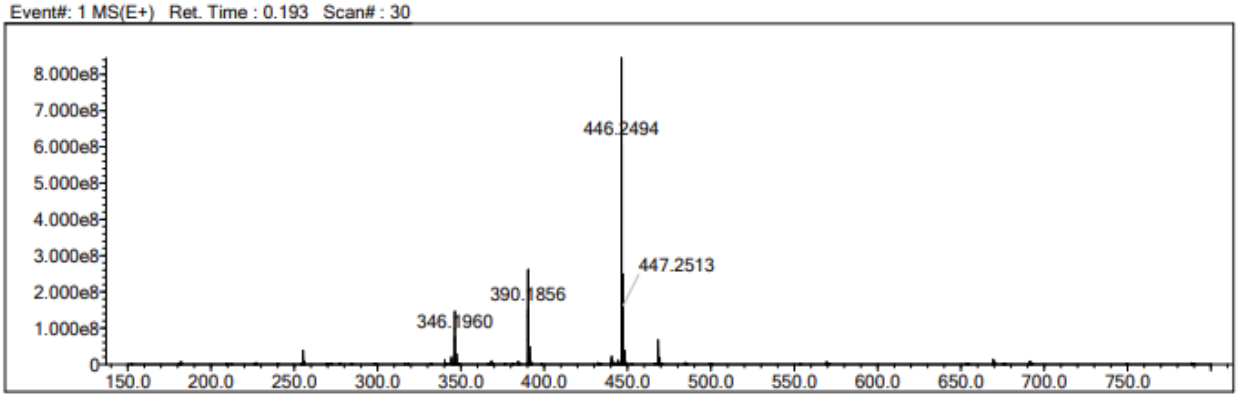

Measured region for 446.2494 m/z

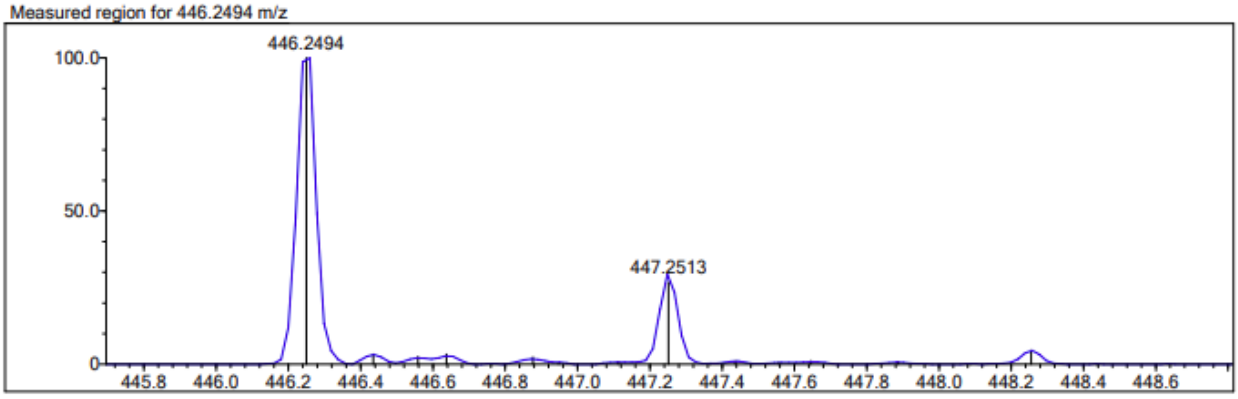

C21 H31 N7 O4 [M+H]+ : Predicted region for 446.2510 m/z

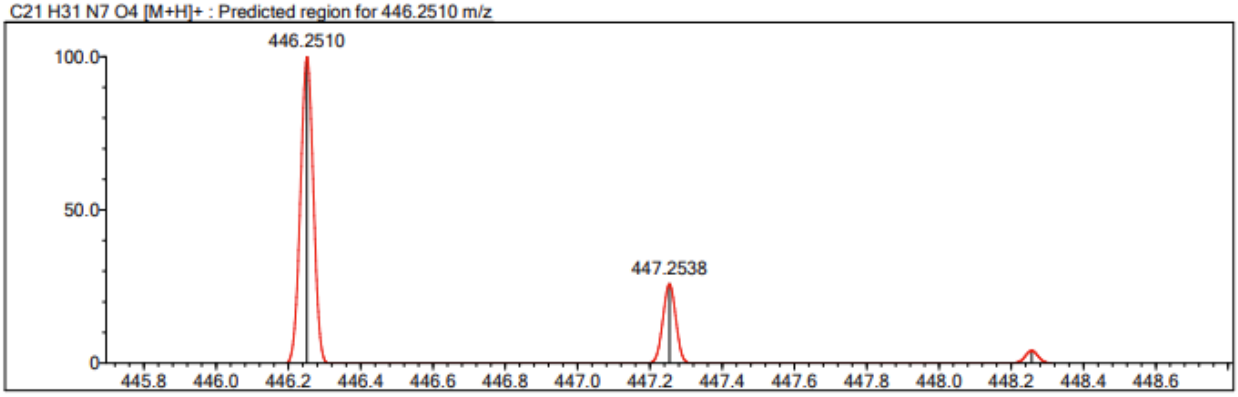

Rank	Score	Formula (M)	Ion	Meas. m/z	Pred. m/z	Df. (mDa)	Df. (ppm)	Iso	DBE
1	88.48	C21 H31 N7 O4	[M+H]+	446.2494	446.2510	-1.6	-3.59	94.61	10.0

Figure S74. HRMS (ESI) of **G^{NNHx}-Ester**.

Elmt	Val.	Min	Max	Elmt	Val.	Min	Max	Elmt	Val.	Min	Max	Use Adduct
H	1	0	300	O	2	0	4	S	2	0	0	H
C	4	0	20	F	1	0	0	Cu	2	0	0	
N	3	0	7	Si	4	0	0					

Error Margin (ppm): 10
HC Ratio: unlimited
Max Isotopes: all
MSn Iso RI (%): 75.00

DBE Range: -2.0 - 1000.0
Apply N Rule: yes
Isotope RI (%): 1.00
MSn Logic Mode: AND

Electron Ions: both
Use MSn Info: no
Isotope Res: 10000
Max Results: 500

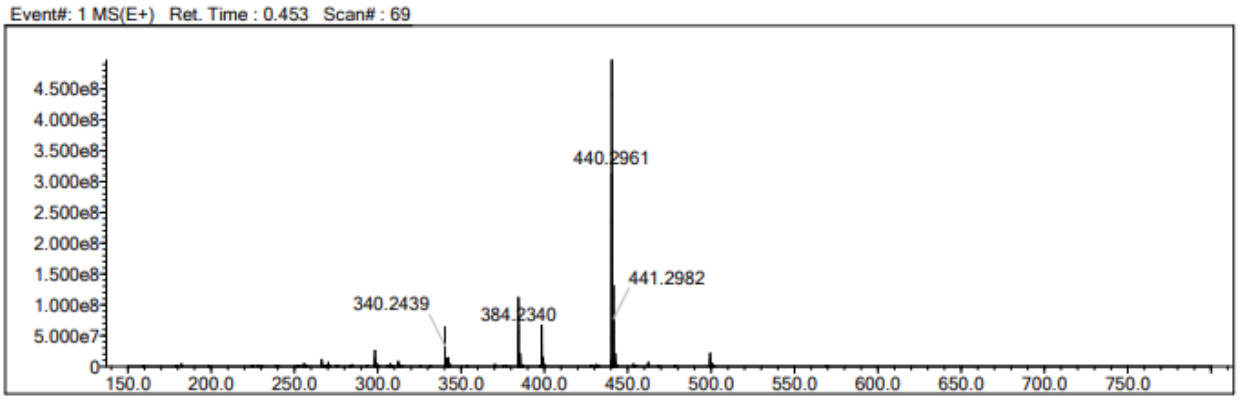

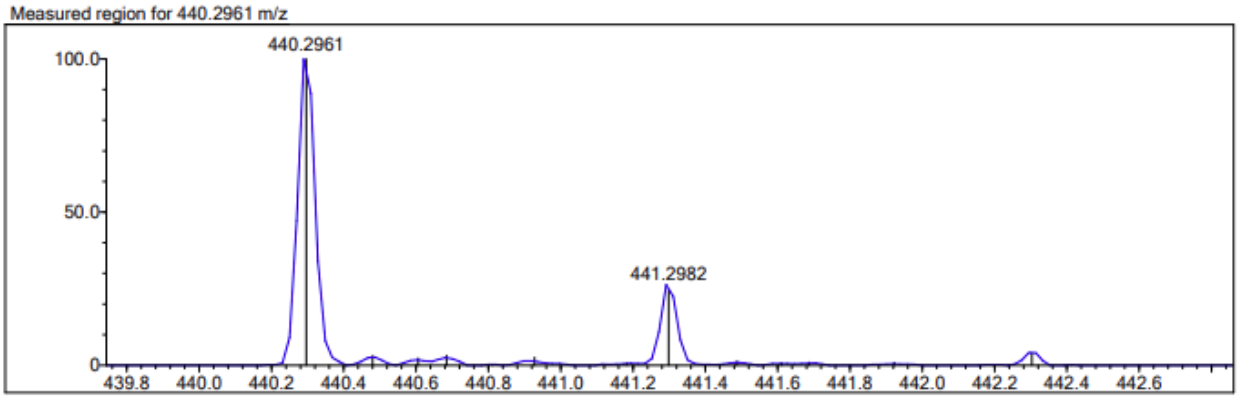

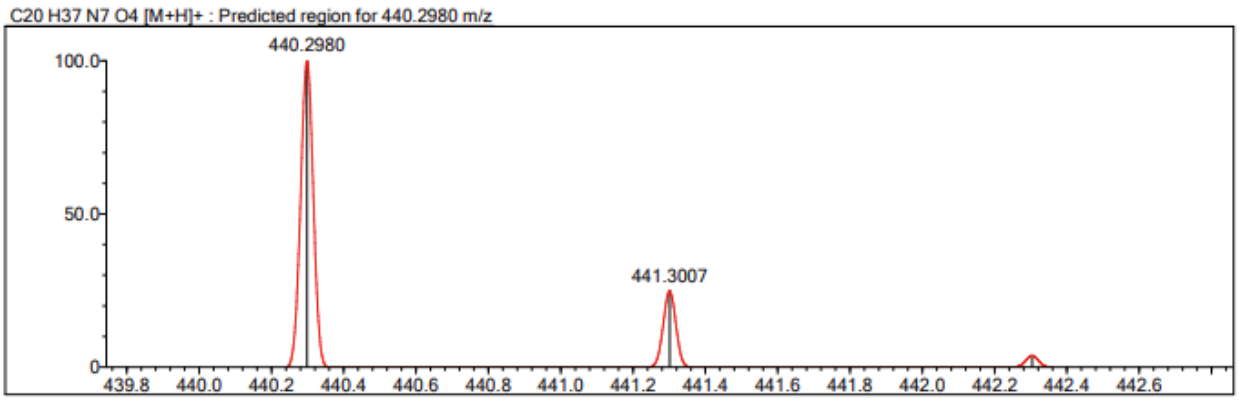

Rank	Score	Formula (M)	Ion	Meas. m/z	Pred. m/z	Df. (mDa)	Df. (ppm)	Iso	DBE
1	86.51	C20 H37 N7 O4	[M+H]+	440.2961	440.2980	-1.9	-4.32	94.34	6.0

SYNTHESIS OF MONOMERS

General synthesis of amide products deriving from the synthesis of **G^{NNHx}-Monomer**. The ester products were amidated with an amino acetal with a mild acidic catalyst and heat as illustrated and described below.

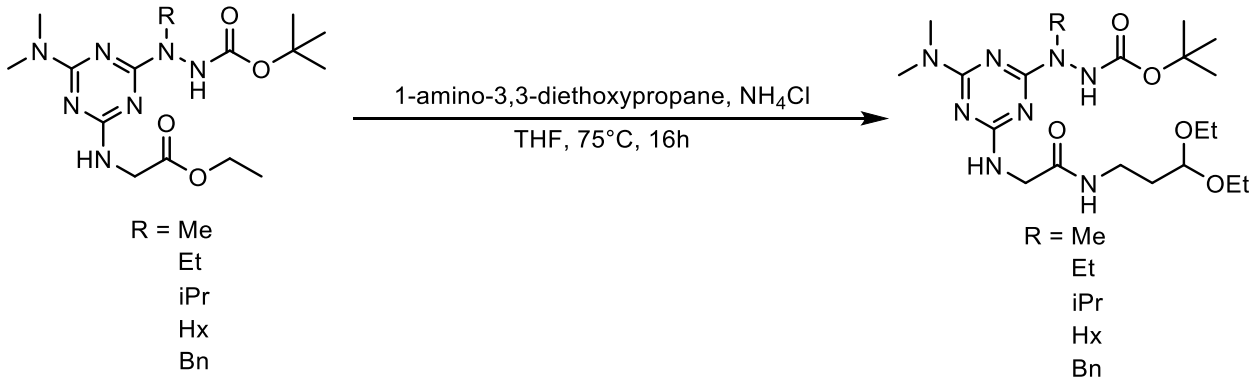

G^{NNHx}-Ester (0.1178 g, 0.27 mmol, 1 eq) was charged to a round-bottom flask along with 1-amino-3,3-diethoxypropane (0.6689 g, 4.5 mmol, 17 eq) and THF (1mL, 0.25 M). Ammonium chloride (0.1789 g, 3.3 mmol, 12.5 eq) was triturated and added to the round-bottom flask. The reaction was then heated to 65°C and a reflux condenser was attached to the round-bottom flask. Extra ammonium chloride (0.1658 g, 3.1 mmol, 11.6 eq) was added to the reaction after two hours of stirring. The reaction was stopped after 19 hours of stirring and was extracted thrice with 50 mL of water and 50 mL of ethyl acetate. The organic layer was collected and dried with magnesium sulfate followed by filtration. The resulting organic layer was concentrated with rotary evaporation. The crude **G^{NNHx}-Monomer** was purified by column chromatography with 75 mL SiO_2 and 3% to 5% methanol in DCM, affording pure **G^{NNHx}-Monomer** (0.036 g, 0.067 mmol, 25% yield). Unreacted **G^{NNHx}-Ester** (0.061 g, 0.18 mmol) was recovered, giving an adjusted yield of 67%.

HRMS (ESI) m/z: $[M + H]^+$ Calculated for $C_{25}H_{48}N_8O_5$ 541.3823; Found 541.3820

^{1}H NMR (DMSO, 400 MHz): δ 8.87 – 8.30 (s, 1 H), 7.81 – 7.13 (m, 1 H), 6.94 – 6.59 (m, 1 H), 4.45 (m, 1 H), 3.89 – 3.67 (m, 2 H), 3.64 – 3.47 (m, 4 H), 3.44 – 3.36 (m, 2 H), 3.08 (q, *J* = 6.4 Hz, 2 H), 3.00 (s, 6 H), 1.63 (q, *J* = 6.4 Hz, 2 H), 1.54 – 1.20 (m, 17 H), 1.08 (t, *J* = 7.0 Hz, 6 H), 0.85 (m, 3 H).

^{13}C{^{1}H} NMR (DMSO, 100 MHz): δ 169.7, 166.4, 165.5, 162.4, 155.5, 100.7, 78.8, 60.7, 54.9, 48.6, 44.1, 35.4, 34.7, 33.4, 31.2, 28.2, 27.1, 26.8, 25.9, 22.1, 15.3, 14.0

G^{NNMe}-Monomer: **G^{NNMe}-Ester** (0.157 g, 0.43 mmol, 1 eq) was charged to a round-bottom flask along with 0.5 mL THF, 1-amino-3,3,-diethoxypropane (0.6478 g, 4.4 mmol, 10.3 eq), and ammonium chloride (0.0634 g, 1.2 mmol, 2.8 eq). The reaction was heated to 70°C and allowed to stir for 16 hours, after which the reaction was finished. The reaction was then concentrated *via* rotary evaporation and the crude reaction was extracted with 50 mL ethyl acetate and 100 mL of water, followed by 30 mL of brine. The organic layer was collected and dried with magnesium sulfate and filtered. The filtrate was collected and ethyl acetate was removed *via* rotary evaporation, affording crude **G^{NNMe}-Monomer**. Pure **G^{NNMe}-**

Monomer (0.158 g, 0.34 mmol, 79% yield) was obtained after column chromatography with 75 mL of SiO_2 and 3% methanol in chloroform.

HRMS (ESI) m/z: $[M + H]^+$ Calculated for $C_{20}H_{38}N_8O_5$ 471.3038; Found 471.3030

^{1}H NMR (DMSO, 400 MHz): δ 8.91 (s, 1 H), 7.75 – 7.54 (m, 1 H), 6.99 – 6.70 (m, 1 H), 4.45 (m, 1 H), 3.88 – 3.69 (m, 2 H), 3.53 (m, 2 H), 3.39 (m, 2 H), 3.14 (s, 3 H), 3.08 (m, 2 H), 3.00 (s, 6 H), 1.63 (m, 2 H), 1.43 – 1.21 (s, 9 H), 1.09 (t, *J* = 7.0 Hz, 6 H).

^{13}C{^{1}H} NMR (DMSO, 100 MHz): δ 169.6, 165.81, 165.76, 165.3, 155.4, 100.6, 78.9, 60.7, 44.0, 37.3, 35.3, 34.7, 33.3, 28.2, 15.3.

G^{NNEt}-Monomer: **G^{NNEt}-Ester** (0.107 g, 0.28 mmol, 1 eq) was charged to a round-bottom flask along with 1-amino-3,3-diethoxypropane (0.2114 g, 1.4 mmol, 5 eq) and THF (0.25 mL) and DMF (0.25 mL, 0.6 M). Ammonium chloride (0.1017 g, 1.9 mmol, 7 eq) was triturated and added to the round-bottom flask. The reaction was then heated to 75°C and a reflux condenser was attached to the round-bottom flask. The reaction was stopped after 19 hours of stirring and concentrated *via* rotary evaporation. The reaction was then extracted thrice with 25 mL ethyl acetate and 25 mL water. The organic layer was then concentrated *via* rotary evaporation. The reaction was then resuspended in 1-amino-3,3-diethoxypropane (1.2437 g, 8.4 mmol, 30 eq) and THF (15 drops, ~0.2 mL). Ammonium chloride (0.0475 g, 0.9 mmol, 3 eq) was triturated and added to the round-bottom flask. The reaction was then heated to 75°C and lightly capped. The reaction was stopped after an additional 4 hours of stirring and concentrated *via* rotary evaporation. The reaction was then extracted thrice with 50 mL water and 50 mL ethyl acetate. The organic layer was dried with magnesium sulfate and filtered. Following concentration *via* rotary evaporation, the crude reaction was purified with column chromatography with 60 mL SiO_2 and 4% methanol in chloroform, yielding pure **G^{NNEt}-Monomer** (0.114 g, 0.23 mmol, 84% yield).

HRMS (ESI) m/z: $[M + H]^+$ Calculated for $C_{21}H_{40}N_8O_5$ 485.3194; Found 485.3188

^{1}H NMR (DMSO, 400 MHz): δ 8.88 – 8.34 (s, 1 H), 7.99 – 7.54 (m, 1 H), 6.96 – 6.64 (m, 1 H), 4.45 (m, 1 H), 3.87 – 3.68 (m, 2 H), 3.67 – 3.58 (m, 2 H), 3.56 – 3.48 (m, 2 H), 3.45 – 3.36 (m, 2 H), 3.08 (q, *J* = 6.5 Hz, 2 H), 3.00 (s, 6 H), 1.67 – 1.59 (m, 2 H), 1.44 – 1.22 (s, 9 H), 1.14 – 1.00 (m, 9 H).

^{13}C{^{1}H} NMR (DMSO, 100 MHz): δ 169.7, 166.2, 165.8, 161.1, 155.6, 100.6, 78.8, 60.8, 44.0, 35.4, 35.3, 34.7, 33.3, 28.2, 15.3, 12.5.

G^{NNiPr}-Monomer: G^{NNiPr}-Ester (0.279 g, 0.70 mmol, 1 eq) was charged to a round bottom flask along with 1-amino-3,3-diethoxypropane (1.5622 g, 10.6 mmol, 15.1 eq) and previously triturated ammonium chloride (0.1139 g, 2.1 mmol, 3 eq) and THF (1 mL). A small stir bar was added to the flask and the reaction was heated to 70°C and lightly capped. The reaction was left to go overnight (18 hours). The reaction was then concentrated *via* rotary evaporation and the crude reaction was extracted thrice with 50 mL of water and 50 mL of ethyl acetate. The organic layer was collected and dried with magnesium sulfate and filtered. Crude **G^{NNiPr}-Monomer** was isolated by removing the ethyl acetate *via* rotary evaporation. Pure **G^{NNiPr}-**

Monomer (0.319 g, 0.64 mmol, 91% yield) was obtained with column chromatography using 75 mL of SiO_2 and 3% methanol in chloroform.

HRMS (ESI) m/z: $[M + H]^+$ Calculated for $C_{22}H_{42}N_8O_5$ 499.3351; Found 499.3342

^1H NMR (DMSO, 400 MHz): δ 8.54 – 8.01 (s, 1 H), 7.75 – 7.51 (m, 1 H), 6.95 – 6.45 (m, 1 H), 4.82 (m, 1 H), 4.46 (m, 1 H), 4.07 – 3.64 (m, 2 H), 3.53 (m, 2 H), 3.39 (m, 2 H), 3.07 (m, 2 H), 3.00 (s, 6 H), 1.63 (m, 2 H), 1.43 – 1.23 (m, 9 H), 1.12 – 0.96 (m, 12 H).

$^{13}C\{^1H\}$ NMR (DMSO, 100 MHz): δ 169.7, 165.8, 165.5, 165.3, 156.2, 100.6, 78.6, 60.7, 46.8, 44.0, 35.4, 34.7, 33.3, 28.1, 19.5, 15.3.

G^{NNBn}-Monomer: **G^{NNBn}-Ester** (91.0 mg, 0.20 mmol, 1 eq) was charged to a round-bottom flask along with 1-amino-3,3-diethoxypropane (0.3307 g, 2.25 mmol, 11 eq), previously triturated ammonium chloride (33.1 mg, 0.62 mmol, 3 eq), and 1 mL of THF. The reaction was then heated to 65°C with gentle stirring. After 13 hours, the reaction was extracted thrice with 50 mL of water and 50 mL of ethyl acetate The organic layer was collected and dried with magnesium sulfate. Ethyl acetate was then removed *via* rotary evaporation, affording crude **G^{NNBn}-Monomer**. Column chromatography with 50 mL SiO_2 and 5% methanol in chloroform afforded pure **G^{NNBn}-Monomer** (41.8 mg, 76.5 µmol, 37% yield) as a clear oil.

HRMS (ESI) m/z: $[M + H]^+$ Calculated for $C_{26}H_{42}N_8O_5$ 547.3351; Found 547.3342

^1H NMR (DMSO, 400 MHz): δ 9.04 – 8.86 (s, 1 H), 7.75 – 7.54 (m, 1 H), 7.37 – 6.89 (m, 6 H), 4.82 (m, 2 H), 4.45 (m, 1 H), 3.92 – 3.67 (m, 2 H), 3.52 (m, 2 H), 3.38 (m, 2 H), 3.09 (m, 2 H), 3.01 (s, 6 H), 1.63 (m, 2 H), 1.43 – 1.16 (s, 9 H), 1.08 (m, 6 H).

$^{13}C\{^1H\}$ NMR (DMSO, 100 MHz): δ 169.6, 166.8, 166.4, 165.9, 155.5, 138.4, 128.0, 127.4, 126.7, 100.6, 79.2, 60.7, 52.4, 44.1, 35.4, 35.3, 34.7, 33.3, 28.1, 15.3.

SYNTHESIS OF MACROCYCLES

General synthesis of macrocycles derived from the synthesis of **G^{NNHx}**.

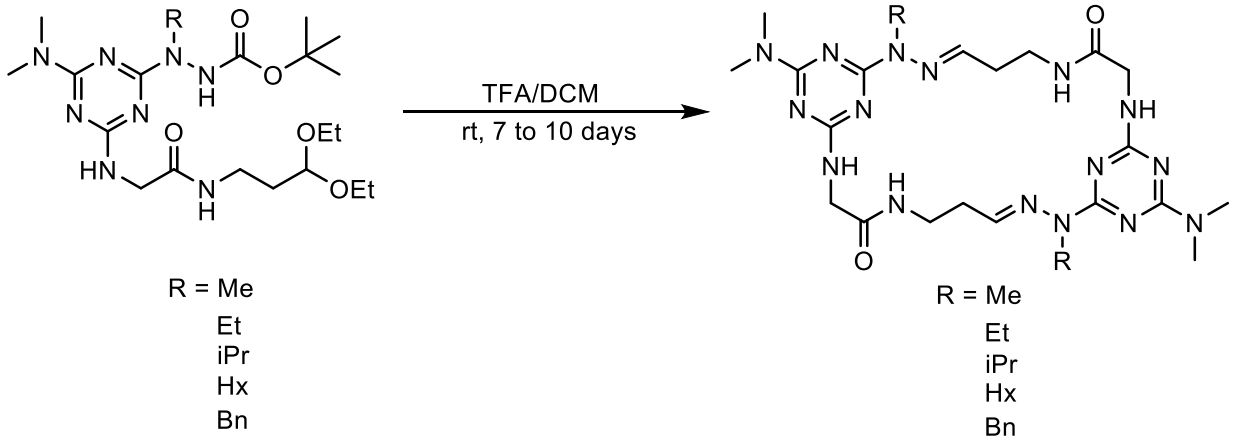

G^{NNHx}-Monomer (24 mg, 44 µmol) was added to a 5 mL scintillation vial along with a magnetic stir bar. 1 mL of dichloromethane was then added *via* pipette and allowed to stir until completely dissolved. 1 mL of TFA was then added to the vial, with an immediate color change from clear to yellow occurring. The reaction was allowed to evaporate to dryness with stirring over the course of 9 days. Pure **G^{NNHx}** was observed with ^{1}H NMR in MeOD, requiring no work-up or purification.

HRMS (ESI) m/z: $[M + H]^+$ Calculated for $C_{32}H_{56}N_{16}O_2$ 697.4845; Found 697.4863

^{1}H NMR (DMSO, 400 MHz): δ 11.88 (s, 1 H), 9.27 (m, 1 H), 7.93 (t, *J* = 6.2 Hz, 1 H), 7.61 (m, 1 H), 4.08 (d, *J* = 5.2 Hz, 2 H), 3.84 (m, 2 H), 3.74 – 3.39 (m, 1 H), 3.10 (s, 3 H), 3.08 (s, 3 H), 3.04 – 2.90 (m, 1 H), 2.69 (m, 2 H), 1.38 (m, 2 H), 1.33 – 1.06 (m, 6 H), 0.85 (m, 3 H).

^{13}C{^{1}H} NMR (DMSO, 100 MHz): δ 175.5, 161.1, 154.3, 152.6, 146.1, 44.0, 40.9, 36.7, 36.3, 33.1, 31.8, 30.7, 25.7, 24.7, 22.0, 13.8.

G^{NNiPr}:

HRMS (ESI) m/z: $[M + H]^+$ Calculated for $C_{26}H_{44}N_{16}O_2$ 613.3906; Found 613.3907

^{1}H NMR (DMSO, 400 MHz): δ 11.64 (s, 1 H), 9.28 (m, 1 H), 8.12 (m, 1 H), 7.81 (m, 1 H), 4.83 (sept, *J* = 7.0 Hz, 1 H), 4.09 (m, 2 H), 3.66 (m, 2 H), 3.11 (s, 3 H), 3.06 (s, 3 H), 2.68 (m, 2 H), 1.31 (d, *J* = 7.0 Hz, 6 H).

^{13}C{^{1}H} NMR (DMSO, 100 MHz): δ 175.9, 169.9, 158.1, 157.8, 152.6, 47.5, 43.8, 36.6, 32.8, 32.3, 18.6.

G^{NNMe}: The cyclization was stopped after 4 hours, showing complete conversion to the macrocycle after rotary evaporation.

HRMS (ESI) m/z: $[M + H]^+$ Calculated for $C_{22}H_{36}N_{16}O_2$ 557.3280; Found 557.3274

^{1}H NMR (DMSO, 400 MHz): δ 11.91 (s, 1 H), 9.31 (m, 1 H), 7.91 (m, 1 H), 7.54 (m, 1 H), 4.07 (m, 2 H), 3.61 (m, 2 H), 3.24 (s, 3 H), 3.12 (s, 3 H), 3.09 (s, 3H), 2.69 (m, 2 H).

^{13}C{^{1}H} NMR (DMSO, 100 MHz): δ 171.7, 161.1, 154.3, 152.9, 146.1, 44.1, 36.8, 36.5, 33.2, 31.8, 28.6.

G^{NNEt}:

HRMS (ESI) m/z: $[M + H]^+$ Calculated for $C_{24}H_{40}N_{16}O_2$ 585.3593; Found 585.3572

^{1}H NMR (DMSO, 400 MHz): δ 11.87 (s, 1 H), 9.26 (m, 1 H), 7.92 (m, 1 H), 7.61 (m, 1 H), 4.07 (m, 2 H), 3.92 (m, 2 H), 3.51 (m, 2 H), 3.09 (s, 3 H), 3.08 (s, 3 H), 2.69 (m, 2 H), 0.99 (m, 3 H).

^{13}C{^{1}H} NMR (DMSO, 100 MHz): δ 171.5, 161.1, 154.3, 152.3, 145.8, 44.0, 36.6, 36.4, 36.1, 33.2, 31.8, 10.3.

G^{NNBn}: The cyclization was stopped after 24 hours, showing complete conversion to the macrocycle after rotary evaporation.

HRMS (ESI) m/z: $[M + H]^+$ Calculated for $C_{34}H_{44}N_{16}O_2$ 709.3906; Found 709.3896

^{1}H NMR (DMSO, 400 MHz): δ 11.99 (s, 1 H), 9.18 (m, 1 H), 7.97 (m, 1 H), 7.55 (m, 1 H), 7.37 – 7.26 (m, 5 H), 5.21 (m, 2 H), 4.12 (m, 2 H), 3.67 (m, 2 H), 3.16 (s, 3 H), 3.15 (s, 3 H), 2.60 (m, 2 H).

^{13}C{^{1}H} NMR (DMSO, 100 MHz): δ 171.8, 161.4, 154.7, 151.6, 146.2, 134.1, 128.8, 127.8, 127.1, 47.8, 44.2, 36.8, 36.7, 33.2, 31.8

Figure S75. The 400 MHz ^{1}H and 100 MHz ^{13}C NMR Spectra of **G^{NNMe}-Monomer** in DMSO.

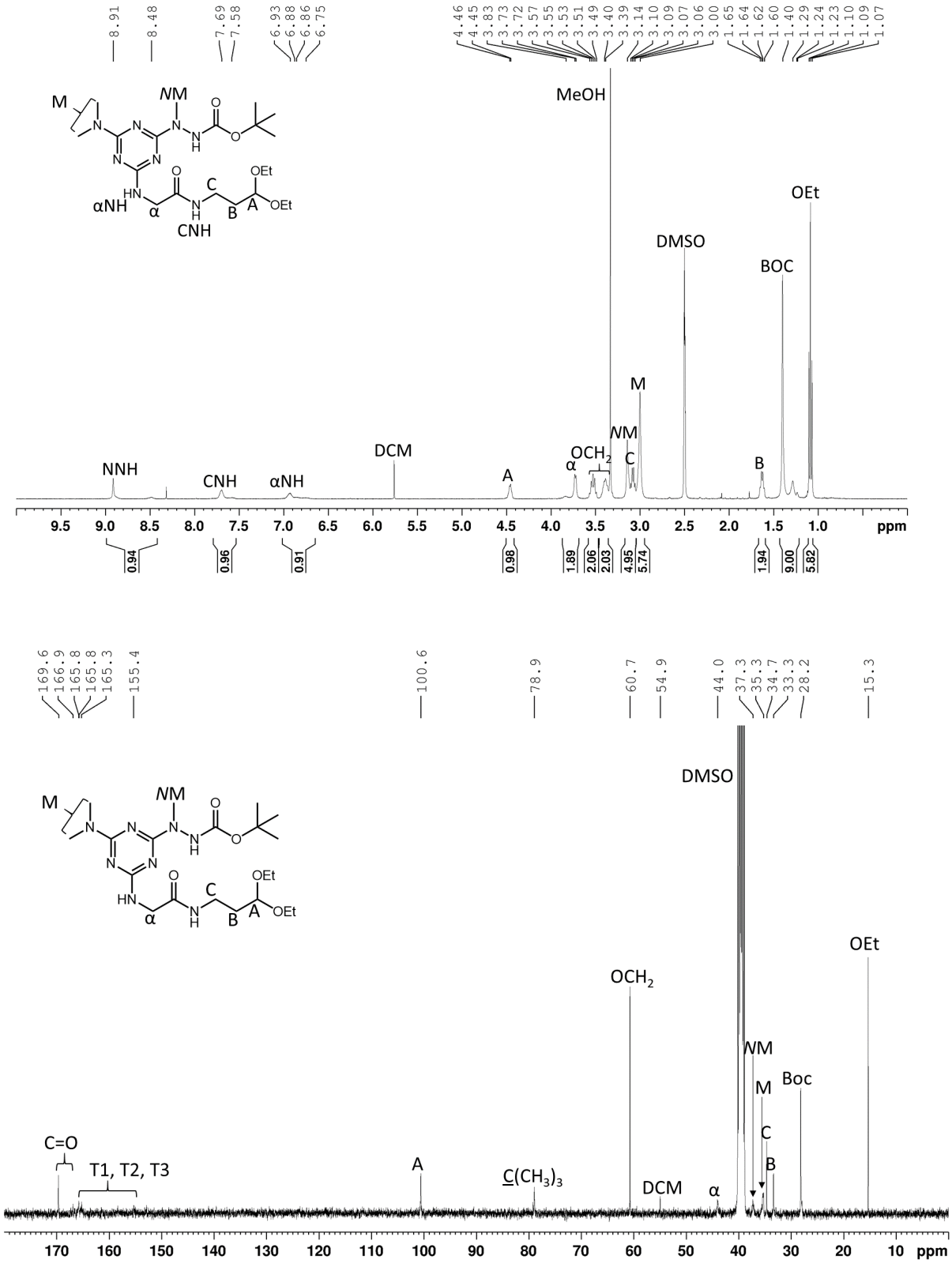

Figure S76. The 400 MHz ^{1}H and 100 MHz ^{13}C NMR Spectra of **G^{NNEt}-Monomer** in DMSO.

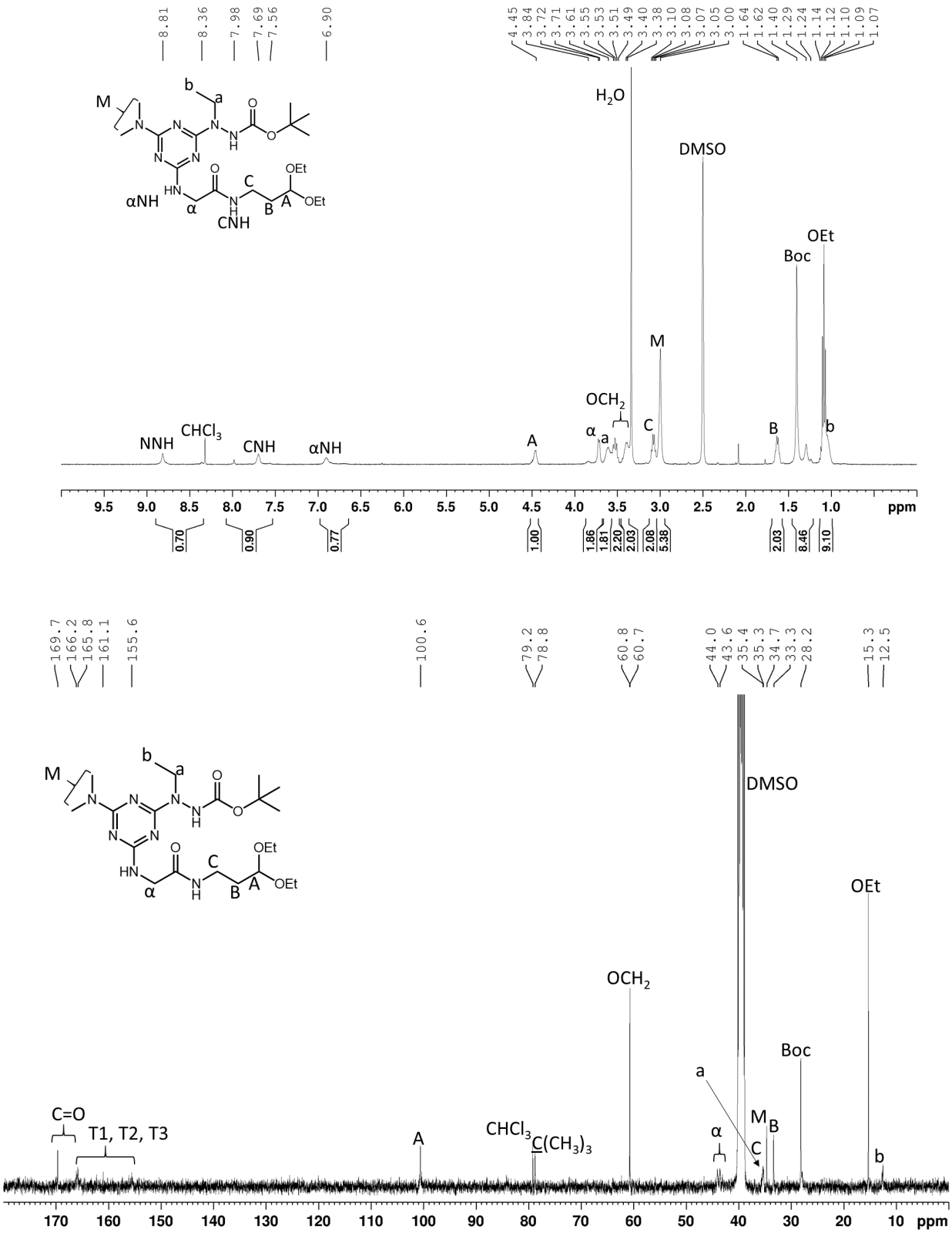

Figure S77. The 400 MHz ^{1}H and 100 MHz ^{13}C NMR Spectra of **G^{NNiPr}-Monomer** in DMSO.

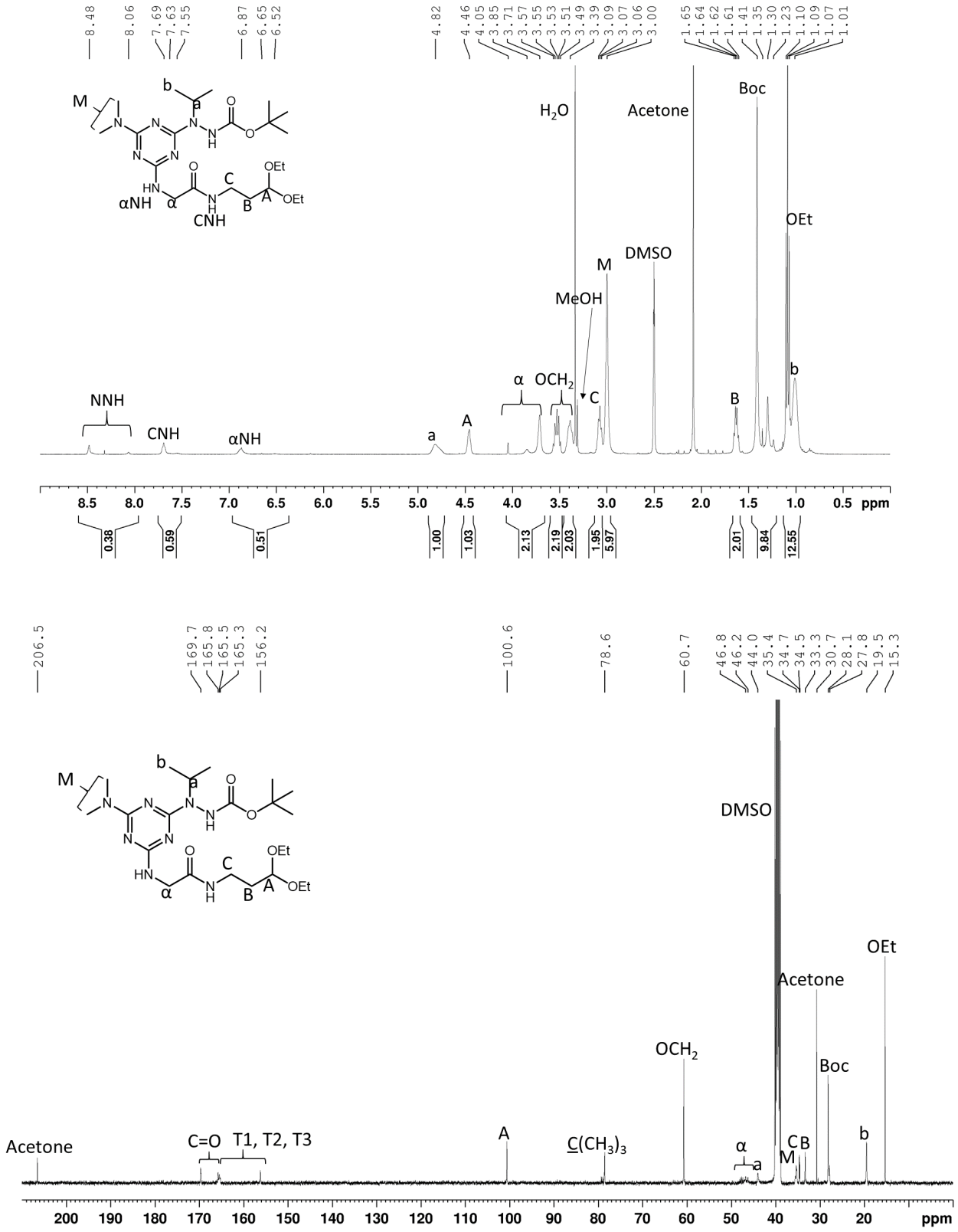

Figure S78. The 400 MHz ^{1}H and 100 MHz ^{13}C NMR Spectra of **G^{NNBn}-Monomer** in DMSO.

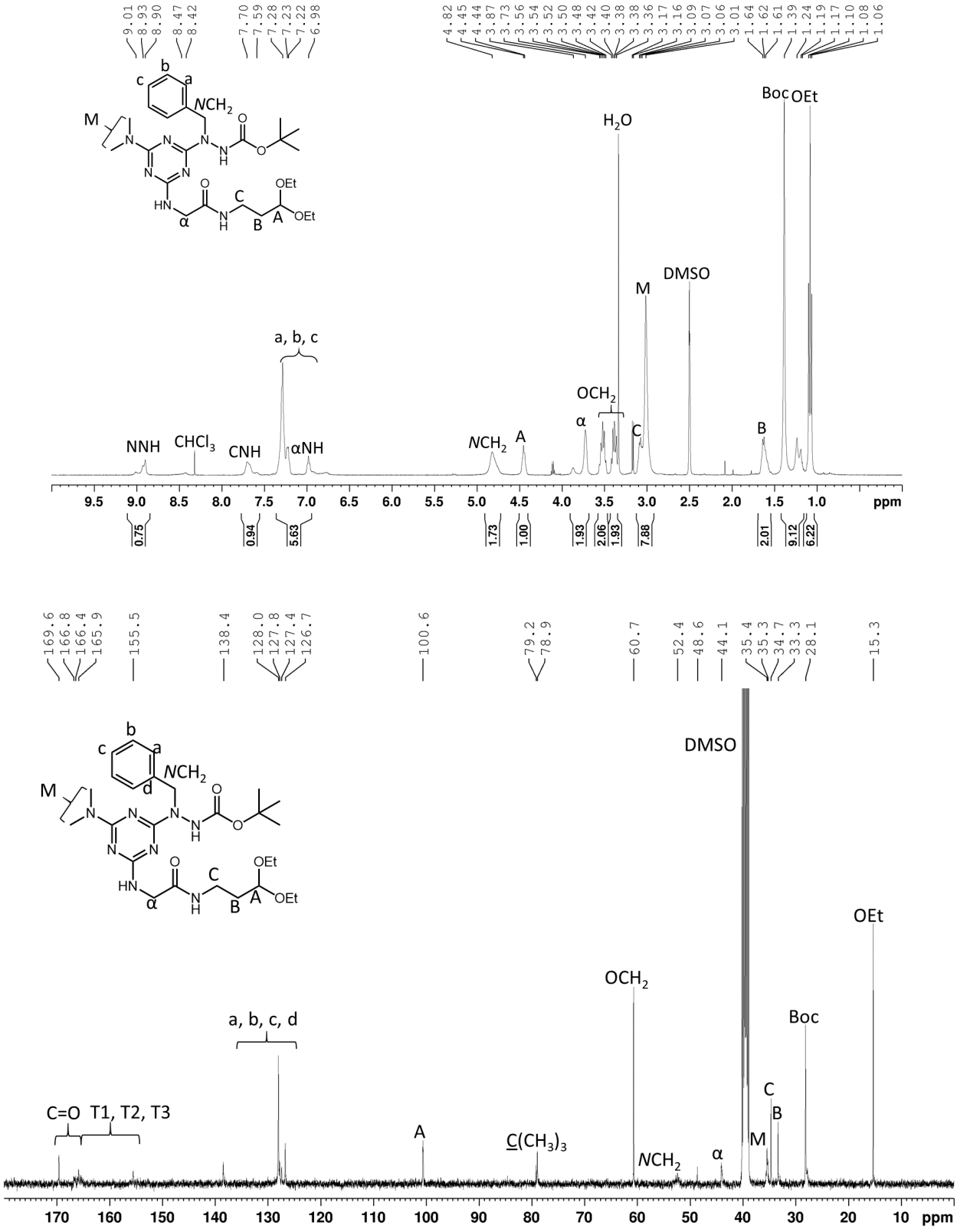

Figure S79. The 400 MHz ^{1}H and 100 MHz ^{13}C NMR Spectra of **G^{NNHx}-Monomer** in DMSO.

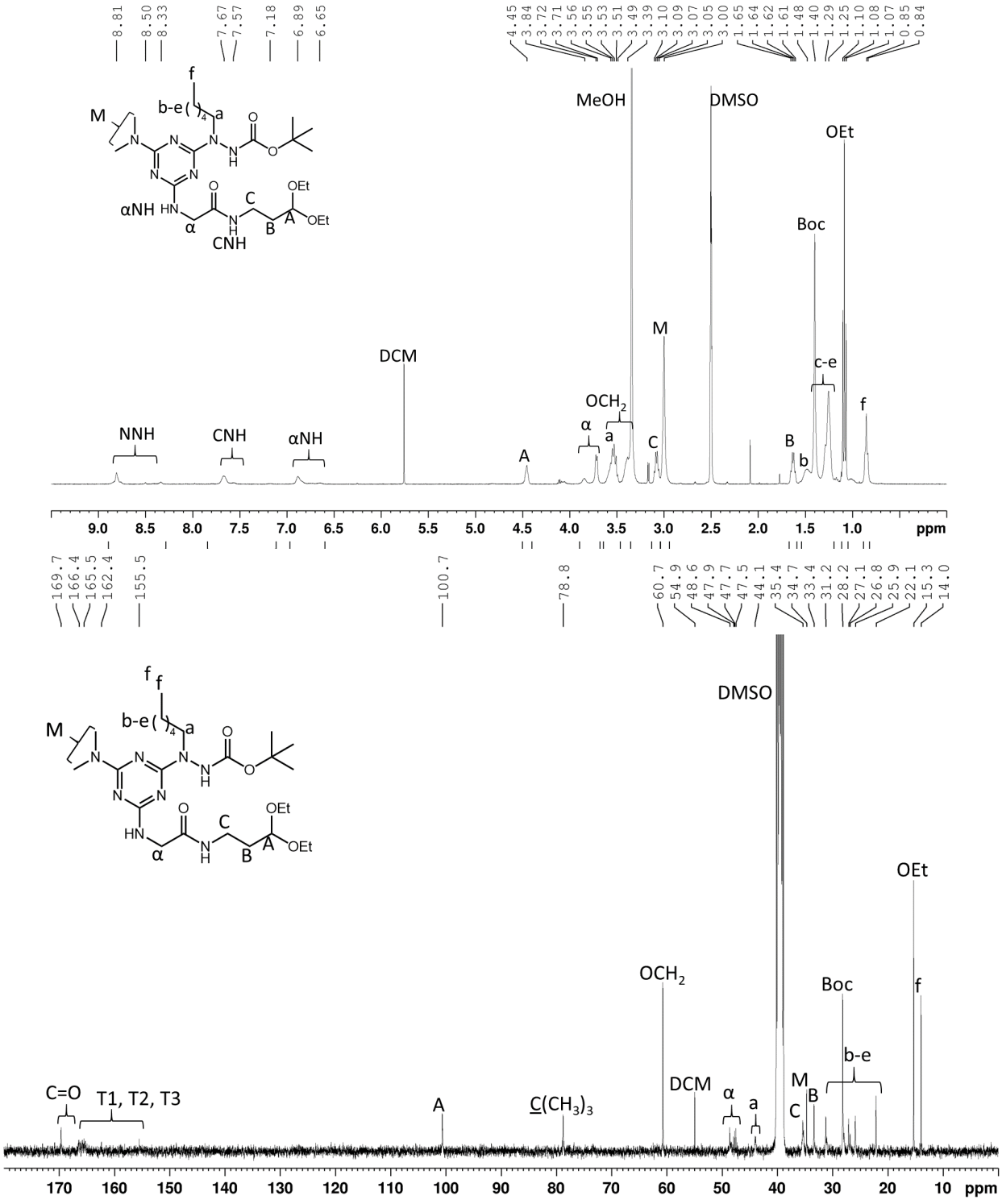

Figure S80. HRMS (ESI) of **G^{NNMe}-Monomer**.

Elmt	Val.	Min	Max	Elmt	Val.	Min	Max	Elmt	Val.	Min	Max	Use Adduct
H	1	0	300	O	2	0	5	S	2	0	0	H
C	4	0	20	F	1	0	0	Cu	2	0	0	
N	3	0	8	Si	4	0	0					

Error Margin (ppm):	10	DBE Range:	-2.0 - 1000.0	Electron Ions:	both
HC Ratio:	unlimited	Apply N Rule:	yes	Use MSn Info:	no
Max Isotopes:	all	Isotope RI (%):	1.00	Isotope Res:	10000
MSn Iso RI (%):	75.00	MSn Logic Mode:	AND	Max Results:	500

Event#: 1 MS(E+) Ret. Time : 0.113 -> 0.127 Scan# : 18 -> 20

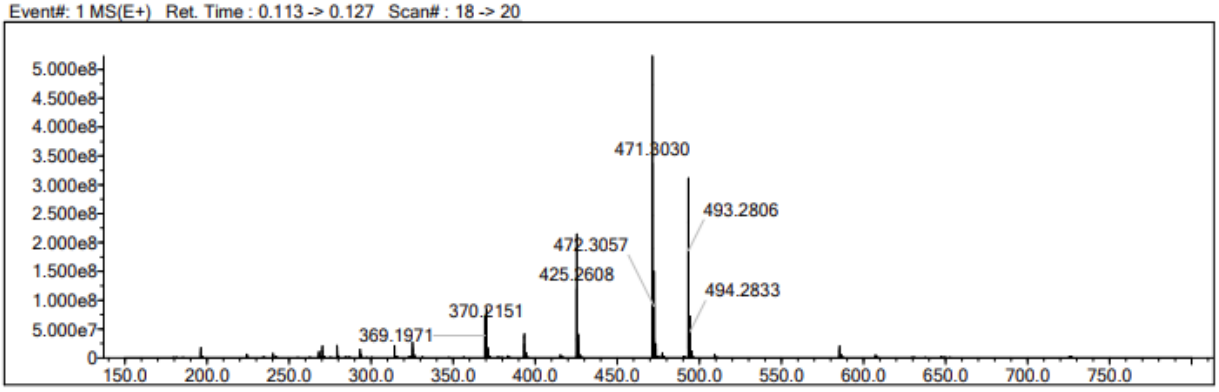

Measured region for 471.3030 m/z

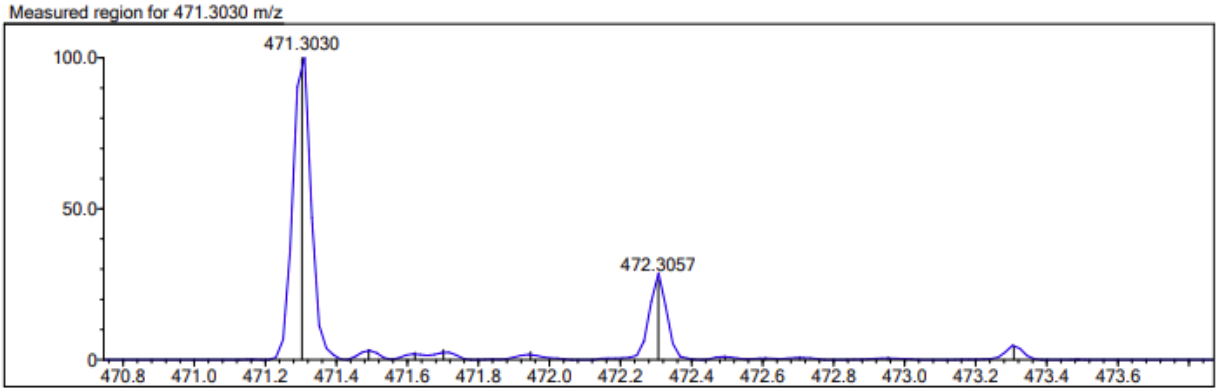

C20 H38 N8 O5 [M+H]+ : Predicted region for 471.3038 m/z

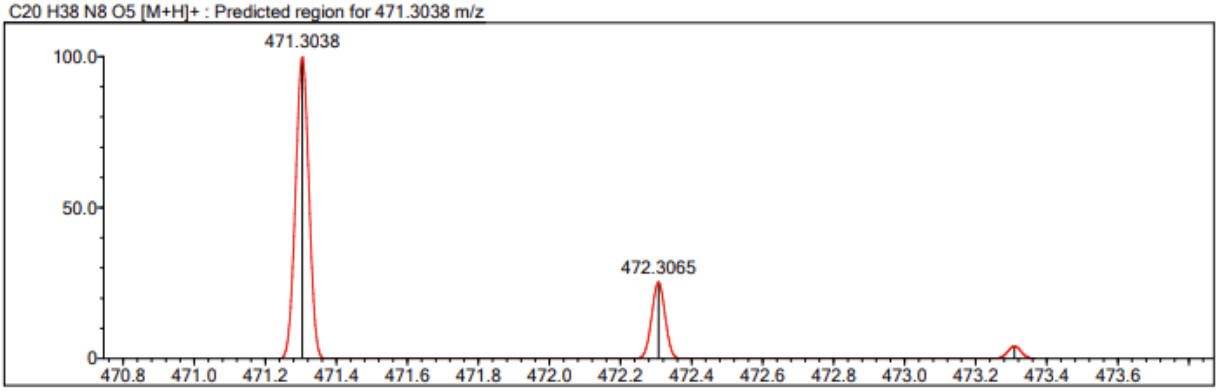

Rank	Score	Formula (M)	Ion	Meas. m/z	Pred. m/z	Df. (mDa)	Df. (ppm)	Iso	DBE
1	94.04	C20 H38 N8 O5	[M+H]+	471.3030	471.3038	-0.8	-1.70	95.71	6.0

Figure S81. HRMS (ESI) of **G^{NNEt}-Monomer**.

Elmt	Val.	Min	Max	Elmt	Val.	Min	Max	Elmt	Val.	Min	Max	Use Adduct
H	1	0	300	O	2	0	5	S	2	0	0	H
C	4	0	21	F	1	0	0	Cu	2	0	0	
N	3	0	8	Si	4	0	0					

Error Margin (ppm): 10
HC Ratio: unlimited
Max Isotopes: all
MSn Iso RI (%): 75.00

DBE Range: -2.0 - 1000.0
Apply N Rule: yes
Isotope RI (%): 1.00
MSn Logic Mode: AND

Electron Ions: both
Use MSn Info: no
Isotope Res: 10000
Max Results: 500

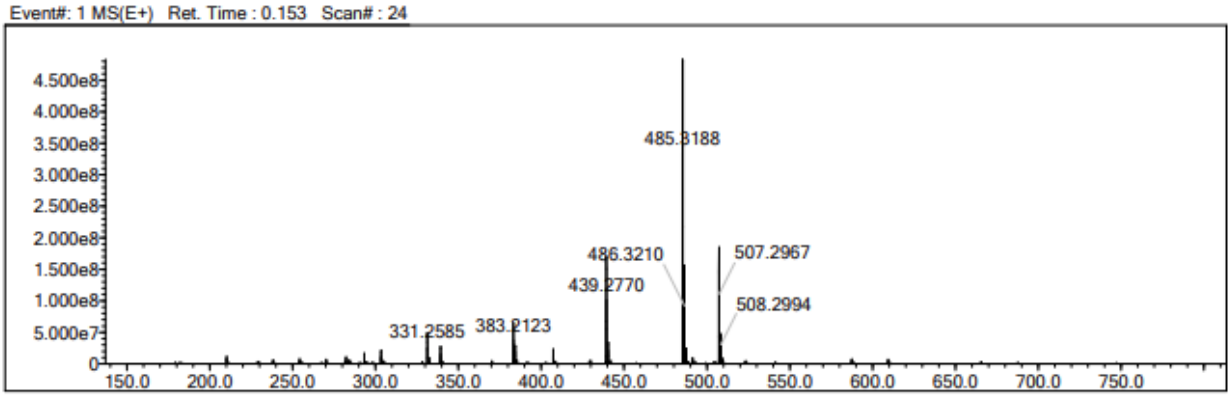

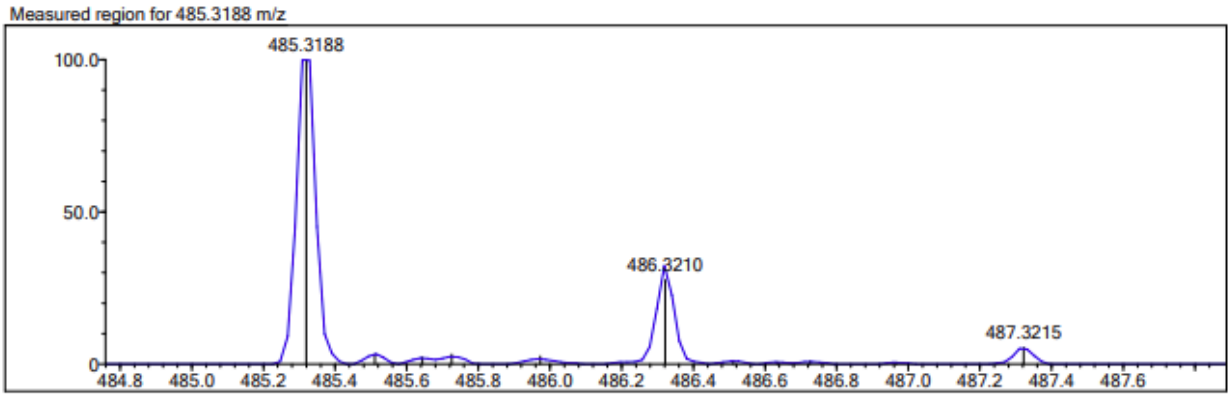

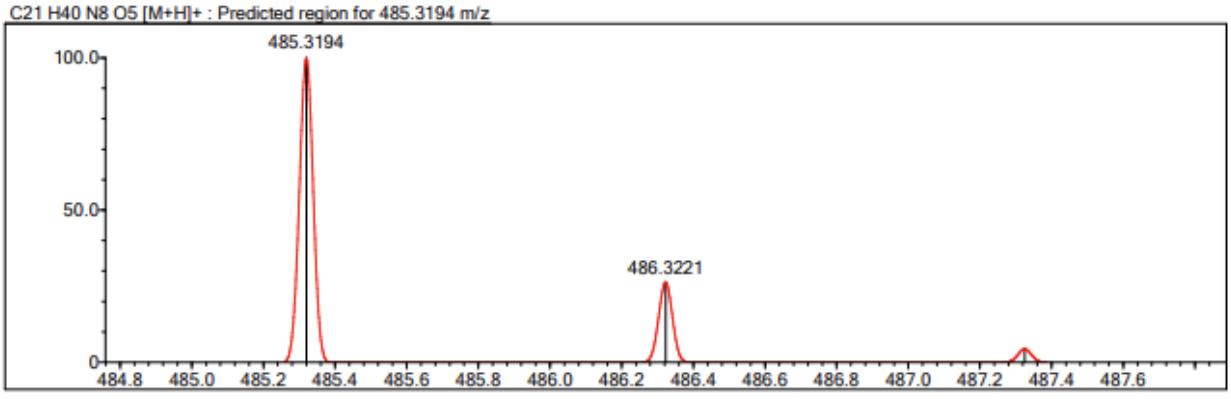

Rank	Score	Formula (M)	Ion	Meas. m/z	Pred. m/z	Df. (mDa)	Df. (ppm)	Iso	DBE
1	95.12	C21 H40 N8 O5	[M+H]+	485.3188	485.3194	-0.6	-1.24	95.69	6.0

Figure S82. HRMS (ESI) of **G^{NNiPr}-Monomer**.

Elmt	Val.	Min	Max	Elmt	Val.	Min	Max	Elmt	Val.	Min	Max	Use Adduct
H	1	0	300	O	2	0	5	S	2	0	0	H
C	4	0	22	F	1	0	0	Cu	2	0	0	
N	3	0	8	Si	4	0	0					

Error Margin (ppm):	10	DBE Range:	-2.0 - 1000.0	Electron Ions:	both
HC Ratio:	unlimited	Apply N Rule:	yes	Use MSn Info:	no
Max Isotopes:	all	Isotope RI (%):	1.00	Isotope Res:	10000
MSn Iso RI (%):	75.00	MSn Logic Mode:	AND	Max Results:	500

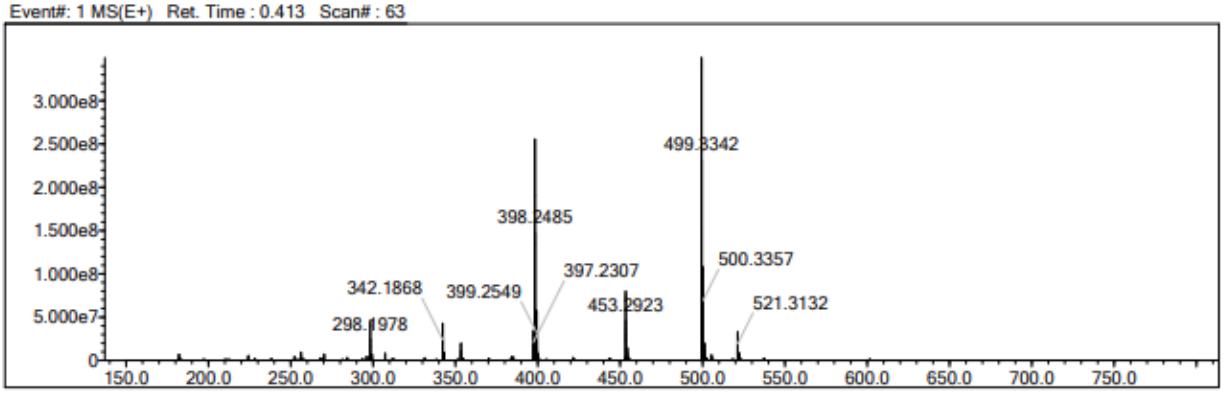

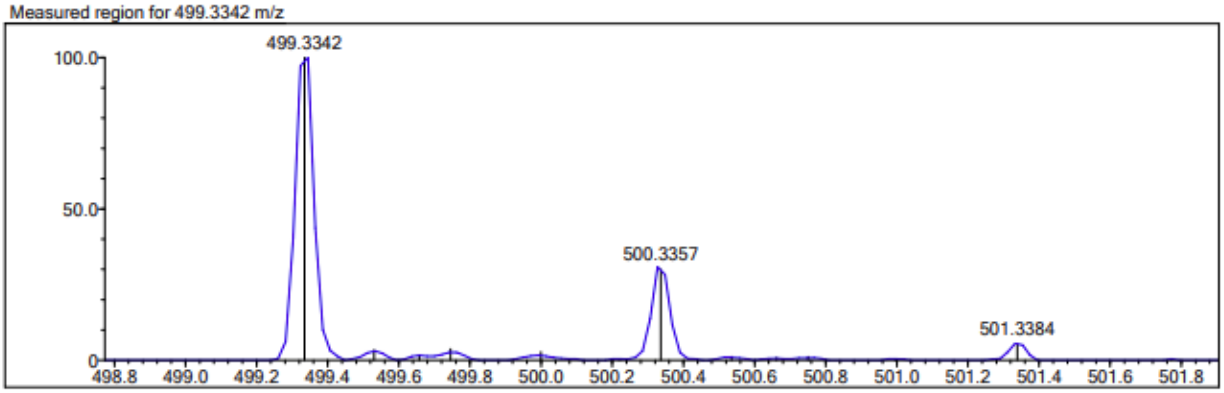

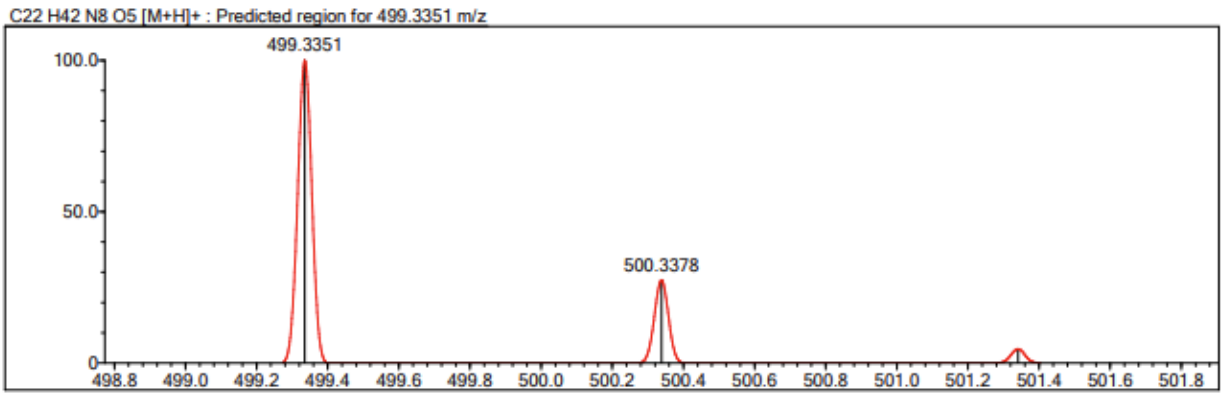

Rank	Score	Formula (M)	Ion	Meas. m/z	Pred. m/z	Df. (mDa)	Df. (ppm)	Iso	DBE
1	98.00	C22 H42 N8 O5	[M+H]+	499.3342	499.3351	-0.9	-1.80	100.00	6.0

Figure S83. HRMS (ESI) of **G^{NNBn}-Monomer**.

Elmt	Val.	Min	Max	Elmt	Val.	Min	Max	Elmt	Val.	Min	Max	Use Adduct
H	1	0	300	O	2	0	5	S	2	0	0	H
C	4	0	26	F	1	0	0	Cu	2	0	0	
N	3	0	8	Si	4	0	0					

Error Margin (ppm):	10	DBE Range:	-2.0 - 1000.0	Electron Ions:	both
HC Ratio:	unlimited	Apply N Rule:	yes	Use MSn Info:	no
Max Isotopes:	all	Isotope RI (%):	1.00	Isotope Res:	10000
MSn Iso RI (%):	75.00	MSn Logic Mode:	AND	Max Results:	500

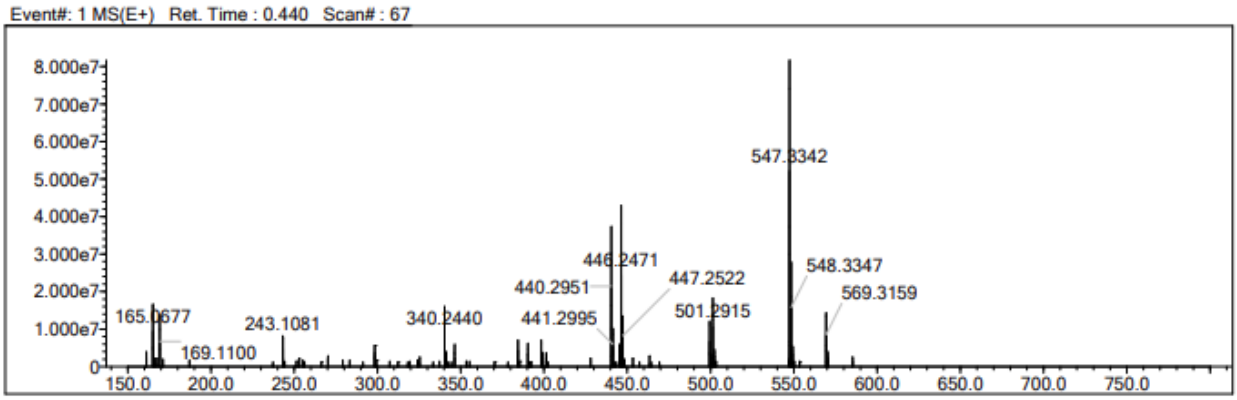

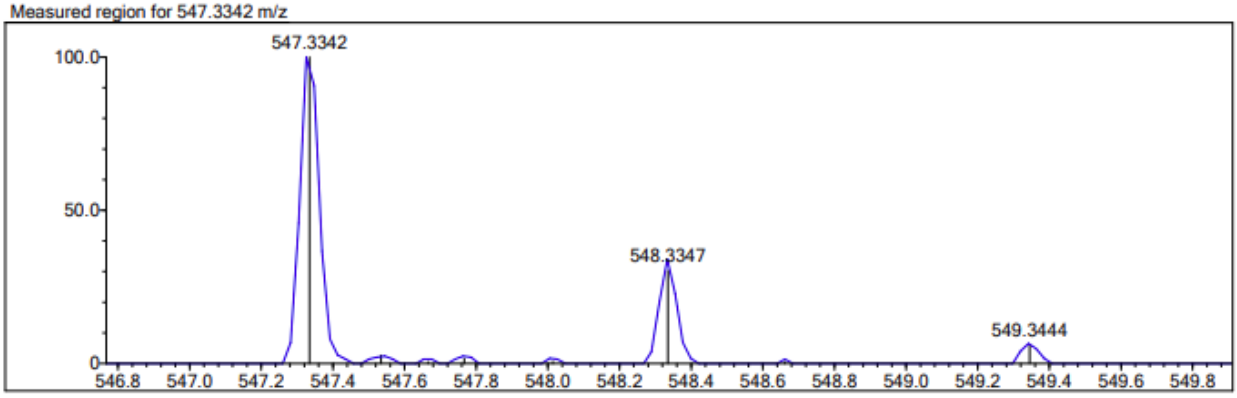

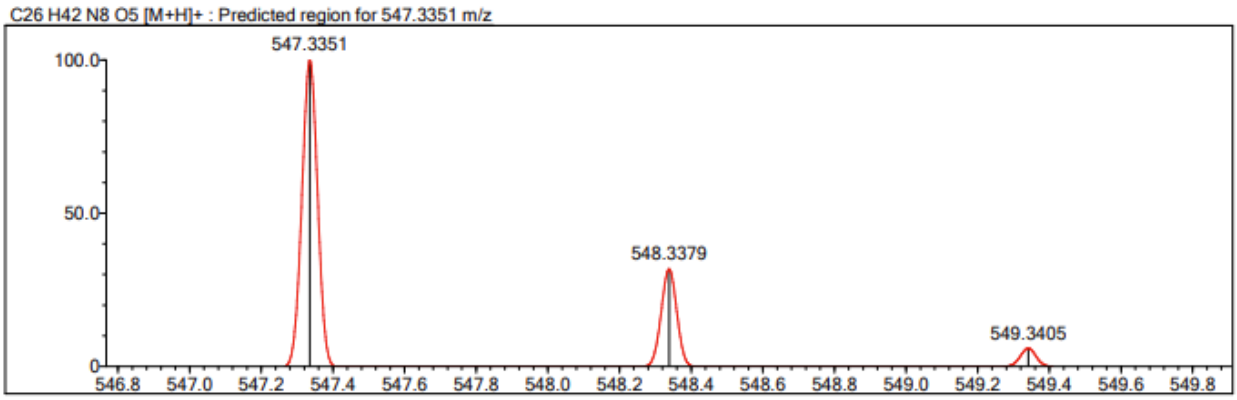

Rank	Score	Formula (M)	Ion	Meas. m/z	Pred. m/z	Df. (mDa)	Df. (ppm)	Iso	DBE
1	89.72	C26 H42 N8 O5	[M+H]+	547.3342	547.3351	-0.9	-1.64	91.18	10.0

Figure S84. HRMS (ESI) of **G^{NNHx}-Monomer**.

Elmt	Val.	Min	Max	Elmt	Val.	Min	Max	Elmt	Val.	Min	Max	Elmt	Val.	Min	Max	Use Adduct
H	1	0	100	O	2	0	5	Si	4	0	0	Cl	1	0	0	H
C	4	25	25	F	1	0	0	P	3	0	0	Cu	2	0	0	
N	3	0	8	Na	1	0	0	S	2	0	0	Br	1	0	0	

Error Margin (ppm): 50
HC Ratio: unlimited
Max Isotopes: all
MSn Iso RI (%): 75.00

DBE Range: -2.0 - 1000.0
Apply N Rule: yes
Isotope RI (%): 1.00
MSn Logic Mode: AND

Electron Ions: both
Use MSn Info: no
Isotope Res: 10000
Max Results: 500

Event#: 1 MS(E+) Ret. Time : 0.317 Scan# : 39

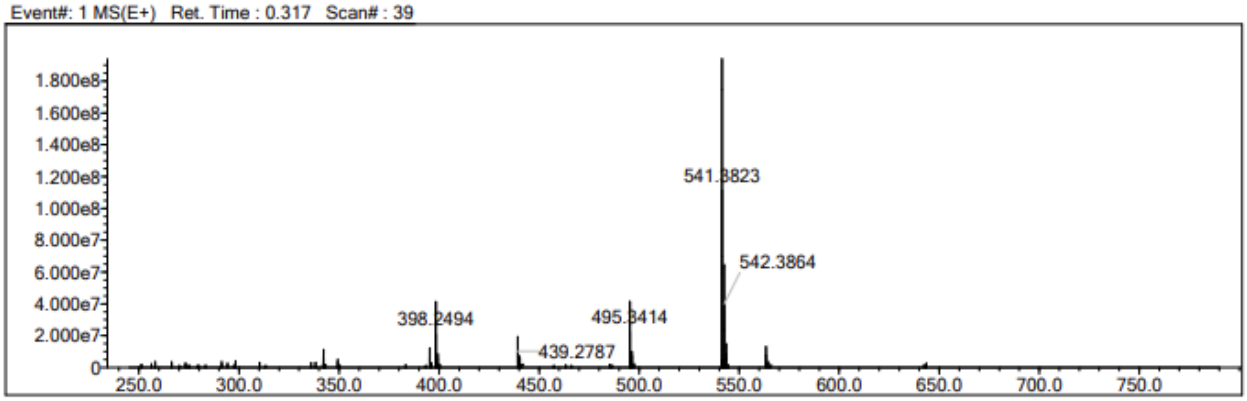

Measured region for 541.3823 m/z

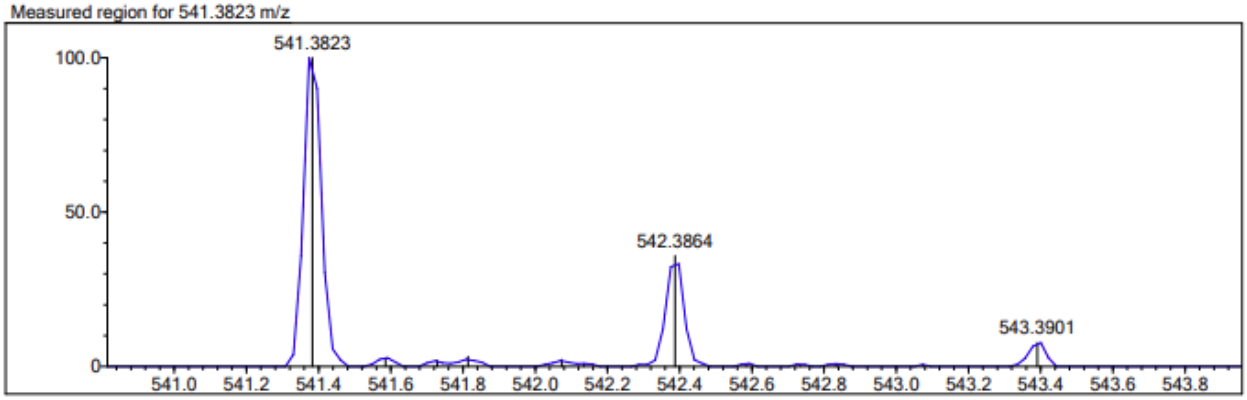

C25 H48 N8 O5 [M+H]+ : Predicted region for 541.3820 m/z

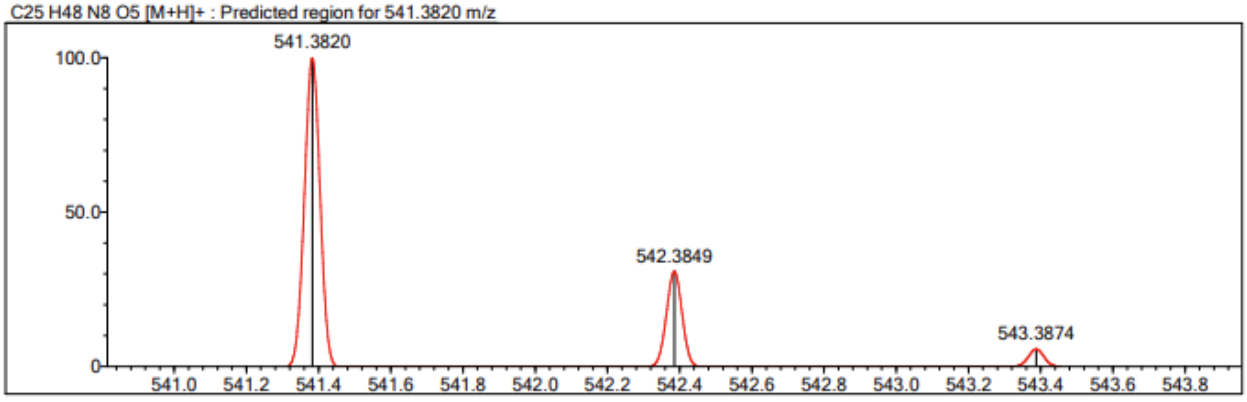

Rank	Score	Formula (M)	Ion	Meas. m/z	Pred. m/z	Df. (mDa)	Df. (ppm)	Iso	DBE
1	93.19	C25 H48 N8 O5	[M+H]+	541.3823	541.3820	0.3	0.55	93.19	6.0

References

A) Yang, Y.-F.; Yu, P.; Houk, K. N. Computational Exploration of Concerted and Zwitterionic Mechanisms of Diels-Alded Reactions between 1,2,3-Triazines and Enamines and Acceleration by Hydrogen-Bonding Solvents. *J. Am. Chem. Soc.* **2017**, *139* (50), 18213-18221.

B) Grimme, S.; Antony, J.; Ehrlich, S.; Krieg, H. A consistent and accurate *ab initio* parametrization of density functional dispersion correction (DFT-D) for the 94 elements H-Pu. *J. Chem. Phy.* **2010**, *132* (15), 154104

C) Melendez, R. E.; Lubell, W. D. Aza-Amino Acid Scan for Rapid Identification of Secondary Structure Based on the Application of *N*-Boc-Aza[1]-Dipeptides in Peptide Synthesis. *J. Am. Chem. Soc.* **2004**, *126* (21), 6759-6764.

D) Casanova, B. B.; Muniz, M. N.; de Oliveira, T.; de Oliveira, L. F.; Machado, M. M.; Fuentefria, A. M.; Gosmann, G.; Gnoatto, S. C. B. Synthesis and Biological Evaluation of Hydrazone Derivatives as Antifungal Agents. *Molecules*. **2004**, *20*, 9229-9241.

E) Škopić, M. K.; Willems, S.; Wagner, B.; Schieven, J.; Krause, N.; Brunschweiger, A. Exploration of a Au(I)-mediated three-component reaction for the synthesis of DNA-tagged highly substituted spiroheterocycles. *Org. Biomol. Chem.* **2017**, *15*, 8648-8654.